HARNESSING HERB-DRUG INTERACTIONS FOR ENHANCED ORAL DELIVERY OF ANTI-HIV AND ANTIMALARIAL DRUGS USING COLLOIDAL FORMULATIONS

by

POLOKO STEPHEN KHEOANE

Submitted in partial fulfilment of the requirements for the degree

DOCTOR TECHNOLOGIAE

in the

Department of Pharmaceutical Sciences

FACULTY OF SCIENCE

TSHWANE UNIVERSITY OF TECHNOLOGY

Supervisor: Prof C Tarirai

Co-supervisor: Prof GM Enslin

October 2020

DECLARATION BY CANDIDATE

“I hereby declare that the thesis submitted for the degree DTech: Pharmaceutical Sciences, at the Tshwane University of Technology, is my own original work and has not previously been submitted to any other institution of higher education. I further declare that all sources cited or quoted are indicated and acknowledged by means of a comprehensive list of references.”

PS Kheoane

DEDICATION

Through it all! Through the highest mountains, through the steep valleys and through rocky and spiky paths, GOD, YOU have seen me through. I dedicate this piece of work to GOD ALMIGHTY for HIS mercy and favour and my lovely spouse, ’Mampho and my daughter Mpho. My lovelies, your selfless support through this study is highly appreciated and is beyond measure.

ACKNOWLEDGEMENTS

I would like to appreciate the selfless efforts of my mentor and supervisor Prof Clemence Tarirai for making this piece of work a success. He had been guiding, grooming, and nurturing me since the very beginning of my career, right from my first degree to the doctoral level. He had indeed been a blessing to me and true pioneer through my academic journey, I cannot emphasise his support enough, because it is unmeasurable. I would also like to thank my co-supervisor Prof Gill Enslin for her mentorship through the pages of this work. Her eagerness and determination to help shine through the pages of this thesis.

I would also like to thank Prof Jerry Shai from the Department of Biomedical Sciences at the Tshwane University of Technology for assisting with his laboratory to perform the cytotoxicity study. The assistance of the A&R abattoir in Pretoria North with the porcine intestinal tissue used in this study is hereby acknowledged. The CSIR is also acknowledged for assisting with the equipment for performing particle size and zeta potential analysis of liposomes.

I would also like to thank the staff of the Department of Pharmaceutical Sciences at the Tshwane University of Technology for their assistance throughout this study, especially Prof Eugene Olivier who helped with the HPLC analysis of the samples.

The financial assistance of the National Research Foundation (NRF) and the Tshwane University of Technology (TUT) (NRF/TUT TTK, UIDs: 87848;117872), and the South African Medical Research Council (SAMRC) Self-initiated research grant of Prof Tarirai towards this research is hereby acknowledged. The financial assistance of the DST-NRF

Innovation Doctoral Scholarship 2017-2018 (UID: 107573) and the Tshwane University of Technology Postgraduate Scholarship (2016) of Mr Kheoane towards this research is hereby acknowledged. Opinions expressed and conclusions arrived at, are those of the authors and are not necessarily to be attributed neither to the DST, NRF, TUT nor SAMRC.

ABSTRACT

Problem: Human immunodeficiency virus/acquired immunodeficiency syndrome (HIV/AIDS) and malaria infect and kill a large population globally. Most of the current clinically used anti-HIV and antimalarial drugs have low bioavailability, either due to poor solubility and permeability, rapid clearance from anatomical reservoirs and poor retention at their site of action (e.g. by the p-glycoprotein efflux system), and extreme first-pass metabolism (e.g. by the cytochrome P450 enzymes). Hence, new approaches such as the incorporation of plant-derived absorption enhancers (PDAEs) into dosage forms, and exploration of nanocarriers as novel dosage forms, are needed and may provide a viable means that could improve the bioavailability of both anti-HIV and antimalarial drugs. **Methods and procedures:** Luminescent-based assay systems were used to screen for the effective inhibitory concentrations of the selected PDAEs against both p-glycoprotein and cytochrome P450 *in vitro*. Thereafter, an everted gut sac model was utilized to further screen for the effective concentrations of PDAEs combinations. Liposomes loaded with efavirenz or mefloquine as well as placebos were prepared using a thin-lipid film hydration technique and characterized for their entrapment efficiency, particle size, zeta potential, *in vitro* drug release, and *in vitro* drug permeability. Liposomes were further investigated for their biocompatibility (safety) with liver using H-4-II-E liver cells *in vitro*. Finally, the everted gut sac model was used for the drug transport studies across an intestinal membrane *ex vivo*. Drug analyses were performed using UV/Vis spectrophotometer for the entrapment efficiency, *in vitro* drug release, and *in vitro* drug permeability studies while high-performance liquid chromatography (HPLC) was used for the *ex vivo* studies. **Main findings:** Quercetin and curcumin had the most significant ($p < 0.05$) inhibitory

effects on both p-glycoprotein and cytochrome P450 at concentrations of 75 µM and 100 µM, respectively. Drug-loaded liposomes prepared using l-α-phospatidylcholine, dioleoyl (DOPC) and cholesterol (CHOL) (1:1 mol/mol) as well as liposomes made of 1,2-distearoyl-sn-glycero-3-phosphocholine (DSPC), CHOL and 1,2-dipalmitoyl-sn-glycero-3-phosphocholine (DPPC) (4:6:26 mol/mol/mol) exhibited better results in terms of their entrapment efficiency, particle size, zeta potential, *in vitro* drug release and permeability. Furthermore, these liposomes were biocompatible (safe) with liver cells. However, drugs and/or liposomes were unable to permeate through the porcine intestinal tissue, possibly due to high protein binding capacities of efavirenz and mefloquine. **Conclusions:** The DOPC:CHOL liposomes and the DSPC:CHOL:DPPC liposomes could provide a useful nanoformulation platform, which could ensure sustained release of both anti-HIV and antimalaria drugs. However, these dosage forms need further investigation using *in vivo* studies that could rectify the effect of protein binding, which was not investigated in this study.

CONTENTS

CHAPTER 5

5 FINAL CONCLUSIONS AND RECOMMENDATIONS

LIST OF FIGURES

LIST OF TABLES

CHAPTER 1

BACKGROUND, AIM, AND OBJECTIVES

1.1 BACKGROUND AND JUSTIFICATION

Malaria and human immunodeficiency virus/acquired immunodeficiency syndrome (HIV/AIDS) affect a large population globally (WHO, 2014; WHO, 2015). Malaria in humans is caused by five species of parasites belonging to the genus *Plasmodium*. Four of these species (*P. falciparum*, *P. vivax*, *P. malariae* and *P. ovale*) spread from one person to another *via* a bite by female mosquitoes of the genus *Anopheles* (WHO, 2015). About 3.2 billion people remain at risk of contracting malaria and in the year 2015 alone, there were an estimated 214 million new cases of malaria and 438 000 deaths attributed to the disease. Approximately 80% of malaria deaths are concentrated in 15 countries, mainly in Africa (WHO, 2015). Figure 1.1 explains how malaria infection is transmitted.

Acquired immunodeficiency syndrome is characterized by a set of symptoms and infections resulting from the specific damage to the immune system caused by infection with HIV, which is a retrovirus of the lentivirus family. Human immunodeficiency virus infects vital components of the human immune system, including $CD4^+$ T cells, macrophages, and dendritic cells. HIV, directly and indirectly, destroys $CD4^+$ T cells, which are required for the proper functioning of the immune system (Kotta *et al*., 2014:129). Figure 1.2 illustrates the progression stages of HIV to AIDS.

Most of the current clinically used drugs have low bioavailability, either due to poor solubility and permeability or due to extreme first-pass metabolism.

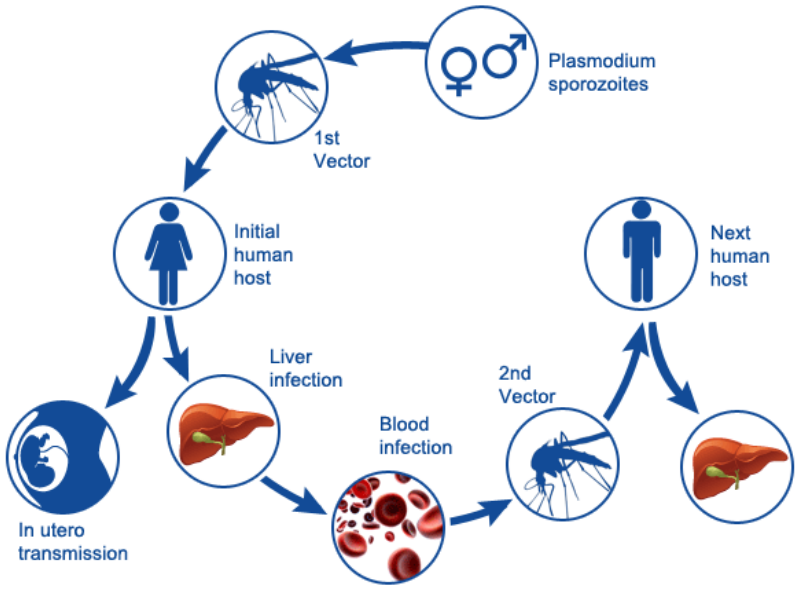

FIGURE 1.1: Schematic illustration of malaria infection and transmission (The Jenner Institute, 2019)

Poor drug bioavailability in the cellular and anatomical reservoirs is affected by the expression of efflux transporters (e.g. p-glycoprotein (P-gp)), the presence of drug-metabolizing enzymes (e.g. cytochrome P-450 (CYP450)), poor permeability properties, non-targeted distribution, and rapid clearance (Kotta *et al*., 2014:129).

Drug absorption can be inhibited by binding between herbal constituents and the drug, resulting in low drug levels. For instance, alkaloids bind to tannins, while pectins, resins, and fibres may bind to several drugs (Fugh-Berman, 2000:1020; Fugh-Berman & Ernest, 2001:588-592). A rapid transit time that may be induced by some herbal products can also result in low drug levels. This is usually the case with diarrhoea or frequent bowel movements due to colitis or laxative (e.g. Senna) intake.

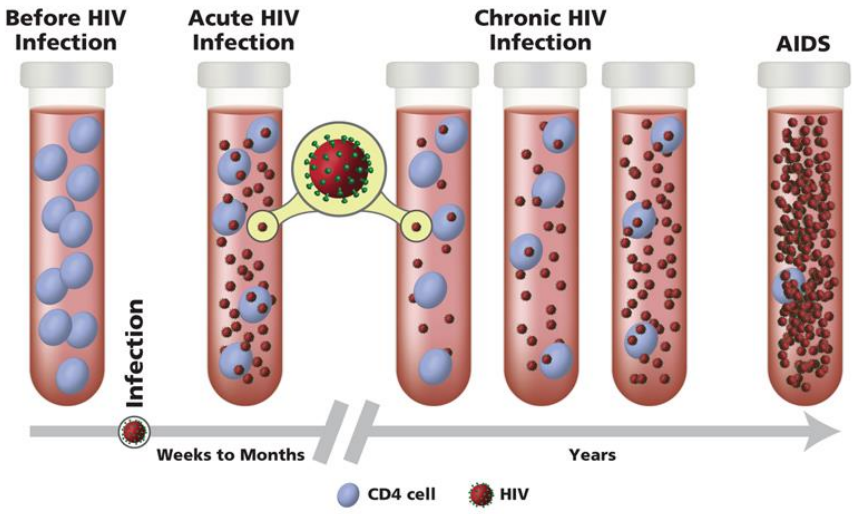

FIGURE 1.2: Schematic illustration of HIV progression to AIDS (CDC, 2019)

Saponins may improve the absorption and elimination of drugs, altering the blood levels and rate of change of drug levels, while strongly acid or alkaline herbs may alter the absorption of drugs by affecting the pH at the absorption window (Blumenthal, 2000:52). Laxative and diuretic herbs may reduce potassium levels in the body. These types of herbs are often given together for weight loss and pose a high risk for cardiac effects when concomitantly administered with cardiac drugs (Tarirai, Viljoen & Hamman, 2010:1550).

Despite the negative effects of herbs outlined above, a vast number of plant-derived natural products have shown potential as excipients to improve the oral absorption of drugs through various pharmacokinetic mechanisms such as their inhibitory effects on efflux transporters or metabolizing enzymes (Tarirai, Viljoen & Hamman, 2010:1550). Literature has indicated that extracts of certain fruits can influence the absorption of allopathic drugs (Lim & Lim, 2006:42; Rodriguez-Fragoso *et al*., 2011:R112; Tarirai, Viljoen & Hamman, 2012:254). For instance, *Psidium guajava* (guava) and *Sclerocarya*

birrea (marula) have shown potential to improve the absorption of cimetidine across Caco-2 cells and excised pig intestinal tissue, probably through inhibition of P-gp-related efflux (Tarirai, Viljoen & Hamman, 2012:254). The P-gp efflux is schematically illustrated in Figure 1.3. Briefly, the already absorbed drug, which is a P-gp substrate is pumped back into the lumen or extracellularly.

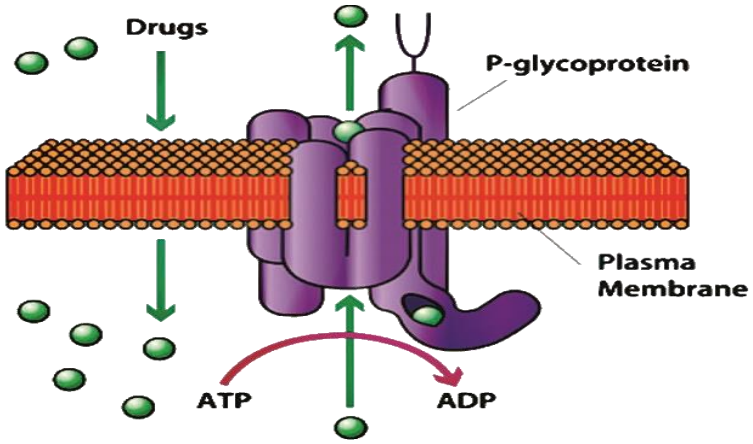

FIGURE 1.3: Schematic illustration of the drug efflux system (Absorption Systems, 2016)

Orally administered Biopharmaceutics Classification System (BCS) class III and IV drugs experience poor drug bioavailability (Tarirai, Viljoen & Hamman, 2010:1551). The BCS class III drugs have low permeability and high solubility, whereas, class IV drugs are less permeable and less soluble. The antimalarial drugs, mefloquine, proguanil, and artemisinin are commonly prescribed in malaria prevalent countries, whereas, anti-HIV drugs such as lamivudine, zidovudine and efavirenz are prescribed throughout the World (WHO, 2015). The World Health Organization (2005) BCS classifies artemether (a semi-synthetic derivative of artemisinin), mefloquine and efavirenz as class IV drugs, whereas, proguanil, lamivudine, and zidovudine are classified as class I drugs, which are susceptible to the effects of drug-metabolizing enzymes and efflux transporters. However,

Strauch et al. (2011:19) concluded that mefloquine hydrochloride could belong to either BCS class II or IV due to lack of reliable permeability data and failure to meet the highly soluble criterion.

Mefloquine (MQ) is a synthetic analogue of quinine commonly used in the treatment and prophylaxis of chloroquine-resistant *Plasmodium falciparum* malaria (Manneck, Haggenmüller & Keiser, 2010:85). Proguanil is a prophylactic antimalarial drug, which is taken in combination with another antimalarial drug, such as atonil. Artemisinin is a Chinese herb, *Artemisia annua* (qinghaosu), which has antimalarial action. Artemisinin can kill a broad range of asexual parasite stages at safe concentrations and therefore, the artemisinin combination therapy (ACT) is used as a frontline treatment drug against malaria (Tripathy & Roy, 2014:673). Lamivudine (3TC) is a nucleoside reverse transcriptase inhibitor, which is active against HIV-1, HIV-2, and hepatitis B virus while zidovudine (3-azido-3-dideoxythymidine, AZT) is a non-nucleoside reverse transcriptase inhibitor, which inhibits viral reverse transcriptase (Rao & Sankar, 2015:73; Joshy *et al*., 2016:40). Efavirenz is a potent non-nucleoside reverse transcriptase inhibitor, is one of the components of highly active antiretroviral therapy (HAART), is highly effective at suppressing HIV-1, and the WHO lists it as a component of the first-line antiretroviral (ARV) treatment (Dalwadi *et al*., 2016:10).

Plant-derived absorption enhancers (PDAEs) are phytochemicals that may enhance the absorption of orally administered drugs. Examples of such materials available on the market include, but are not limited to, quercetin and naringin from citrus fruits (e.g. grapefruit), curcumin from *Curcuma longa*, sinomenine from *Sinomenium acutum* and glycyrrhizic acid from *Glycyrrhiza glabra* root (liquorice). Quercetin, a flavonoid, has been

reported to inhibit P-gp-mediated drug efflux (Choi, Jo & Kim, 2004:313). *Hypoxis hemerocallidea* was found to inhibit the efflux of nevirapine (anti-HIV drug) across intestinal epithelial cells (Brown *et al*., 2008:588), while the bioavailability of diltiazem was increased by quercetin through inhibition of P-gp and cytochrome P450 3A4 (CYP3A4) in rabbits and by naringin in rats (Choi & Li, 2005:313; Choi & Han, 2005:122). Glycyrrhizic acid inhibited P-gp-mediated efflux of daunorubicin in P-gp-overexpressing KB-C2 cells (Nabekura *et al*., 2008:867).

Colloidal formulations, such as nanoparticles, nanoemulsions and liposomes have several advantages over conventional drug delivery systems as platforms for enhanced bioavailability. These advantages include high stability, high specificity, high drug-carrying capacity, controlled release applications, possibility to administer through different routes and the capability to deliver both hydrophilic and hydrophobic drug molecules (Pal *et al*., 2011:228). Colloidal formulations containing PDAEs could also play a vital role in the delivery of the BCS class III and IV drugs.

1.2 PROBLEM STATEMENT

Several studies indicate that phytochemicals may improve the absorption of orally administered drugs through herb-drug interactions (Tarirai, Viljoen & Hamman, 2012:254; Lim & Lim, 2006:42; Rodriguez-Fragoso *et al*., 2011:112). Mechanistic herb-drug interactions are therefore a potentially viable means of enhancing drug absorption (e.g. through the inhibition of efflux transport and metabolising enzymes by phytochemicals from natural products) and this avenue could be beneficial to patients. However, it is not clear whether the same results would be obtained when the phytochemicals are

incorporated in a dosage form as functional phytoexcipients. There is also a need to develop excipients that can increase the permeability of both BCS Class III and IV drugs to enable their oral administration in the lowest effective doses possible. Furthermore, there is continuing interest in excipients of natural origin because of their continuing massive production, which is cost-effective. Although the mechanisms of drug absorption enhancement are not well understood for many of these compounds, drug absorption enhancement can be achieved by harnessing different herb-drug interaction mechanisms. The proposed study will provide scientific information that can be used by policymakers, the medical fraternity and professionals in the pharmaceutical arena to advocate for the incorporation of phytochemicals into various dosage forms as phytoexcipients. The study will provide detailed scientific information about the application of colloidal formulations for improved drug delivery.

1.3 AIM

This study is aimed at investigating the effects of phytochemicals as plant-derived absorption enhancers and nanocarrier drug delivery systems towards the improvement of the bioavailability of antimalarial and anti-HIV drugs.

1.4 SPECIFIC OBJECTIVES

The objectives of this study were:

1.4.1 To identify phytochemicals with potential functional excipient properties with regards to bioavailability enhancement using existing literature.

1.4.2 To screen the selected PDAEs using P-gp and CYP450 kits to determine their effective concentrations.

1.4.3 To formulate and characterise a nanocarrier (e.g. liposomes) containing selected PDAEs and model drugs.

1.4.4 To conduct the *ex vivo* drug permeability studies on colloidal formulations across pig intestinal tissue.

1.5 LAYOUT OF THE THESIS

Chapter one is the introduction to the thesis. The justification, the problem statement, the aim, and specific objectives of the study were defined. The literature of different PDAEs that act on both the CYP450 enzymes and the P-gp were reviewed in chapter two. In chapter two, the *in vitro* effective concentrations of different PDAEs were also reviewed; different nanocarriers in drug delivery, liposomes preparation, and liposomes characterisation were discussed. The biocompatibility or toxicity levels of different liposomal formulations, the selected PDAEs and the selected anti-HIV and antimalarial drugs were discussed in chapter two. Chapter two finally, identified different nanoformulations, which are approved by the Food and Drug Administration (FDA). The selected PDAEs were investigated for their effective concentrations *in vitro* and *ex vivo* in chapter three. The formulation and characterisation of liposomes were performed, and their toxicity level and/or biocompatibility were investigated in chapter four. The *ex vivo* permeability studies of liposomal formulations for this study were also assessed and reported in chapter four. Conclusion, recommendations, and the limitations of the study were given in chapter five.

CHAPTER 2

LITERATURE REVIEW

2.1 INTRODUCTION

Studies indicate that phytochemicals may improve the absorption of orally administered drugs through herb-drug interactions and involvement of the p-glycoprotein (P-gp) and the cytochrome P450 enzymes (CYP450) (Tarirai, Viljoen & Hamman, 2012:254; Lim & Lim, 2006:42; Rodriguez-Fragoso *et al*., 2011:112). CYP3A4 is one of the most important CYP isoforms involved in the metabolism of xenobiotics in the human body (Li, Kaminski & Rasmussen, 1995:1). CYP2C9 makes up approximately 18% of the CYP450 protein in liver microsomes and metabolizes certain therapeutic drugs, including those with a narrow therapeutic index, such as warfarin (Rettie & Jones, 2005:477). CYP2E1 is involved in the metabolism of xenobiotics in the body (Kolble, 1993:702) and mediates many important drug interactions (Touw, 1997:55).

Many therapeutic drugs or molecules such as nucleic acid, proteins, peptide, anticancer drugs and other agents (including anti-HIV and antimalarial drugs) have less bioavailability, low solubility profile, rapid clearance, high toxicity, rapid elimination from body, side effects and adverse effects and may therefore, require special drug delivery platforms (e.g. colloidal nanocarriers) to counter these properties. The development of delivery methods and drug delivery carriers, that will convey needful and effective delivery for therapeutic agent or drugs is required (Singh, Gangadharappa & Mruthunjaya, 2017:166). Liposomes and other nanoformulations (also referred to as colloidal

nanocarriers) as compared to the conventional types of formulations have numerous advantages (Sercombe *et al*., 2015:1).

2.2 PLANT-DERIVED ABSORPTION ENHANCERS

Plant-derived absorption enhancers (PDAEs) are the absorption enhancers of plant origin, also called bioavailability enhancers of herbal origin. Many herbal compounds including quercetin, genistein, naringin, sinomenine, piperine, glycyrrhizin and nitrile glycoside have demonstrated the capability to enhance the bioavailability (Kesarwani & Gupta, 2013:253). PDAEs can be further classified according to their mechanism of action. For example, *Carum carvi* (caraway), genistein, sinomenine, *Cuminum cyminum* (black cumin) naringin and quercetin can be classified as the inhibitors of the P-gp. Naringin, gallic acid, and quercetin can be classified as the suppressors of the CYP-450 enzymes, while the *Aloe vera* (aloe), niaziridin (drumstick pods), *Zingiber officinale* (ginger) and glycyrrhizic acid (liquorice) are classified as regulators of the gastrointestinal tract (GIT) function to facilitate better absorption (Tatiraju *et al*., 2013:57).

2.2.1 Quercetin

Quercetin [2-(3,4-dihydroxyphenyl)-3,5,7-trihydroxy-4H-chromen-4-one] (Figure 2.1) is a bioactive flavonoid compound found in many common foodstuffs such as nuts, vegetables and fruits. Quercetin increased the bioavailability, blood levels and efficacy of several drugs including diltiazem, digoxin and epigallocatechin gallate (Hoi & Li, 2005:297; Dupuy *et al*., 2003:112; Wang *et al*., 2004:1191; Anup *et al*, 2005:89), possibly through the inhibition of the p-glycoprotein efflux pump and the metabolizing enzyme, CYP3A4 in the intestinal mucosa (Scambia *et al*., 1994:460; Shapiro & Ling, 1997:588).

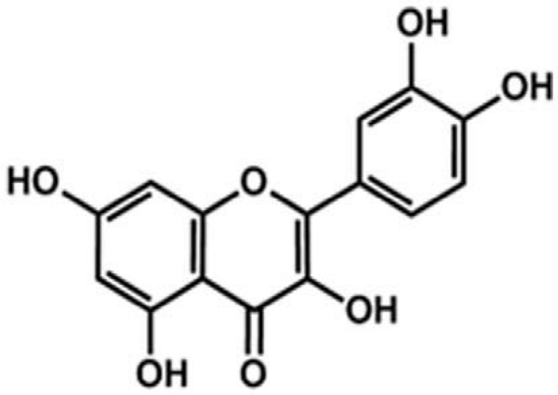

FIGURE 2.1: Chemical structure of quercetin (Vilaca *et al*., 2012: e45494)

2.2.2 Curcumin

Curcumin (1E,6E)-1,7-bis(4-hydroxy-3-methoxyphenyl)-1,6-heptadiene-3,5-dione) is a major yellow pigment and dietary component derived from *Curcuma longa* (Figure 2.2). Curcumin inhibited CYP1A2 (IC_{50}, 40.0 µM), CYP3A4 (IC_{50}, 16.3 µM), CYP2D6 (IC_{50}, 50.3 µM), CYP2C9 (IC_{50}, 4.3 µM) and CYP2B6 (IC_{50}, 24.5 µM) (Appiah-Opong *et al*., 2007:83).

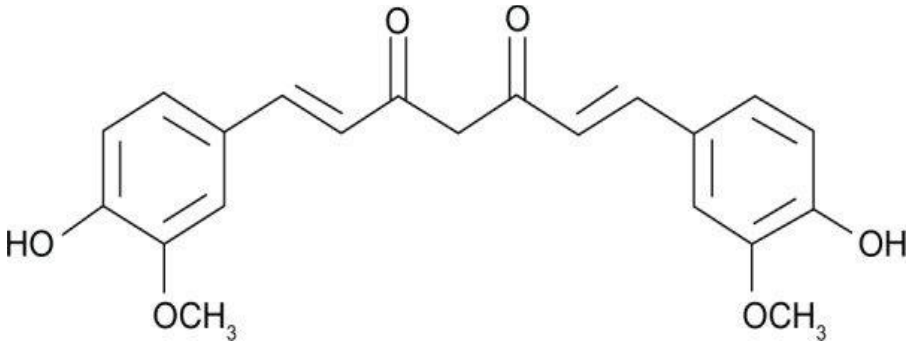

FIGURE 2.2: Chemical structure of curcumin (Farazuddin *et al*., 2014:1140)

2.2.3 Naringin

Naringin (chemical structure illustrated in Figure 2.3) is the major flavonoid glycoside found in grapefruit and makes grapefruit juice taste bitter. Naringin inhibited a CYP3A1/2 and p-glycoprotein in rats (Zhang *et al*., 2000:351; Lim & Choi, 2006:443).

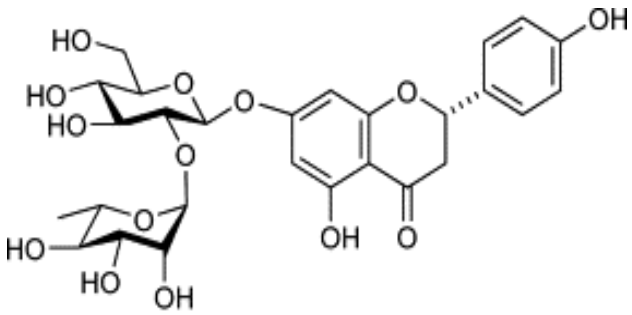

FIGURE 2.3: Chemical structure of naringin (Izawa *et al*., 2010:651)

2.2.4 Sinomenine

Sinomenine (7,8-didehydro-4-hydroxy-3,7-dimethoxy17-methylmor phinan-6-one) (Figure 2.4) is an alkaloid extracted from *Sinomenium acutum Thunb* (Cheng *et al*., 1964:177).

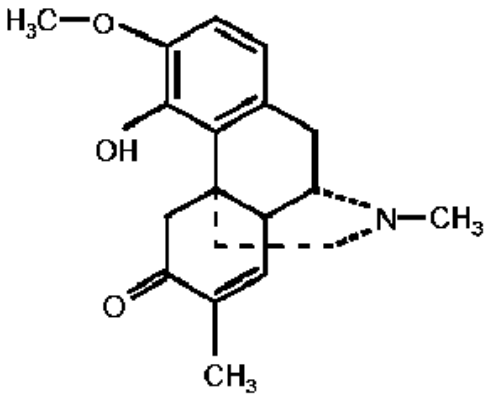

FIGURE 2.4: Chemical structure of sinomenine (Zeng *et al*., 2007:1439)

Sinomenine at 16 and 136 μM concentrations could significantly enhance the absorption of paeoniflorin (20 μM) by 1.5- and 2.5-fold (Chan *et al*., 2006:425).

2.2.5 Glycyrrhizic acid (liquorice)

Glycyrrhizic acid or glycyrrhizin [(3,18)-30-hydroxy-11,30-dioxoolean-12- en-3-yl 2-O-glucopyranuronosyl-Dglucopyranosiduronic acid] (the chemical structure is shown in Figure 2.5) is a triterpenoid saponin found in *Glycyrrhiza glabra L*. (Fabaceae). Lv et al. (2016:1) evaluated the effect of glycyrrhizin on the activity of five cytochrome P450 enzymes, namely, CYP2A6, CYP2C9, CYP2C19, CYP2D6, and CYP3A4, in human liver microsomes (HLMs) and recombinant cDNA-expressed enzyme systems using an HPLC-MS/MS CYP-specific probe substrate assay. The results of their study revealed that glycyrrhizin decreased CYP3A4 activity with IC_{50} values of 8.195 μM in HLMs and 7.498 μM in the recombinant cDNA-expressed CYP3A4 enzyme system, respectively.

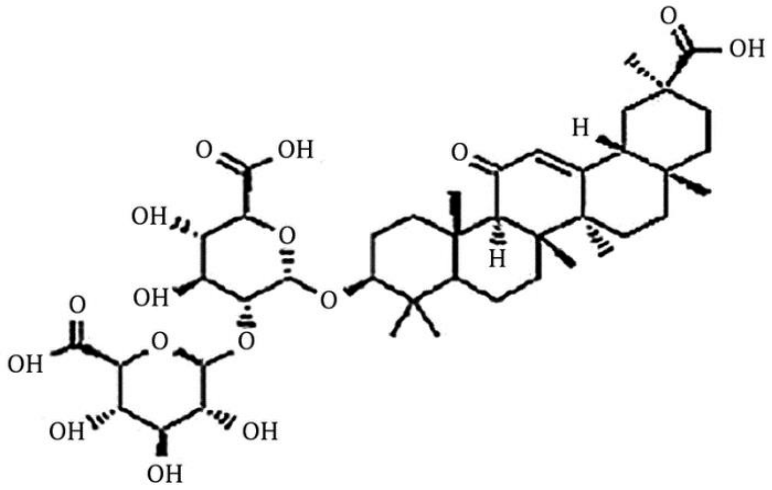

FIGURE 2.5: Chemical structure of glycyrrhizic acid (Refahi *et al*., 2016: e21012)

2.3 EFFECTIVE *IN VITRO* CONCENTRATIONS AND TOXICITIES OF THE SELECTED PLANT-DERIVED ABSORPTION ENHANCERS REPORTED IN THE LITERATURE

2.3.1 Quercetin

Quercetin inhibited CYP3A4 enzyme activity in a concentration-dependent manner with a 50% inhibition concentration (IC_{50}) of 1.97 µM. In addition, quercetin significantly enhanced the intracellular accumulation of rhodamine-123 in MCF-7/ADR cells overexpressing P-gp. Flavonoids (morin, quercetin and phloroglucinol) were tested for their ability to modulate the function of p-glycoprotein ATPase of the insecticide-resistant pest *Helicoverpa armigera* (Ha-Pgp). A 100 µM concentration of quercetin inhibited the activity of Ha-Pgp ATPase by 80 - 90% (Aurade *et al*., 2011:214-215).

For Caco-2 cells exposed to 1.1 µM PH-interacting protein (PhIP) in the presence of 25 µM quercetin the increase in flux value amounted to 367 ± 49% of the flux value for PhIP in the absence of quercetin (Schutte *et al*., 2008:3425). It was further confirmed *in vitro* using erythromycin-N-demethylase (EMD) assay. These studies indicated potent inhibition of CYP3A activity by quercetin 10 µM, *in vitro* (Umathe *et al*., 2008:1673-1674).

Quercetin inhibited P-gp activity, down-regulated P-gp expression and decreased ABCB1 mRNA (in a wide range of concentrations 10–100 µM) in different experimental models (cancer cell lines such as HK-2, MCF7, etc.) and thus enhanced the sensitivity to anti-tumor agents (cisplatin, tamoxifen, paclitaxel) (Chieli *et al*., 2010:287).

Experiments performed on cell lines of human pancreatic carcinoma, exposed to selected

concentrations of quercetin (3, 6 and 12 µM) and daunorubicin, confirmed that the polyphenol affects the expression and function of P-gp in a concentration-dependent manner. Moreover, it decreased the expression of ABCB1 (Borska *et al*., 2010:859-862).

The reviewed literature on quercetin demonstrated its effectiveness in a wide range of concentrations from 1.97 µM to 100 µM (Aurade *et al*., 2011:214-215; Chieli *et al*., 2010:287). Therefore, quercetin effective concentrations could be investigated on different *in vitro* models using this concentration range.

The chemotherapeutic effects of quercetin were tested by Raja et al. (2017:95) on HCT15 and HT29 cells using various concentrations of quercetin (0 - 100 µM) for 12, 24, 36, 48, and 60 hours and viability of the cells was assessed using the MTT assay. HT29 cells were more sensitive to quercetin with the IC_{50} of 42.5 µM at 24 hours was, which was lower than the IC_{50} of quercetin treated HCT15, which was 77.4 µM.

Liu et al. (2017:33) examined the effects of quercetin on cell viability, cell cycle progression, and migration in U251 cells, a human glioblastoma cell line. Quercetin inhibited cell proliferation after treating cells for 24 hours with the IC_{50} of 113.65 µg/mL or 48 hours with the IC_{50} of 48.61 µg/mL. Quercetin treatment also induced apoptosis via deregulating the expression of apoptotic genes, including Bax and Bcl-2, and arrested cell cycle at G2/M phases.

Assessment of cell viability was done based on qualitative colony formation and quantitative growth curve studies of CHO10B2 (CHO wild type) cells. The effects of 3.3 µM and 33 µM quercetin treatments compared to the untreated control sample showed a drastic reduction in the size of colony formations. Growth inhibition studies showed that

quercetin was the strongest inhibitor with an extrapolated IC_{50} of 11.5 µM, where isoquercetin and maltooligosyl isoquercetin had an IC_{50} of 238 µM and 159 µM, respectively (Engen *et al*., 2015:18).

The *in vitro* cytotoxicity against breast cancer cell lines (MCF-7) was studied by Saraswathi, Saravanan and Santhakumar (2017:25) for various concentrations of both the isolated and crude extract of quercetin (25, 50, 100, 250 and 500 µg/mL) and compared with control. The number of dead cells increased with the increase in the concentration of the isolated compound when compared to the crude extract. At 500 µg/mL the enlargement of cells was noticed, nearly 30–35% of the cells showed small protrusions of the membrane. The apoptotic bodies observed in the isolated quercetin compound (MEI) was good compared to the crude extract of the treated cells. The cells showed big vacuoles in the cell cytoplasm indicating the autophagy (similar to cell death mechanism).

The combination of metformin and quercetin induced more apoptosis of human prostate cancer cell lines PC-3 and LNCaP ATCC (American Type Culture Collection) than treatment of metformin or quercetin alone. The combinational effect of metformin and quercetin on tumour growth was further investigated *in vivo* in a xenograft model in BALB/c nude male mice injected with PC-3 cells and then treated with metformin (500 mg/kg body weight) and quercetin (600 mg/kg body weight), alone or in combination, for 40 days. Both the tumour volume and weight in the combination treatment group was less than in the single-agent treatment groups, suggesting that the combination of metformin and quercetin suppressed the growth of PC-3 cells in BALB/c mice (Sun *et al*., 2018:52).

An *in vitro* model treated with quercetin and quercetin nanoparticles was used to investigate the effects of quercetin nanoparticles on MCF-7 breast cancer cell line. MCF-7 cells were cultured with different concentrations (1 -100 µM) of quercetin nanoparticles at the 24^{th}, 48^{th} and 72^{nd} hours, and cell cycle and apoptosis assays were detected by flow cytometry (FCM). Quercetin nanoparticles (1 - 100 µM) reduced cell vitality, growth rate and colony formation of MCF-7 cells (Aghapour *et al*., 2018:860).

Dell'Albani et al. (2017:56) administered quercetin-derivatives such as acylated and brominated quercetin, which caused a sharp increase in cell death. Of all the tested derivatives, 3-O decanoylquercetin 10 showed the strongest cytotoxic effect at a concentration of 25 µM both in the human U373-MGU373-MG (40% viability after 24 hours) and in murine 9L glioma cells (20% viability after 24 hours).

Anti-proliferative effects of quercetin, PLGA nanoparticles loaded with quercetin (QrPLGA) and transferrin conjugation on QrPLGA (Tf-QrPLGA) were assessed against both the human triple-negative breast (MDA-MB-231) and larynx epidermoid carcinoma (HEp-2) cell lines. A substantial reduction in viability of the cancer cells was recorded in MTT assay. The IC_{50} in cell viability was achieved by Tf-QrPLGA in the lowest dose of 4 ug/mL, followed by QrPLGA at 7 ug/mL and free quercetin at 10 ug/mL (Halder *et al*., 2018:9702).

Singh et al. (2018:105) analysed the cytotoxicity of cells incubated in different concentration (50–200 µg/mL) of chitin-glucan-aldehyde-quercetin (chi-glu-ald-que) conjugate for 12 hours in PBMCs and 48 hours in J774 (macrophage cancer cell line). Their result showed no sign of cell death of PBMCs whereas in J774 cell death increased

substantially with increasing concentration of chi-glu-ald-que conjugate. The chi-glu-ald-que-conjugate was concluded to be nontoxic and biocompatible for normal cell line and provided excellent cytotoxicity in cancerous cell line. Cell viability decreased with increase in concentration of chi-glu-ald-que conjugate. The cell viability J774 for chi-glu-ald-que conjugate decreased up to 60% when exposed for 48 hours at maximum concentration whereas the cell death in case of PBMCs in all case were found to be negligible with increasing concentration.

2.3.2 Curcumin

Curcuminoid extract inhibited multiple CYPP450 enzymes of human liver microsomes and recombinant CYP3A4 and CYP3A5 at different concentrations ranging from 0.19 - 200 µM (Volak *et al*., 2008:1598). Volak et al. (2008:1600) observed the moderate to potent inhibition (IC_{50} < 50 µM) with the curcuminoid extract for most CYP isoforms with a relative order of inhibitory potency of CYP2C19 > CYP2B6 > CYP2C9 > CYP3A. Relatively weak inhibition (IC_{50} > 60 µM) was observed for CYP2D6 and CYP1A2, while less than 20% inhibition was observed for CYP2E1 activity at the highest concentration of 200 µM.

At concentrations of 1, 3, 10, and 30 µM, curcumin inhibited the ethoxyresorufin deethylation (EROD) activity in β-naphthoflavone (βNF)-induced liver microsomes by 36 up to 93%, the pentoxyresorufin depentylation (PROD) activity in phenobarbital (PB)-induced microsomes by 13 up to 88%, and the p-nitrophenol (PNP) hydroxylation activity in pyrazole-induced microsomes only by 0.5 up to 9%, respectively (Oetari *et al*., 1996:42).

Cho, Lee and Choi (2012:124) evaluated the effects of curcumin on p-glycoprotein (P-gp) and CYP3A4. Curcumin inhibited CYP3A4 activity with 50% inhibition concentration (IC_{50}) values of 2.7 µM. In addition, curcumin significantly ($p<0.01$ at 10 µM) enhanced the cellular accumulation of rhodamine-123 in MCF-7/ADR cells overexpressing P-gp in a concentration-dependent manner.

Curcumin achieved minimal inhibition at all concentrations in the CYP450 3A4 or 2D6 *in vitro* studies. Only 10.5% and 22.5% inhibition of CYP450 2C9 and CYP450 2C8 was achieved at curcumin concentration of 58.3 µM, respectively. The curcumin concentration required to achieve 50% inhibition of CYP450 activity (IC_{50}) was 276.8 µM for CYP450 2C9 and 129.7 µM for CYP450 2C8 (Mach *et al*., 2010:813).

Curcumin inhibited CYP1A2 (IC_{50}, 40.0 µM), CYP3A4 (IC_{50}, 16.3 µM), CYP2D6 (IC_{50}, 50.3 µM), CYP2C9 (IC_{50}, 4.3 µM) and CYP2B6 (IC_{50}, 24.5 µM) and showed a competitive type of inhibition towards CYP1A2, CYP3A4 and CYP2B6, whereas a non-competitive type of inhibition was observed with respect to CYP2D6 and CYP2C9 (Appiah-Opong *et al*., 2007:87-88).

Caco-2 cell monolayers were treated with methanol extracts of *Curcumas* (0.1 mg/mL) or curcumin (30 µM) for 72 hours to investigate the relationship between the potential effects of *Curcuma*s and curcumin on P-gp. All *Curcumas* increased the activity of P gp by up-regulating the expressions of P-gp protein and *MDR1* mRNA levels (Hou *et al*., 2008:226-227).

Appiah-Opong et al. (2008:1622-1623) screened the 33 curcumin analogues (each at 100 µM concentration) for inhibitory potentials towards human CYP1A2, CYP3A4, CYP2B6,

CYP2C9 and CYP2D6. The curcumin analogues demonstrated a wide range of inhibitory activities towards CYP-mediated metabolism of probe substrates. Results on 29 selected compounds (with % inhibition >20%) revealed 75.8% (22), 27.5% (8), 13.7% (4), 62.0% (18) and 41.3% (12) of the compounds inhibiting CYP1A2, CYP3A4, CYP2B6, CYP2C9 and CYP2D6, respectively. The compounds showed a comparatively stronger inhibitory potency towards CYP1A2 and CYP2C9 than towards CYP3A4, CYP2B6 and CYP2D6 activities.

Methanolic extracts from two *Curcuma* rhizomes (0.1 mg/mL) or curcumin (30 µM) decreased the activity of CYP3A4 by about 85 - 98%. The 50% inhibitory concentrations of *C. longa* and *C. zedoaria* extracts were 0.019 and 0.014 mg/mL, respectively. They caused a 60 - 70% decrease in CYP3A4 protein. Otherwise, curcumin treatment caused a 30 - 40% decrease in CYP3A4 catalytic activity and a 38% decrease in CYP3A4 protein expression (Hou *et al*., 2007:172-173).

In both freshly plated hepatocytes, containing low levels of P-gp, and 72 hour-cultured hepatocytes, containing high levels of P-gp, the Rhodamine- (R-123) efflux, which represents a specific functional test for P-gp-mediated transport, was inhibited by curcumin in a dose-dependent manner. Western blot analysis showed that 25 µM curcumin when included in the culture medium throughout the experimental observation (72 hours), lowered the increase of mAb C219-immunoreactive protein spontaneously occurring in the cells during culture (Romiti *et al*., 1998:2351-2352).

Curcumin at concentrations less than 25 µM inhibited the growth of the tumour by increasing the sensitivity of cells to vincristine, cisplatin, fluorouracil, and

hydroxycamptothecin. The intracellular Rhodamine123 accumulation was increased ($p < 0.05$), and the expression of the multidrug resistance gene and p-glycoprotein were significantly suppressed ($p < 0.05$) (Lu *et al*., 2013:694).

Curcumin mixture inhibited the activity of Ha-Pgp ATPase by 80 - 90% at 100 µM concentration. Along with curcuminoids I, II and III, it inhibited the verapamil- and ethylparaoxonstimulated Ha-Pgp ATPase activity (Aurade, Jayalakshmi & Sreeramulu, 2010:271).

Based on the literature outlined above, it is evident that curcumin exhibit varying effective concentrations depending on different types of CYP450 isoenzymes (Appiah-Opong *et al*., 2007:87-88) and on the selected CYP or P-gp model. However, curcumin at 30, 50, 129.7 and 276.8 µM concentrations were reported most effective for CYP450 inhibition (Volak *et al*., 2008:1600; Oetari *et al*., 1996:42; Mach *et al*., 2010:813) while 10, 25 and 30 µM concentrations were more effective for P-gp inhibition (Cho, Lee & Choi, 2012:124; Hou *et al*., 2008:226-227; Lu *et al*., 2013:694).

Fourteen diverse analogues of curcumin were evaluated against a panel of human cancer cell lines. The best analogue of the series i.e. compound 6a exhibited potent cytotoxicity against A431, epidermoid carcinoma cell line (IC_{50} = 1.5 µM) and DLD1, colorectal adenocarcinoma cell line (IC_{50} = 6.9 µM). In tubulin kinetics experiment, compound 6a destabilized polymerisation process (IC_{50} = 4.68 µM). In cell cycle analysis, compound 6a exerted G2/M phase arrest in A431 cells and induced apoptosis (Khwaja *et al*., 2018:51).

The nanocurcumin had the anticancer activity with the IC_{50} of 0.05 µg/mL against AGS cancer cells. This formulation had little effect at concentrations lower than its IC_{50} and this

could be attributed to its poor *in vitro* bioavailability when a carrier is not used (Dhivya *et al*., 2017:66).

Cytotoxic potential and cellular uptake of curcumin-loaded zinc oxide (ZnO) nanoparticles were assessed by cell viability assay, cell cycle assays along with the cell imaging studies were done in addition to MTT using AGS gastric cancer cells. These studies revealed the clinical potential of the curcumin-loaded PMMA-PEG/ZnO to induce the apoptosis of cancer cells through a cell cycle mediated apoptosis corridor (Dhivya *et al*., 2017:59).

Cytotoxicity of the free-drug, curcumin-loaded diphenyl carbonate (DPC) and pyromellitic dianhydride (PMDA) nanosponges and their blank nanosponges were studied in MCF-7 (human breast adenocarcinoma) cell lines. Cell viability was estimated using MTT assay and the study revealed increased toxicity of curcumin nanosponges with two different types of crosslinker namely DPC-CDNS and PMDA-CDNS to MCF-7 cells at a lower concentration. IC_{50} value of the drug (22.51 µg/mL) was reduced by 2.2 fold (10.44 µg/mL) by CUR-PMDA-CDNS against 1.4 fold (15.92 µg/mL) by CUR-DPC-CDNS (Pushpalatha, Selvamuthukumar & Kilimozhi, 2018:45).

Hodgkin's lymphoma heterotopic xenograft model was used to assess the chemotherapeutic potential of curcumin *in vivo*. All the treatment groups were treated with curcumin at a dose of 100 mg/kg/d, 5 days per week. Curcumin, significantly inhibited L-540 xenograft growth, starting on day 15 of treatment until the end of the study ($p < 0.05$, vs. control). Formulation of curcumin in SLN and TPGS enhanced its inhibitory effect. Compared to control, SLN-curc and TPGS-curc reduced the rate of growth over baseline, by 50.5% ($p<0.02$) and 43.0% ($p<0.04$), respectively (Guorgui *et al*., 2018:14).

A comparative cytotoxicity study to prospect the capability of curcumin-loaded marinosomes (CURMS) to deliver highly hydrophobic drugs such as curcumin to lung cancer cells has been performed. After incubation of A549 cells for 24 hours, free-CUR has a cytotoxic effect of 63.4 ± 6.5% (the highest) while CURMS showed 10.9 ± 5.9% at 20 µg/mL of curcumin concentration. After 48 hours incubation, free-CUR and CURMS showed nearly the same cytotoxic effect of 59.3 ± 4.0% and 55.7 ± 2.5% at 20 µg/mL, respectively. However, when the incubation time was extended to 72 hours, the cytotoxic effect of CURMS increased to 90.9 ± 2.2% (the highest) and that of free-CUR decreased to 45.7 ± 9.2% at the same curcumin concentration (20 µg/mL) (Ibrahim *et al*., 2018:46-47).

The curcumin-loaded marinosomes (CURMs) showed its maximum cytotoxic effect (IC_{50}; 11.7 ± 0.24 µg/mL) after incubation for 72 hours against A549 lung cancer cells. Additionally, CURMs inhibited the proliferation of HUVECs in a dose-dependent manner with an IC_{50} of 2.64 ± 0.21 µg/mL after incubation for 24 hours (Ibrahim *et al*., 2018:40).

The 5-fluoro-2-deoxyuridine (FdU) containing hairpin and curcumin bound to DNA hairpin with natural nucleotide (AT-hairpin), demonstrated cytotoxicity towards human oral squamous carcinoma cell line (UPCI-SCC-131) in a dose-dependent manner, at concentrations ranging from 0.125–4.0 µM (Ghosh *et al*., 2018:490).

The MTT assay was carried out for assessing the cell viability in the presence of different materials in both normal (CHO) and cancer cells (A549, MCF-7 and B16F10). Initially, cell viability assay was carried out in normal cells (CHO) with different MSU-2 and MCM-41 based functionalized materials (V1-V6) that did not exhibit any cytotoxicity suggesting

the biocompatible nature of silica-based mesoporous materials and materials loaded with curcumin. However, it was observed that curcumin loaded mesoporous materials V3 and V6 were cytotoxic in various cancer cell lines in a dose-dependent (5 -10 µM curcumin) manner compared to free curcumin (Bollu *et al*., 2016:399-400).

Cytotoxicity studies of curcumin-loaded oleic acid ultra-deformable nanovesicles were performed using MTT assay on human breast cancer cell lines (MCF-7 cells). The results of the MTT assay demonstrated cell death at an IC_{50} of 20 µg/mL making these new curcumin-loaded nanovesicles a potential delivery system for breast cancer therapy (Abdel-Hafez, Hathout & Sammour, 2018:63).

In vitro cytotoxicity of the synthesized curcumin derivatives (2a-2n) were evaluated by MTT assay method using three selected human tumour cell lines HeLa, HCT-116 and QG-56. Among 3,4-dihydropyrimidines (2a-2n), derivatives 2b, 2c, 2h, 2m and 2n showed more or less equal cytotoxicity with range of 50 - 100 µM IC_{50} against HeLa, HCT-116 and Hep-G2 (Sahu, 2016:512). Curcumin showed less cytotoxicity (% growth inhibition) of 7.5, 11, and 19% for 2.5, 25, and 250 µg/mL concentration respectively, on lung cancer cells A549 line (Gaikwad *et al*., 2017:663).

In vitro cytotoxicity potentials of nanocurcumin, zinc oxide (ZnO), and curcumin/ poly(methyl methacrylate-co-acrylic acid)/ zinc oxide nanoparticles (Cur/PMMA-AA/ZnO NPs) on AGS cells were evaluated by Dhivya et al. (2018:187) using a standard MTT assay. The IC_{50} of ZnO NPs was 0.05 µg/mL. The IC_{50} of nanocurcumin was approximately the same as for the ZnO NPs, 0.05 µg/mL. The nanocurcumin had little

concentration effect on AGS cancer cells than its IC_{50}. The Cur/PMMA-AA/ZnO NPs had the largest observable effect on AGS cancer cell viability with IC_{50} close to 0.01 µg/mL.

The MTT colorimetric assay was carried out to study the cytotoxic potential of free curcumin, cholesterol-curcumin solid lipid nanoparticles (Chol-Cur SLN), and blank cholesterol SLN against MDAMB- 231 (Human breast cancer) cells. Higher cytotoxicity was seen for free CUR and Chol-CUR SLN treated for 24 hours against 6 hours treatment. For all concentrations, Chol-CUR SLN was found to be more effective in killing the cells in comparison with the free drug. A 50 µg/mL concentration of curcumin, cells exhibited 71.83 ± 2.64% cell viability compared to 52 ± 2.94% in Chol-CUR SLN treated cells after 6 hours treatment. The cell viability decreased to 55.1 ± 2.65% and 39.04 ± 3.43% for free CUR, and Chol-CUR SLN, respectively after 24 hours treatment (Rompicharla *et al*., 2017:17).

The cytotoxicity of free curcumin was evaluated *in vitro* by exposing HeLa cells to curcumin and curcumin-loaded and unloaded genipin-crosslinked CS-CH nanoparticles (G-CCNPs). There was no decrease in cell viability observed in the presence of unloaded G-CCNPs at all concentrations used, indicating that G-CCNPs were biocompatible and nontoxic. Cell viability decreased in a concentration-dependent manner in the presence of free curcumin or curcumin-loaded G-CCNPs. However, the cytotoxicity of curcumin-loaded G-CCNPs was enhanced compared with that of free curcumin, with the IC_{50} values of free curcumin and curcumin-loaded G-CCNPs for these cells at 10 and 6.5 µg/mL, respectively (Razi *et al*., 2018:312).

MCF-7 cell line was used to study its inhibition and proliferation after treating with curcumin and the CSSH coated curcumin liposomes (Cur-Lip-CSSH). Treatment of MCF-7 with curcumin and Cur-Lip-CSSH showed dose and time-dependent cytotoxicity, with growth suppression at 200 μM, after 72 hours of incubation (Li *et al*., 2017:156).

The IC_{50} of free paclitaxel (Tax) and curcumin in breast cancer cells was 0.19 μM and 53.16 μM, respectively. The synergy of Tax/Cur mixture in breast cancer cells was further investigated by designing a series of concentration ratios. The results indicated that Tax and Cur had some synergistic effects in the presence of 0.4 to 0.0125 μM Tax. Considering the synergistic effect and encapsulation efficiency of Tax and Cur synthetically, the 5:1 Cur/Tax mole ratio was used in subsequent *in vitro* experiment. The *in vitro* anti-tumour activity of Tax/Cur mixture and their dual delivery in lipid bilayer coated mesoporous silica nanoparticles (LMSNs) and PEGylated lipid bilayer coated mesoporous silica nanoparticles (PLMSNs) against breast cancer cells after 24 hours, 48 hours, 60 hours and 72 hours incubation was assessed by CCK8 assay. The cell viabilities of all loaded mesoporous silica nanoparticles (MSNs) and drug effect were inhibited by a fixed concentration of Cur ranging from 1 μM to 0.25 μM and the concentration of Tax 0.2 μM/Cur 1 μM at different time points. At each single time point, Tax-Cur-PLMSNs exhibited the strongest cytotoxic effect against breast cancer cells. For example, cell viability of Tax-Cur-PLMSNs group was significantly decreased at 48 hours ($p<0.01$), 72 hours ($p<0.01$) and 60 hours ($p < 0.05$) compared to Tax-Cur-mixture group (Lin *et al*., 2018:278-279).

HCT-15 cells and HT-29 cells were treated with (5 - 90 μg/mL) curcumin, (5 - 90 μg/mL) cur-monosuccinate (5 - 90 μg/mL) xylan-curcumin (xyl-cur) prodrug nanoparticles (NPs)

for 24 hours and 48 hours. The *in vitro* cytotoxicity of the free drugs (curcumin and cur-monosuccinate) and the xyl-cur prodrug NPs was investigated in HT-29 and HCT-15 colon cancer cells lines by MTT assay. The cell viability results showed that the xyl-cur prodrug NPs and the free drugs exhibited the cytotoxicity in a dose-dependent and time-dependent manner and the substantial differences in cytotoxicity were observed after 48 hours treatment. The results showed that xyl-cur prodrug NPs possessed over 2.8 fold lower IC_{50} value than free curcumin for HT-29 cell line, and over 1.28-fold lower IC_{50} value than free curcumin for the HCT-15 cell line, indicating the expressively enhanced cytotoxicity of xyl-cur prodrug NPs (Sauraj *et al*., 2018:257).

The N,N,N-trimethyl chitosan (TMC), TMC/sodium tripolyphosphate (TPP) and TMC/TPP/CUR cytotoxic concentration (CC_{50}) toward healthy VERO cells were 145 ± 2, 53 ± 4 and 158 ± 7 µg/mL, respectively. So, TMC/TPP was more cytotoxic against VERO cells than TMC and TMC/TPP/CUR. On the other hand, the TMC/TPP/CUR was slightly cytotoxic on SiHa cells, but the non-loaded TMC/TPP particles were more cytotoxic to SiHa cells. TMC and TMC/TPP CC_{50} were 217 ± 23 and 275 ± 4 µg/mL, respectively. N,N-dimethyl chitosan (DMC), DMC/TPP and DMC/TPP/CUR CC_{50} on VERO cells were 137 ± 13, 135 ± 5 and 172 ± 7 µg/mL, respectively. The CUR slightly increased the DMC/TPP/CUR biocompatibility, whereas DMC and DMC/TPP showed almost the same cytotoxic effect on VERO cells. The loaded CUR into NPs matrices increased the biocompatibility onto SiHa cancerous cells, because DMC/TPP/CUR CC_{50} was 235 ± 23 µg/mL, while DMC and DMC/TPP CC_{50} were 190 ± 5 and 165 ± 7 µg/mL, respectively. The CUR presence on TMC/TPP/CUR structures induced slight cytotoxic activity only on cancerous cells (SiHa), and in general, the CUR into NPs (DMC/TPP/CUR or

TMC/TPP/CUR) matrices promoted greater biocompatibility on healthy VERO cells, especially when the biocompatibility of unloaded and loaded TMC/TPP were compared (Facchi *et al*., 2016:244).

The cytotoxicity of free curcumin, curcumin-loaded amino-functionalized mesoporous silica nanoparticles (MSN-N=C-Cur) and curcumin-loaded folic acid conjugated mesoporous silica nanoparticles (FA-MSN-N=C-Cur) were evaluated, respectively. Curcumin showed a concentration-dependent toxicity effect to MCF-7 and HEK-293 T cells, respectively. There was no much difference observed in cell viability incubated with free curcumin between MCF-7 and HEK-293T cells. Compared to curcumin loaded nanoparticles, a little bit low cytotoxicity of free curcumin against both cell lines was observed. The cytotoxic efficacy of FA-MSN-N=C-Cur was higher than that of free curcumin and MSN-N=C-Cur at all treated concentrations (i.e. 0.5 – 32 µg/mL), especially obvious toward MCF-7 cells (Chen *et al*., 2018:95).

2.3.3 Naringin

Naringin inhibited the metabolism of simvastatin in rat hepatocytes (the intrinsic clearance of simvastatin decreases from 26.2 µL/min/10^6 cells in the absence of naringin to 4.15 µL/min/10^6 cells in the presence of 50 µM naringin, indicating the inhibition of CYP metabolizing enzymes. This inhibition was more pronounced in hepatocytes (Ki value = 5 µM) than in liver microsomes (Ki = 23 µM and = 30 µM in human and rat liver microsomes respectively) (Ubeaud *et al*., 1999:1403).

There are few reports on the *in vitro* effective concentrations of naringin as compared to the *in vivo* studies. The concentration range of naringin, therefore, needs to be expanded

when this absorption enhancer is screened for effective concentrations.

2.3.4 Sinomenine

The intestinal kinetic absorptive characteristics of paeoniflorin, as well as the absorptive behaviour influenced by co-administration of sinomenine using an *in vitro*, everted rat gut sac model was investigated by Chan et al. (2006:425-432). Sinomenine at 16 and 136 µM concentrations enhanced the absorption of paeoniflorin by 1.5 and 2.5-fold, respectively (Chan *et al*., 2006:427-428).

A 50 µM concentration of sinomenine decreased the activity of CYP2C19 by 69% (p=0.012) in human microsomes (Yao *et al*., 2007:113).

Exposure of Caco-2 cells monolayer to sinomenine 0.5% w/v resulted in a decrease in the expression of claudin-1, which represented tight-junction weakening and paracellular permeability enhancement of octreotide (Li *et al*., 2013:12874-75).

The *in vitro* reports on the IC_{50} values concentrations of sinomenine revealed more CYP450 inhibition at 50 µM concentration and P-gp inhibition at the concentration ranges of 16 to 136 µM. However, there are only a few studies on the absorption enhancement activity of sinomenine, therefore, there is a need to expand on the concentration range when the effective concentration of sinomenine is investigated.

2.3.5 Glycyrrhizic acid (liquorice)

Alcoholic liquorice root extract (1.4 to 69 µg/mL) inactivated CYP3A4 in a time- and concentration-dependent manner. The inactivation was NADPH-dependent and not

reversible by extensive dialysis, which was also demonstrated to be correlated with the loss of the P450-reduced spectrum and the intact heme-moiety (Kent *et al*., 2002:709). Liquorice root (0.5 mg/mL) also inhibited the p-glycoprotein (P-gp) in an *in vitro* ATPase assay (Satoh *et al*., 2009:2018).

Glycyrrhizic acid (GA) at a concentration of 50 μM inhibited CYP3A4-catalyzed testosterone 6-β-hydroxylation with an IC_{50} of 25.96 μM (Liu *et al*., 2011:81). Recent research has demonstrated that glycyrrhizin (100 μM) and its major metabolite GA (25 μM) increased the CYP3A4 activity by 25.5% and 30.2% individually (Hou, Lin & Chao, 2012:2307).

Glycyrrhizic acid inhibited the 4-hydroxylation of diclofenac by the CYP2C9 with an IC_{50} value of 16.21 μM; this concentration was 8-fold higher than that observed following specific inhibition with sulfaphenazole (Liu *et al*., 2011:81). Isoliquiritigenin (20 μM) inhibited the CYP2E1 activity and the mRNA expression by 75.7% and 78.7%, respectively (Zhang *et al*., 2008:293).

As the inhibitory action of p-glycoprotein was enhanced by a combination of liquorice and Kansui (*Radix euphorbiae kansui*), the inhibition of P-gp may be the mechanism that underlies the toxicity of the mixture (Sun *et al*., 2010:510). Similarly, the action of P-gp was inhibited by coadministration of liquorice and *Daphne genkwa* (Huang *et al*., 2008:2521). This phenomenon highlights the possibility of synergy when combining PDAEs.

According to the reviewed literature on the effective concentration of glycyrrhizic acid, it is clear that this absorption enhancer is extensively researched on CYP inhibition than

the P-gp inhibition. It is therefore particularly important to explore its effective inhibitory concentrations on the P-gp. The effective inhibitory concentrations of glycyrrhizic acid on the CYP enzymes falling within the ranges of the reviewed literature could also be investigated using other *in vitro* models.

2.4 COLLOIDAL NANOCARRIERS IN DRUG DELIVERY

Nanoscale drug delivery, commonly referred to as nanocarriers, are nanosized materials, which can carry multiple drugs or imaging agents (Peer *et al*., 2007:751). Colloidal nanocarriers, in their various forms, have the possibility of providing endless opportunities in drug delivery systems (Mishra, Bhavesh & Tiwari, 2010:9).

2.4.1 Advantages of colloidal nanocarriers over conventional dosage forms

Nanocarriers deliver the drug precisely and safely to its target site at the right time and deliver a controlled release and thereby insuring the maximum therapeutic effect (Mishra, Bhavesh & Tiwari, 2010:9). Nanocarriers, because of their higher ratio of surface area to volume, show improved pharmacokinetics and biodistribution of therapeutic agents and thus minimize the toxicity of drugs (Alexis *et al*., 2008:74). They improve the solubility of hydrophobic compounds and render them suitable for parenteral administration. Furthermore, they increase the stability of a variety of therapeutic agents, like peptides, oligonucleotides accumulation at the target site (Koo, Rubinstein & Onyuksel, 2005:193). They can be used to deliver the drug to the central nervous system owing to their smaller size and higher barrier permeability. Use of biodegradable materials minimizes the possibilities of hypersensitivity reactions and affords good tissue compatibility. A desirable pharmacokinetic and pharmacodynamics pattern of a drug can be delivered by the

nanocarrier by modifying the size and shape of the nanocarrier used. Delivering hydrophobic drugs is a major advantage of nanocarriers. They enhance the dose efficacy and reduce the side effects and helps in a sustained controlled and targeted delivery of a drug (Qian *et al*., 2012:5781). Phospholipids-based nanocarriers (e.g. liposomes) enhance the bioavailability of drugs with low aqueous solubility or low membrane penetration, improve or alter the uptake and release profile of drugs, protect sensitive active agents from degradation in the GIT tract, reduce side effects and mask bitter taste of drugs (Singh, Gangadharappa & Mruthunjaya, 2017:166).

2.4.2 Different types of drug delivery nano-scale dosage forms

Nanocarriers including liposomes, dendrimers, gold nanoparticles, magnetic nanoparticles, mesoporous silica, polymeric nanoparticles and polymer conjugates gains much attention for combination therapy by enhanced permeability and retention (EPR) (Oerlemans *et al*., 2010:2569; Riehemann *et al*., 2009:872).

2.4.2.1 Liposomes

Liposomes (depicted in Figure 2.6) are spherical in structure, size ranging from 20 nm to micrometre with an aqueous core and a vesicle shell. Liposomes are made of a single or multiple bilayer membrane structure containing natural or synthetic lipids, and cholesterol in various proportions to get desired texture (Pushpalatha, Selvamuthukumar & Kilimozhi, 2017:273-274).

2.4.2.2 Dendrimers

Dendrimers (shown in Figure 2.7) are highly branched globular macromolecules

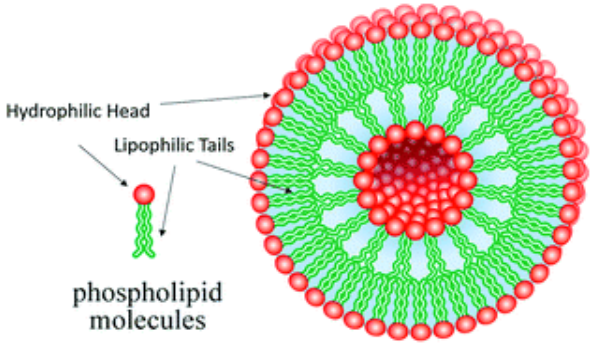

FIGURE 2.6: Liposome structure (Hwang, Li & Loh, 2016:70593)

structured by an initiator core, layers of branched repeating units and functional end groups on the outermost layer. Dendrimers are one of the most favourable delivery systems to carry both water-soluble and insoluble drugs in a single platform (Pushpalatha, Selvamuthukumar & Kilimozhi, 2017:365). Michlewska et al. 2018 studied the delivery of ruthenium dendrimers into cancer cells and their study reported the ability of dendrimers to deliver small interfering ribonucleic acid (siRNA) as non-viral vectors into the cancer cells as well as the ability to protect siRNA against nuclease degradation.

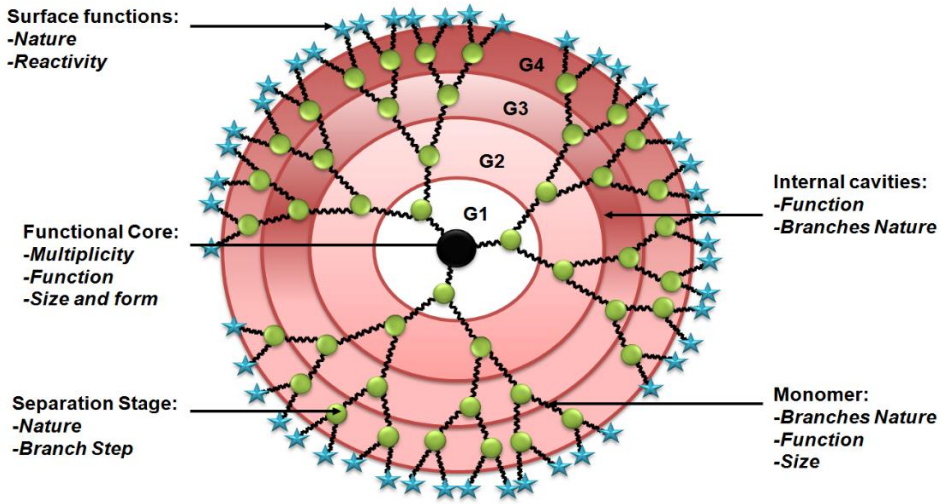

FIGURE 2.7: Dendrimer structure (Nanotransmed, 2019)

2.4.2.3 Gold nanoparticles

Nanoparticles (portrayed in Figure 2.8) are submicron particles (size less than 1000 nm) with a high surface area that facilitates the interaction and cellular uptake by biological membranes (Dias *et al*., 2018:1107). Some features of gold nanoparticles that have attracted interest among researchers in different fields of science include: high X-ray absorption coefficient, ease of synthetic manipulation, enabling precise control over the particle's physicochemical properties, strong binding affinity to thiols, disulfides and amines, unique tunable optical and distinct electronic properties (Elahi, Kamali, & Baghersad, 2018:537). The potential applications of gold nanoparticles (AuNPs) include their usage in catalysis, as antimicrobials, as anti-cancers, in drug delivery, and agriculture (Mythili *et al*., 2018:318). In addition, Lin et al. (2018:49) used DNA-modified gold nanoparticles to develop colorimetric detection for reactive oxygen species (e.g. hydrogen peroxide). The AuNPs can be easily synthesized and have high chemical and thermal stability (Noruzi, 2015:1). The green vegetable waste synthesized AuNPs showed antibacterial activity against clinical pathogens (Mythili *et al*., 2018:318). Halder et al. (2018:413) studied the antiviral efficacy of gallic acid stabilized highly mono-dispersed gold nanoparticles (GAunps) against HSV infections in Vero cells, whereby GAunps were effective in a dose-dependent manner with EC_{50} of 32.3 µM in HSV-1 and 38.6 µM in HSV-2. HER2-targeted gold nanoparticles (T-AuNPs) showed stronger cytotoxic effects than controls against trastuzumab-resistant (MKN7) and trastuzumab-sensitive (NCI-N87) cells (Kubota *et al*., 2018:1919).

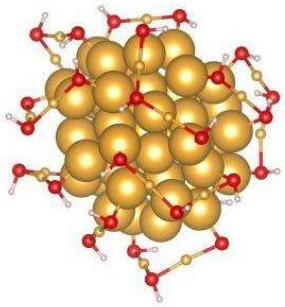

FIGURE 2.8: Atomic structure of gold nanoparticles (University of Nebraska-Lincoln, 2015)

2.4.2.4 Magnetic nanoparticles

Magnetic nanoparticles (represented in Figure 2.9) typically consist of a magnetic core, a coating and, in some cases, a layer with biomarkers or antibodies (Baker, 2018:197). Baker (2018:197) also reported the use of magnetic nanoparticles for a variety of biomedical applications such as: conjugation with antibodies and injected intravenously for diagnostic purposes; used as contrast agents in techniques such as magnetic resonance imaging; delivery of drugs via intravenous or local injection with or without conjugated antibodies that can be released over time or all at once; for magnetic hyperthermia; can be incorporated into silica shells or liposomes in order to enable *in situ* enzyme-linked immunosorbent assay (ELIZA) measurements and can be used to sort *ex vivo* rare, magnetically labelled cells from a heterogeneous mixture of cells in blood samples.

2.4.2.5 Mesoporous silica

Mesoporous silica nanoparticles (MSNs) (structure depicted in Figure 2.10) and hollow

mesoporous silica nanoparticles (HMSN) can be synthesized from iron silicate via selective etching of iron oxide (Adhikari *et al*, 2018:303).

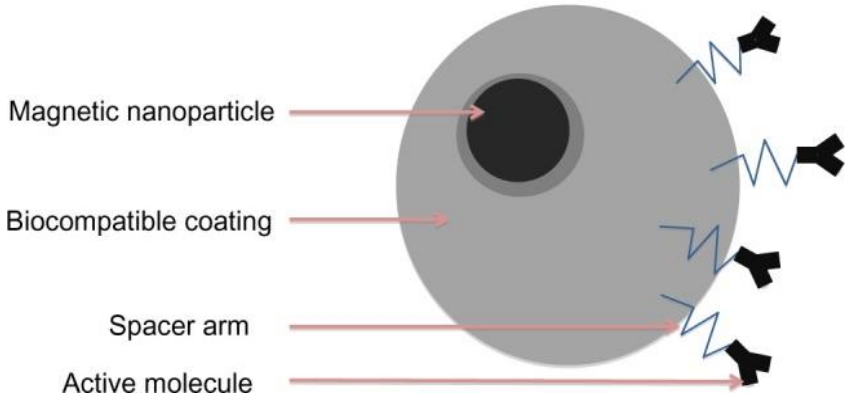

FIGURE 2.9: Magnetic nanoparticle structure (Bull *et al*., 2014:1643)

MSNs possess the following advantages: increased surface area and pore volume, selective surface functionality, as well as morphology control, MSNs exhibit high loading capacity for therapeutic agents and controlled release properties if modified with stimuli-responsive groups, polymers or proteins (Zhou *et al*., 2018:165). Oliveira et al. (2018:62) reported the suitability of MSNs for drug delivery systems, notably, the delivery of photo-initiator camphorquinone and the anaesthetic ethyl 4-aminobenzoate. Activated biocompatible hydrogel nanocomposites containing mesoporous silica was shown to be a determinant factor in inhibiting initial burst by nearly 90% and the drug was released with minimal burst kinetics, thus making this nanomaterial suitable for controlled release (i.e. sustained-release) of a drug. This system was also biocompatible with human immortalized RWPE-1 prostatic epithelial cells (de Lima *et al*., 2018:126).

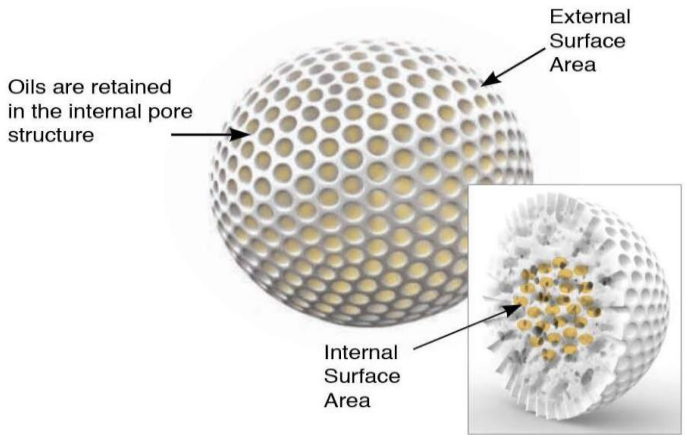

FIGURE 2.10: Mesoporous silica structure (Pharma Excipients, 2019)

2.4.2.6 Polymeric nanoparticles

The water-dispersible conjugated polymeric nanoparticles (WDCPNs) (structure represented in Figure 2.11) exhibited bright fluorescence in cellular imaging and showed good biocompatibility demonstrating them as ideal fluorescent probes for biological imaging and detection (Wang *et al*., 2018:1). Imiquimod-loaded polymeric nanoparticles showed an antiangiogenic activity in chicken embryo chorioallantoic membrane (CAM) and some chemo-preventive potential in multistage DMBA and croton oil model of skin carcinogenesis in mice. Their antiangiogenic activity and antitumoral activity were superior to the negative control, placebo dispersion and market imiquimod (Dias *et al*., 2018:1107).

2.4.2.7 Polymeric micelles

A novel three-dimensional macroporous hydroxyapatite/chitosan foam (HA/CS)-supported polymer micelle enhanced the solubility and bioavailability of a poorly soluble drug (Zhang *et al*., 2018:497).

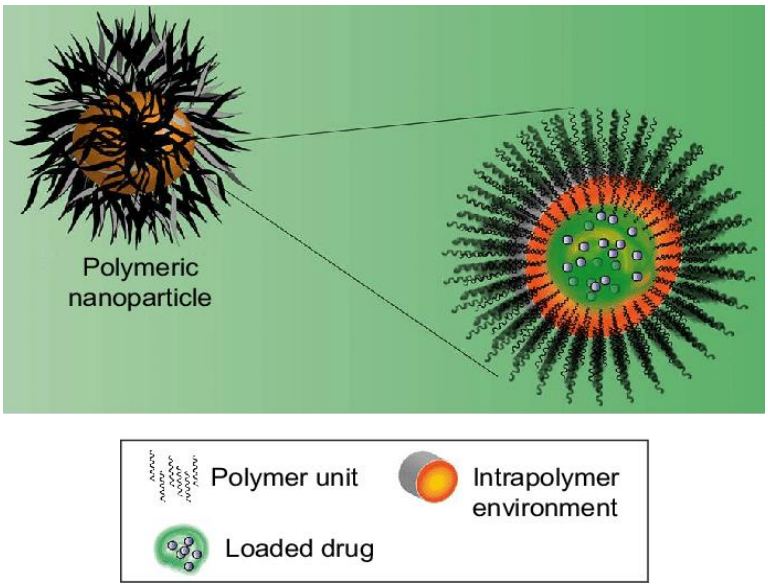

FIGURE 2.11: Polymeric nanoparticle structure (Ramos *et al*., 2018:1199)

The doxorubicin-loaded polymeric micelles killed about 80% of the tumour cells after 48 hours incubation and this indicates their potential to deliver anticancer drugs in a controlled release manner (Chen *et al*., 2018:1). Polymeric micelles made from hydrophobized hyaluronic acid (HA) compared to non-polymeric micelle solutions containing similar drug amount indicated three times larger deposition of drug in the epidermis and six times larger drug deposition in the dermis after 5 hours of topical treatment in Franz diffusion cells, indicating the potential of polymeric micelles as suitable nanomaterial for the topical drug delivery (Smejkalova *et al*., 2017:86). The schematic structure of the polymeric micelle is shown in Figure 2.12.

2.4.2.8 Polymersomes

Animal experiment results showed that the antigen-specific prophylactic vaccination by PEDP polymersomes delivery was much more rapid and efficient in depressing tumour

growth and progress when compared with the therapeutic vaccination (Gao *et al*., 2018:1609).

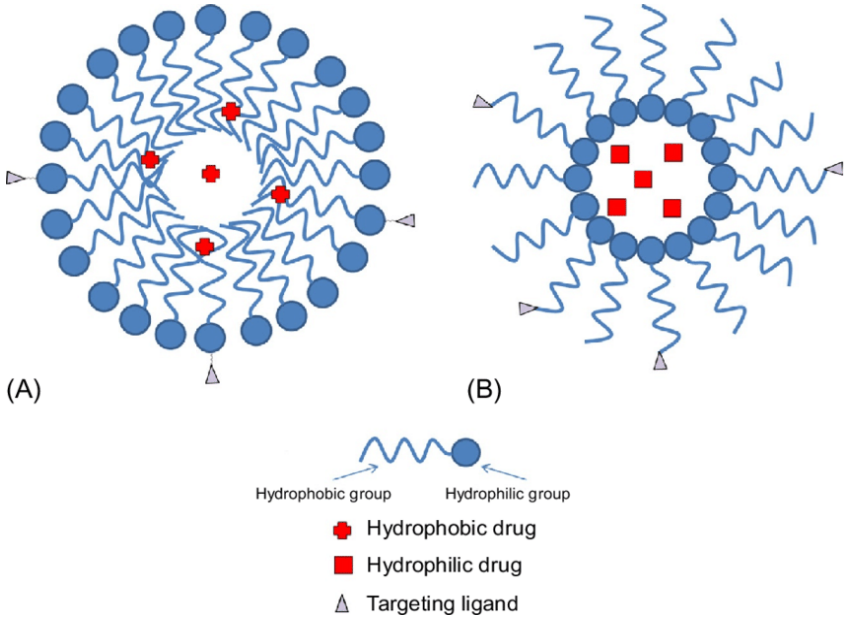

FIGURE 2.12: Schematic structure of polymeric micelle (Garcia *et al*., 2017:51)

Empty polymersomes were non-toxic and were quickly and more efficiently internalised by melanoma cells compared to healthy cells, in addition, PMPC25-PDPA70 polymersomes encapsulated doxorubicin for long periods of time without significant drug release (Pegoraro *et al*., 2013:328). Drug-loaded polymersomes exhibited enhanced drug penetration and thus improved cytotoxic potential against MCF-7 cancer cell line and were highly hemo-compatible (Curcio *et al*., 2018:568). The structure of the polymersome is illustrated in Figure 2.13.

2.4.2.9 Nanosponges

Nanosponge (structure shown in Figure 2.14) carrier enhanced the solubility of poorly

water-soluble drugs (Pushpalatha, Selvamuthukumar & Kilimozhi, 2018:45; Gangadharappa, Prasad & Singh, 2017:488).

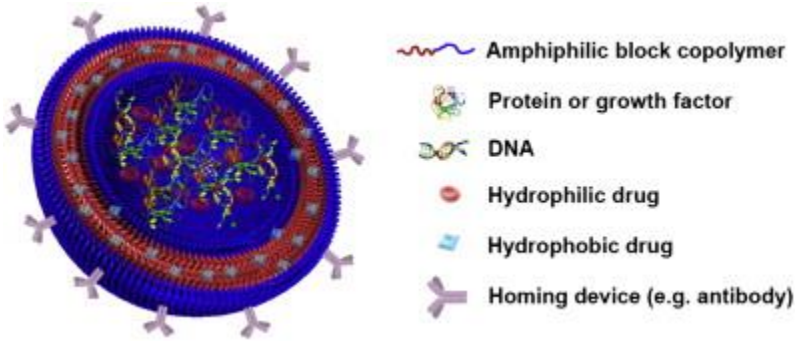

FIGURE 2.13: Schematic structure of polymersome (Lee & Feijen, 2012:474)

In vitro studies demonstrated pH-dependent slow and prolonged release kinetics of the drug from the nanosponges (Caldera *et al*., 2018:111). Norfloxacin-loaded nanosponges exhibited higher *in vitro* permeation of norfloxacin in comparison to norfloxacin drug alone and revealed a mucoadhesive property that could increase norfloxacin absorption thus improving its antibiotic activity in an *in vivo* sepsis model (Mendes *et al*., 2018:586).

A dual drug nanosponge of tamoxifen and quercetin reduced the metabolism of tamoxifen by 2 to 3-fold and that of quercetin by 3 to 4-fold (Lockhart *et al*., 2015:751). The *in vitro* drug release of cyclosporin based nanosponges exhibited a burst release for the first 4 hours then delivered a drug in a sustained manner for subsequent 24 hours. These nanosponges also enhanced the oral bioavailability of nifedipine in comparison to control formulation (Shringirishi *et al*., 2017:344).

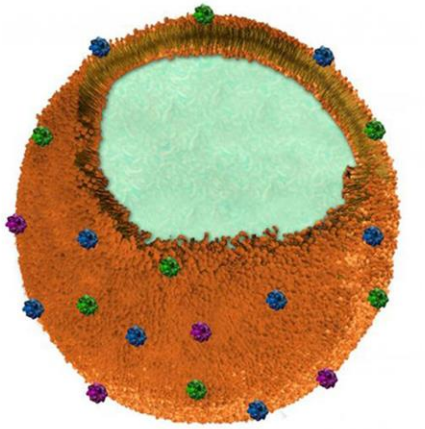

FIGURE 2.14: Nanosponge structure (Souppouris, 2013)

2.5 ANTI-HIV AND ANTIMALARIAL NANOMEDICINES APPROVED BY THE FDA AND UNDER CLINICAL TRIALS

Liposomes are the first nano-drug delivery systems that have been successfully translated into real-time clinical applications. The significant contribution of liposomes as drug delivery systems in the healthcare sector is known by many clinical products, e.g. Doxil®, Ambisome®, and DepoDur™ (Bulbake *et al*., 2017:1), of which Doxil® was the first FDA-approved nano-drug (Barenholz, 2012:117). About 51 FDA-approved nanomedicines and 77 products in clinical trials were identified, with approximately 40% of trials listed in clinicaltrials.gov started in 2014 or 2015 (Bobo *et al*., 2016:2373).

ClinicalTrials.gov listed the following anti-HIV nanoformulations as completed: MK-1439 100 mg film-coated tablet, MK-1439 150 mg tablet (40% drug loaded granule), MK-1439 150 mg tablet (30% drug loaded granule), MK-1439 150 mg tablet (50% drug loaded granule), MK-1439 100 mg tablet (30% drug loaded granule). The other listed nanoformulation, which the status of their clinical trials had been suspended include nano-

efavirenz 50 mg, nano-lopinavir 400 mg, nano-lopinavir 200mg, ritonavir 100 mg, nano-efavirenz 300 mg, sustiva 600 mg, nano-efavirenz 200 mg, kaletra® (lopinavir 400mg/ritonavir 100mg), nano-lopinavir 200 mg, ritonavir NORVIR, 200 mg and sustiva 400 mg. There were no antimalarial nanoformulations listed in ClinicalTrials.gov website.

2.6 PHOSPHOLIPIDS FOR LIPOSOMES PREPARATION

Phospholipids are amphiphilic lipids consisting of a glycerol backbone or an amino-alcohol sphingosine backbone, which is esterified to one or two fatty acids, a phosphate group and a hydrophilic residue (Zhou & Rakariyatham, 2018). Phospholipids (main component of cellular membrane) have the exceptional biocompatibility and remarkable amphiphilicity characteristics (i.e. self-assembly, which generates different super-molecular structures, when it mixes with aqueous media, which are dependent on their specific properties and conditions) that make phospholipids the major and suitable agent or excipient for the formulation and to achieve better therapeutic applications in drug delivery system (Singh, Gangadharappa & Mruthunjaya, 2017:166). Furthermore, phospholipids have the following characteristics:

- *Excellent biocompatibility*: Phospholipids are compatible with drug or phyto-compound, which can be employed as the drug carriers (Cullis & De Kruijff, 1979:399).

- *Emulsifying*: Phospholipids have a good emulsifying property, which can stabilize the emulsions (Yang *et al*., 2013:434).

- *Wetting characteristics*: As surface-active wetting agents, phospholipids can enhance

the hydrophilicity of hydrophobic drugs through the surface coat of crystals (Li *et al*., 2015:82).

2.6.1 Structures of phospholipids for liposomes preparation

Phospholipid molecules consist of two hydrophobic fatty acids “tails” and a hydrophilic phosphate “head”, joined together by an alcohol or glycerol molecule. Phospholipids are divided into two classes, depending on whether the alcohol backbone is glycerol (glycerophospholipids), or sphingosine (sphingophospholipids) (Engelking, 2015; Singh, Gangadharappa & Mruthunjaya, 2017:166).

2.6.1.1 Glycerophospholipids

Glycerophospholipids are the most abundant phospholipids. They are found in highest amounts in the membranes of all cells and are present in very small quantities in fat stores and are a source of physiologically active compounds (Blanco & Blanco, 2017:99).

According to Pollard et al. (2017:227-239), the alcohol head groups give phosphoglycerides their names as follows:

- Phosphatidic acid [PA] (no head group);
- Phosphatidylglycerol [PG] (glycerol head group);
- Phosphatidylethanolamine [PE] (ethanolamine head group);
- Phosphatidylcholine [PC] (choline head group);
- Phosphatidylserine [PS] (serine head group);

- Phosphatidylinositol [PI] (inositol head group).

Zhou and Rakariyatham (2018:1) illustrated the structure of different glycerophospholipids in Figure 2.15 below. Where the letter X signifies different alcohol head groups.

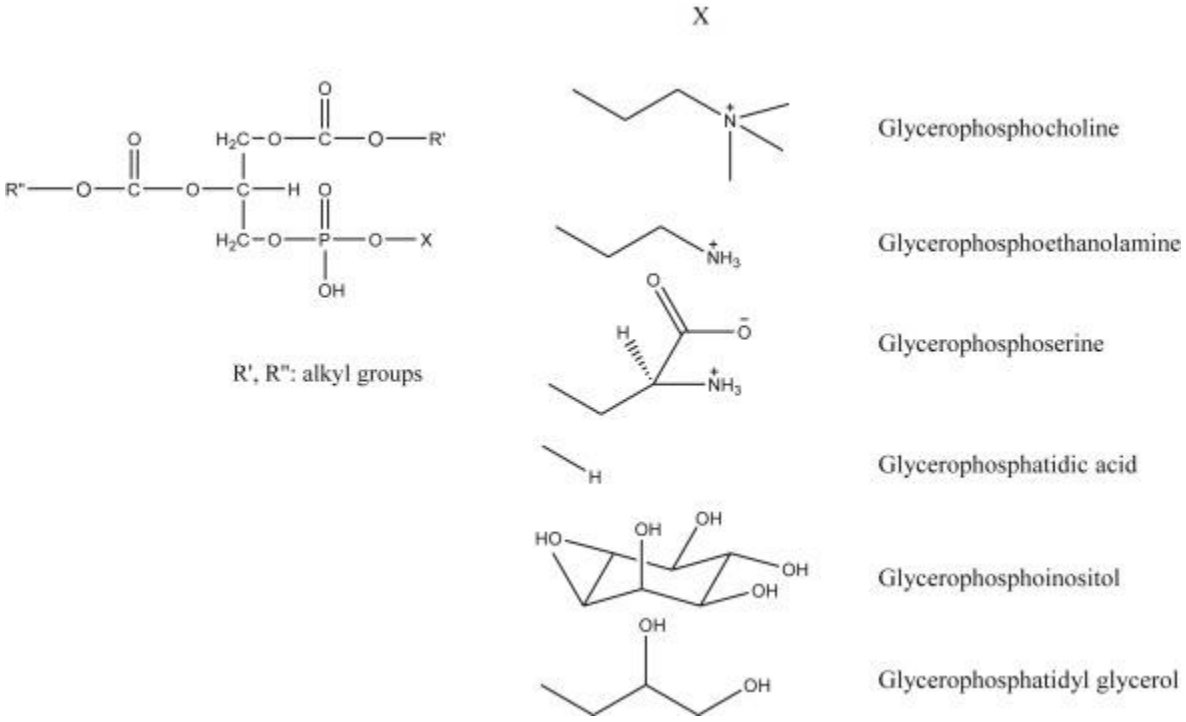

FIGURE 2.15: Chemical structures of different glycerophospholipids (Zhou and Rakariyatham, 2018:1)

2.6.1.2 Sphingophospholids

Sphingolipids are some of major lipid components of eukaryotic biomembranes, like the plasma membrane, and are involved in several physiological functions such as cell adhesion, signalling, immunity, skin barrier formation, neural functions, and glucose metabolism (Holthuis *et al*., 2001:1689; Mizutani *et al*., 2009:784; Pontier & Schweisguth,

2012:92; Hla & Dannenberg, 2012:420; Mitsutake & Igarashi, 2013:271). Sphingolipids comprise a polar head group and a hydrophobic backbone called ceramide. The polar head group of mammalian sphingolipids is either phosphocholine (sphingomyelin (SM)) or a sugar chain (glycosphingolipids) (Holthuis *et al*., 2001:1689).

2.6.2 Sources of phospholipids

The sources of phospholipids can be categorized as natural or synthetic based on the variation in their chemical structure. Examples of natural phospholipids include soybean phosphatidylcholine, egg phosphatidylcholine, whereas synthetic phospholipids include synthetic phosphatidylcholine, hydrogenated phosphatidylcholine (Singh, Gangadharappa & Mruthunjaya, 2017:166-167). Natural phospholipids are isolated from natural sources such as soybeans, rape (canola) seed, wheat germ, sunflower, flaxseed, and animal material, like egg yolk, milk, or krill using non-toxic solvent extraction and chromatographic procedures with low consumption of energy and minimum possible waste, whereas synthetic phospholipids with specific polar head group and fatty acid composition can be manufactured using various synthesis routes (Van Hoogevest & Wendel, 2014:1088).

2.7 CHARACTERISATION OF LIPOSOMES

2.7.1 Particle size and zeta potential

Zeta potential is a scientific term for electrokinetic potential in colloidal systems, which has a major effect on various properties of nano-drug delivery systems (Honary & Zahir, 2013:255). Wang et al. (2018:736) formulated mesoporous silica nanoparticles (MSN)

with size ranging from 100 to 500 nm and conjugated them with polyethylenimine-coated carbon dots (PCD) and coated them with polyethylene glycol (PEG) to study the influence of particle size and surface chemistry on transepithelial transport and bioavailability. Their findings revealed that MSN with a diameter of 250 nm had the highest transepithelial transport and oral bioavailability compared to other formulations. Physicochemical properties, such as particle size, shape and surface charge, play a key role in the cellular uptake of nanoparticles. The uptake of nanoparticles by cells is a two-step process: first, a binding step on the cell membrane and second, the internalization step (Honary & Zahir, 2013:255).

2.7.2 Entrapment efficiency

Entrapment efficiency (EE) is a crucial parameter for the evaluation of nanocarriers (Lv *et al*., 2018:395). Some possible sample pre-treatment methods that can be in liposomal entrapment efficiency study include size-exclusion chromatography (SEC), solid-phase extraction (SPE), centrifugation ultrafiltration (CF-UF) and hollow fibre centrifugal ultrafiltration (HF-CF-UF), of which CF-UF was the most effective exclusion method, followed by SEC (Ran *et al*., 2016:56). The addition of polyethylene glycol (PEG) enhanced the encapsulation efficiency of egg phosphatidylcholine (PC) and cholesterol (CH) based liposomes as compared to conventional liposomes based on the same phospholipid combinations (Panwar *et al*., 2010:101).

2.7.3 *In vitro* drug release

Drug release is assessed using a variety of methods including sample and separate (SS),

continuous flow (CF), dialysis membrane (DM) methods, and a combination these methods, as well as voltammetry and turbidimetry (D'Souza, 2014:1). Dialysis is mostly used for determining the rate of drug release from different types of liposomal dispersions and gels for both hydrophilic and hydrophobic drugs (Nounou *et al*., 2006:311). The release agent such as bovine serum could be used for the *in vitro* drug release studies because it has components that interact with liposomes to cause the encapsulated drug to be released (Cipolla *et al*., 2014:314).

2.8 CYTOTOXICITY OF LIPOSOMAL FORMULATIONS

2.8.1 Toxicity

Cytotoxicity effects of some liposomal formulations had been evaluated against three cell lines Hep-G2, HCT-116 and QG-56 by MTT assay method, where compound 3c, (IC_{50} value 6.25 µM) showed better cytotoxicity effect against three cell lines (Sahu *et al*., 2016:1342).

Compared to Doxil, the CD30-targeted Doxil showed a significantly higher binding affinity to ALCL cells (5.3% versus 27%, p=0.005) and a lower inhibitory concentration at 50% (IC_{50}) *in-vitro* (32.6 mg/mL versus 12.6 mg/mL, p=0.006). In a SCID mouse xenograft model, CD30-targeted Doxil inhibited tumour growth more significantly than the unconjugated formulation; specifically, tumours in mice treated with CD30-targeted Doxil were significantly smaller than those in mice treated with Doxil (average, 117 mm^3 versus 270 mm^3, p=0.001) at 18 days after the tumours were inoculated (Molavi *et al*., 2013:8718).

The *in vitro* cytotoxicity of docetaxel-loaded RIPL liposomes (DTX-RIPL- L) was dose-dependent with IC_{50} values of 36.10 ng/mL (SK-OV-3 cells) and 48.62 ng/mL (MCF-7 cells) for hepsin-positive, and 61.12 ng/mL (DU145 cells) and 53.04 ng/mL (PC-3 cells) for hepsin-negative cell lines. Live or dead cell imaging was further carried out to visualize the proportion of viable and non-viable SK-OV-3 cells. Compared to DTX solution, DTX-RIPL-L inhibited tumour growth more (Yoon *et al*., 2017:229).

DKD/paclitaxel liposomes (DKD/PTX-Lips) promoted the death of A549 cell at lower pH. The DKD/PTX-Lips were more cytotoxic than Taxol and SPC/PTX-Lips to A549/Taxol cells. IC_{50} of DKD/PTX-Lips in A549/Taxol cells was 20-fold lower than that of Taxol under the same pH condition. Thus, DKD/PTX-Lips have the greatest inhibitory effects against A549 and A549/Taxol cell growth compared to Taxol and traditional PTX liposomes, especially at pH 6.8 (Jiang *et al*., 2015:134-135).

Duopafei®, docetaxel loaded liposomes (DTX-PSL) and RGD(Arg-Gly-Asp)/DTX-PSL, decreased viability of MCF-7 cells from 83.2% to 17.6%, from 85.0% to 11.1%, and from 77.9% to 7.9%, respectively. Furthermore, RGD/DTX-PSL demonstrated stronger antiproliferative effects than Duopafei® and DTX-PSL (Zuo *et al*., 2016:96-97).

The *in vitro* antitumor activity of DTX solution (DTX-sol), DTX-PLPs and DTX/RGD-PLPs against cancer cells after 24 hours of incubation caused a decrease in the viabilities of the MCF-7, HepG2 and A549 cells with all loaded liposomes and free DTX in a DTX concentration-dependent manner. However, the IC_{50} values of DTX-loaded liposomes were significantly ($p < 0.05$) lower than that of DTX solution (Chang *et al*., 2015:180).

The RIPL peptides (IPLVVPLRRRRRRRRC; 16mer; 2.1 kDa) and RIPL peptide-

conjugated liposomes (RIPL-LPs) were cytotoxic in human prostate cancer cells (LNCaP) and human keratinocyte cells (HaCaT) in a concentration-dependent manner. For example, a 50 μM concentration of RIPL peptide exhibited minor toxicity (cell viability >90%) in both cells, but cell viability decreased to less than 70% at concentrations above 100 μM for LNCaP and 500 μM for HaCaT cells (Kang *et al*., 2014:495-496).

When the *in vitro* antitumor effects of ursolic acid (UA) solution, UA formulated in the conventional and the PEG-modified liposomes were compared at the equivalent drug concentration on EC-304 cancer cells after 24 hours incubation, UA solution had the poor effect leading to a minimum inhibition rate of 57% at 250 μg/mL. The cell inhibitory rate of conventional liposomes (without PEG) was higher than that of PEG-modified liposome. The EC-304 cells treated with conventional liposomes and PEG-modified liposomes exhibited up to 71.26% and 68.27% cell inhibitory rates at 250 μg/mL, respectively (Zhao *et al*., 2015:201).

The anti-proliferative effects of various UA suspensions on HeLa cells were determined by MTT assay. All the UA formulations could induce tumour cell death in a dose-dependent manner. A 125 μg/mL volume of UA solution had the worst effect leading to a minimum inhibition rate of 55.14%, whereas, at the same UA concentration, HeLa cells treated with ursolic acid liposomes (UA-L) and chitosan-coated ursolic acid liposome (CS-UA-L) exhibited up to 69.51% and 76.46% cell inhibitory rates respectively. According to these results, it was clear that the anti-tumour effect of UA was improved by entrapping in liposomes. Notably, modifying chitosan on the surface of liposomes further enhanced the antitumor effect of UA (Wang *et al*., 2017:1237).

The cytotoxic effect of SPION@APTES@FA-PEG nano-drug was investigated on A549 (FR-) and MCF-7, HeLa (FR+) cancer cell lines. Cells were exposed to nanoparticles for 48 hours at 37 ºC. The cytotoxic effects of SPION@APTES@FA-PEG@CQ nano-drug (10 - 200 µg/mL) on HeLa, MCF-7 and A549 cell lines were studied. The 10, 50, 100 and 200 µg/mL concentrations of SPION@APTES@FA-PEG@CQ nano-drug had lower cell viability on A549 cells compared with HeLa and MCF-7 cells at 24th and 48th hours (Akal, Alpsoy & Baykalc, 2016:579).

Singh et al. (2018:241) incubated cells in different concentrations (50 µg/mL and 100 µg/mL) of compounds for 12 hours in peripheral blood mononuclear cells (PBMCs) and macrophage cancer cell lines (J774) were incubated for 24 hours. There was no sign of cell death in case of PBMCs whereas in macrophage cancer cell line cell death increased in a concentration-dependent manner with drug-loaded ChGCQ i.e. Cu-ChGCQ showing more cell death (Singh *et al*., 2018:241).

According to the reviewed reports on the toxicity of liposomal formulations, the free form of the test compounds is not as effective as when they are formulated as liposomal formulations or in any other forms of nanocarriers. Although most liposomal formulations are effective towards cancer treatment, the contribution of the liposomal platform itself is of interest and forms a basis, from which such platforms may be used with other drugs when cytotoxic effects are not desired.

2.8.2 Biocompatibility

Liposomes have been widely accepted in many scientific disciplines because of their versatility and biocompatibility (Mallick & Choi, 2014:755). The PEG-modified liposomes

demonstrated the biocompatibility in an *ex vivo* model of haemolysis in human erythrocytes indicating the suitability of liposomes in this model (Caddeo *et al*., 2018:40). Polymeric liposomes, on the other hand, are biocompatible and conductive kind of liposomes (Tian *et al*., 2016:41). Treatment with the blank liposomes caused negligible toxicity in the MCF-7 cells (>89% survival rate), indicating the good biocompatibility and safety of the vectors (Zuo *et al*., 2016:96-97).

The cytotoxicity of a series of synthesized histidine-rich (RH) cell-penetrating peptides (CPPs) toward HepG2 and A549 cells were evaluated by using MTT assay. The cell viabilities of all the RH CPPs with the different concentrations (i.e. 10 and 50 μM), except R9H3 with the concentration of 100 μM, were higher than 80% in HepG2 and A549 cells indicating no significant cytotoxicity of RH CPPs toward both cell lines (Jiang *et al*., 2012:9249-9250).

The 5, 20, 50 and 100 μg/mL concentrations of pure MCM-41, MCM-41 nanoparticles functionalized with CREKA (MCM-41-APTES-mal-DTPA-CREKA) and of those complexed with copper (MCM-41-APTES-mal-DTPA-CREKA-Cu) showed similar profiles of cell viability of the MRC-5 fibroblast cells in relation to pure MCM-41. The three samples presented less or no cytotoxicity against the fibroblast strain up to a concentration of 100 μg/mL indicating the biocompatibility potential on live cells (Freitas *et al*., 2017:280-281).

Cytotoxicity of blank 1,2-distearoyl-sn-glycero-3-phosphoethanolamine (DSPE)- peptide $_{D}$[KLAKLAK]$_{2}$ (KLA)- 2,3-dimethylmaleic anhydride (DMA) (DSPE-KLA-DMA)/(DKD) liposomes against NIH 3T3 cells with various lipid concentrations was evaluated at pH 7.4 and 6.8 by the cell counting kit-8 (CCK-8) assay. Blank DSPE-KLA-DMA (DKD)

liposomes (DKD-Lips) were nontoxic even at high lipid concentrations at either pH, so DKD-Lips may be a safe drug delivery carrier (Jiang *et al*., 2015:134-135).

When haemolysis potential of both free ursolic acid (UA) and the UA-loaded poly-lactic acid (PLA) nanoparticles was assessed as a function of time and UA concentration, the results revealed more haemolysis of erythrocytes with free UA than UA-loaded PLA nanoparticle, indicating the biocompatibility and protective potential of the nanocarriers (Antônio *et al*., 2017:162). Similarly, the cytotoxic activity evaluation of free and nano-encapsulated UA over B16-F10 cells (murine melanoma) was evaluated and the results showed that the UA-loaded nanoparticles presented a cytotoxic profile concentration- and time-dependent, but due to prolonged drug release, the cytotoxicity was less expressive ($p=0.05$). Blank nanoparticles showed no cytotoxicity in B16-F10 cells (Antônio *et al*., 2017:162).

The MTT assay evaluation of the cytotoxicities of blank pH-sensitive liposomes (PLPs) and blank arginine-glycine-aspartic acid peptide modified liposomes (RGD-PLPs) indicated small cell death with blank liposomes in MCF-7, HepG2 and A549 cells even up to the highest dose of 3000 µg/mL. All cell viabilities were greater than 75% after incubating blank liposomes for 24 hours, indicating that liposomes had good biocompatibility and low toxicity (Chang *et al*., 2015:180).

2.9 EFAVIRENZ AS A MODEL ANTI-HIV DRUG

Efavirenz (also known and branded as Sustiva®) is a human immunodeficiency virus type 1 (HIV-1) specific, non-nucleoside, reverse transcriptase inhibitor (NNRTI). Efavirenz is chemically described as (S)-6-chloro-4-(cyclopropylethynyl)-1,4-dihydro-4-

(trifluoromethyl)-2H-3,1-benzoxazin-2-one. Its empirical formula is $C_{14}H_9ClF_3NO_2$ and its structural formula is shown in Figure 2.16. Efavirenz is a white to slightly pink crystalline powder with a molecular mass of 315.68. It is practically insoluble in water (< 10 µg/mL) (Bristol-Myers Squibb, 2005).

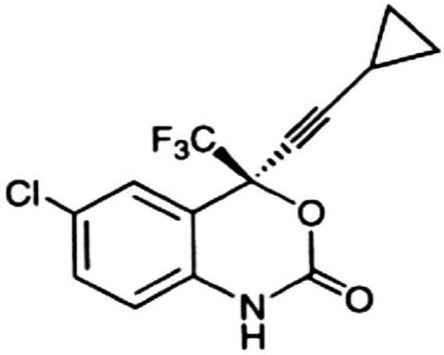

FIGURE 2.16: Chemical structure of efavirenz (Madhusudhan *et al*., 2012:85)

Incubation of Hep3B cells with 25 µM EFV for only 8 h significantly modified the expression of several genes involved in drug metabolism: up-regulation was observed with cytochrome P450, family 1, subfamily A, polypeptide 1 (CYP1A1), which indicated metabolic stress. Several genes directly related to oxidative stress and damage exhibited increased expression, including methalothionein 2A (MT2A), heat shock 70 kDa protein 6 (HSPA6), growth differentiation factor 15 (GDF15) and DNA-damage-inducible transcript 3 (DDIT3) (Gomez-Sucerquia *et al*., 2012:232). The *in vitro* EC_{50} of the EFV in the BxPC-3 pancreatic cancer cells was 31.5 µM/L (= 9944 ng/mL) (Hecht *et al*., 2015:1).

2.10 MEFLOQUINE AS A MODEL ANTIMALARIAL DRUG

Mefloquine (also known as mefloquine hydrochloride) is an antimalarial agent. It is a 4-quinolinemethanol derivative with the specific chemical name of (R*,S*)-(±)-α-2-

piperidinyl-2,8-bis (trifluoromethyl)-4-quinolinemethanol hydrochloride. It is a 2-aryl substituted chemical structural analogue of quinine. The drug is a white to almost white crystalline compound, slightly soluble in water. Mefloquine hydrochloride has a calculated molecular weight of 414.78 and the following structural formula (Figure 2.17) (Roche, 2008):

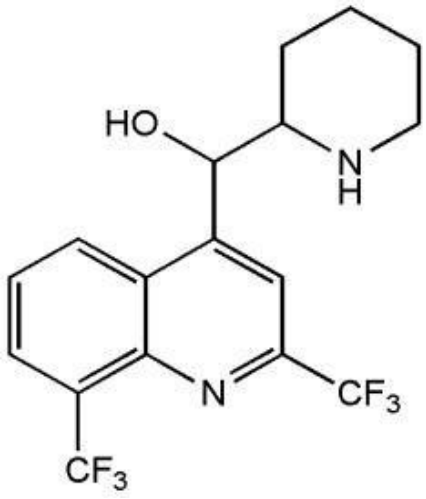

FIGURE 2.17: Chemical structure of mefloquine (Osonwa *et al*., 2017:249)

A high dose of mefloquine (MQ) (40 mg/mL) resulted in a decreased mitotic index. Furthermore, the results obtained from the spermatocyte diakinesis-metaphase 1 test and sperm abnormalities suggest that MQ may contribute to a high incidence of birth defects and congenital abnormalities (El-Habit & Al-Khamash, 2012:277).

The effect of MQ on autophagy in neuroblastoma cells was investigated and the results revealed that MQ treatment highly induced the formation of autophagosomes and the conversion of LC3I protein into LC3II protein. Moreover, MQ-induced autophagy was

efficiently suppressed by an autophagy inhibitor and by downregulation of ATG6 (Shin *et al*., 2012:162).

2.11 CONCLUSION

Studies identify several PDAEs as promising therapies for future drug development. Most of these PDAEs act through inhibition of both the P-gp and the CYP450 enzymes, which forms the basis of this study. From the reviewed literature, it is evident that inhibiting either the P-gp or CYP450 enzymes or both, can indeed improve the absorption of many drugs. However, the effective concentrations of these PDAEs remain an important factor that needs to be considered for the proper design of dosage forms. Different studies reported different concentrations as effective, and it is important to work within those ranges for future research. There are several colloidal nanocarriers, which are extensively researched and the choice of one nanocarrier over others should be based on merits and its compatibility with the active pharmaceutical ingredient. In nanomedicine, the particle size of the formulation, it's surface charge, the loading efficiency, drug release, and its biocompatibility with the living cells are some of the important aspects of an effective therapy. In the next chapter, the PDAEs that act through the inhibition of either the P-gp or the CYP450 enzymes or both were identified and selected. The selected PDAEs were further screened for their *in vitro* and *ex vivo* effective concentrations.

CHAPTER 3

MANUSCRIPT 1

IDENTIFICATION AND SELECTION OF PLANT-DERIVED ABSORPTION ENHANCERS AND SCREENING OF THEIR EFFECTIVE CONCENTRATIONS

3.1 INTRODUCTION

The effective concentration of the pharmaceutically active ingredient is an important aspect in the formulation of drugs and therefore needs to be quantified. This is so important because any concentration above therapeutic levels can pose a toxic effect to the body whereas less concentrations can be sub-therapeutic. The same is true for the PDAEs. This chapter identified and explored different concentrations of PDAEs *in vitro*, to determine the lowest effective concentrations of each PDAEs. Table 3.1 lists different PDAEs that according to past research had either an inhibitory or enhancing activity or are substrates for the CYP450 enzymes and the P-gp.

The selection criteria for PDAEs investigated in this study was based on their activity on either the CYP450 enzymes or the P-gp or both. According to the review written by Tatiraju et al. (2013:57), the following PDAEs are the inhibitors of either the CYP450 enzymes or the P-gp and were therefore selected and screened for their effective concentrations *in vitro*: quercetin, curcumin, naringin, sinomenine, piperine, glycyrrhizin.

Both the recombinant human p-glycoprotein and the recombinant human cytochrome P450 3A4 enzyme *in vitro* models were utilized in this study. P-gp, also known as MDR1 and ABCB1, is a 170kDa integral plasma membrane protein that functions as an ATP-

TABLE 3.1: Plant-derived absorption enhancers that act on the cytochrome P450 and/or p-glycoprotein

Plant-derived absorption enhancer	**Sources**	**CYP450/P-gp inhibitor/enhancer/substrate**	**References**
Quercetin	Citrus fruits	P-gp and CYP3A4 inhibitor	Scambia *et al*., 1994:460; Vijayakumar *et al*., 2015:4537.
Curcumin	*Curcuma longa*	P-gp and CYP3A inhibitor	Ganta, Devalapally & Amiji, 2010:4630; Appiah-Opong *et al*., 2007:83.
Sinomenine	*Sinomenium acutum thumb* (Orient vine stem)	P-gp inhibitor	Chan *et al*., 2006:425.
Naringin	Citrus paradise (Grapefruit)	P-gp, CYP3A1 and CYP3A2 inhibitor	Zhang *et al*., 2000:351; Lim & Choi, 2006:443.
Glycyrrhizic acid	*Glycyrrhiza glabra L.*	CYP3A4 inhibitor	Lv *et al*., 2016:1.
Genistein	Soy, Genista tinctorial, lupin, fava beans, soybeans, coffee	P-gp inhibitor	Sparreboom *et al*., 1997:2031; Doyle & Ross, 2003:7340; Huisman *et al*., 2005:824.
Piperine	Black pepper (*Piper nigrum)*	P-gp and CYP3A4 inhibitor	Bhardwaj *et al*., 2002:642.
Luteolin	*Cuminum cyminum linn*	P-gp inhibitor	Boumendjel *et al*., 2002:512.

dependent drug efflux pump and plays an important role in multi-drug resistance and certain adverse drug-drug interactions. Compounds that interact with P-gp can be identified as stimulators or inhibitors of its ATPase activity. Compounds that are substrates for transport by P-gp typically stimulate its ATPase activity (Ambudkar *et al*., 1999:361). The Pgp-Glo assay relies on the ATP-dependence of the light-generating reaction of firefly luciferase. After a pool of ATP is first exposed to the P-gp ATPase, ATP consumption is detected as a decrease in luminescence from a second reaction with recombinant firefly luciferase (Promega, 2015:2). For example, if a test compound is a P-gp inhibitor it means the ATP will not be used up thereby an increase in luminescence, but the luminescence will decrease if the test compound is a P-gp substrate or enhancer. The recombinant human p-glycoprotein model simulated the efflux of drugs back into the lumen following their absorption into the mesenteric blood vessels located on the basolateral region of the lumen thereby affecting the bioavailability of such drugs. The Pgp-Glo assay system and its mechanism of operation are illustrated in Figure 3.1.

The recombinant human cytochrome P450 3A4 enzyme model simulated pre-systemic metabolism of drugs both in the lumen and in the liver. Inhibiting both the CYP450 enzymes and the P-gp could enhance the absorption and thus the bioavailability of drugs, which are the substrates for these proteins. The current study, therefore, sought to investigate the minimum quantities of the PDAEs that could inhibit both the CYP450 enzymes and the P-gp. The P450-Glo Assay System is illustrated in Figure 3.2.

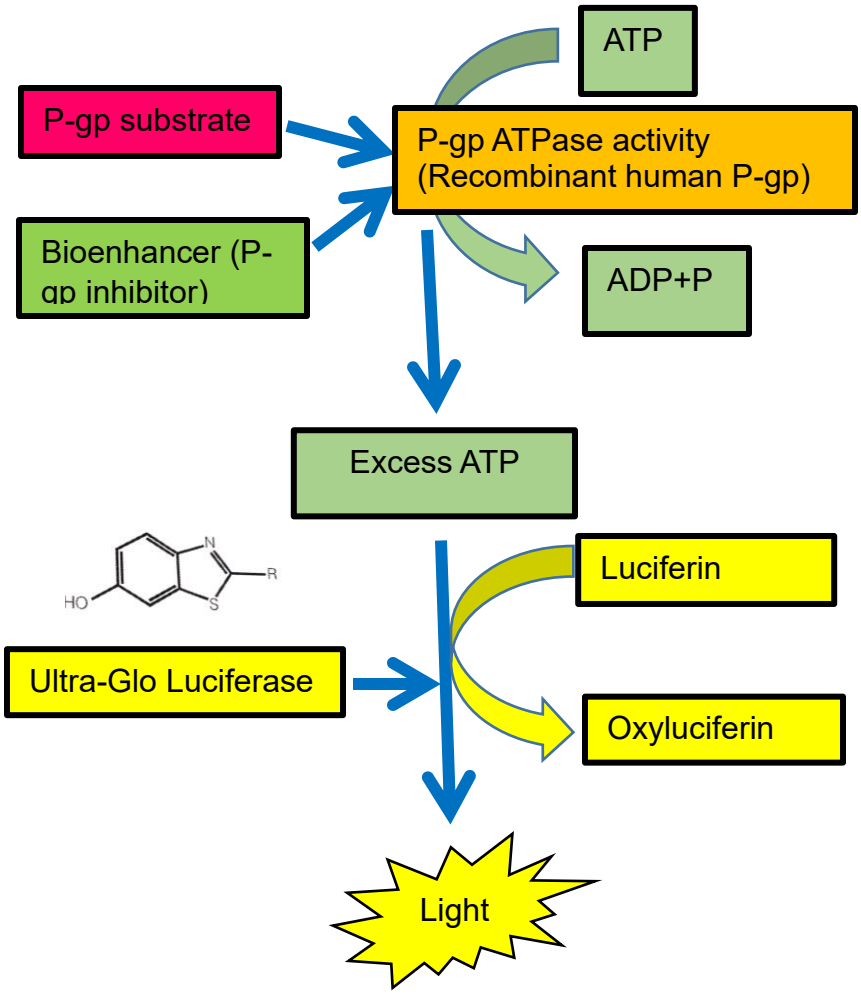

FIGURE 3.1: Schematic illustration of Pgp-Glo assay system (adapted with modifications from Promega (2015))

3.2 MATERIALS AND METHODS

3.2.1 Materials

Each system contained sufficient reagents for 96 assays at 50 µL per assay in 96-well plates. The reagents included:

- *A 500 µL volume of Recombinant Human P-gp Membranes*: These are the synthetic membranes, which contain the p-glycoprotein. The p-glycoprotein is responsible for

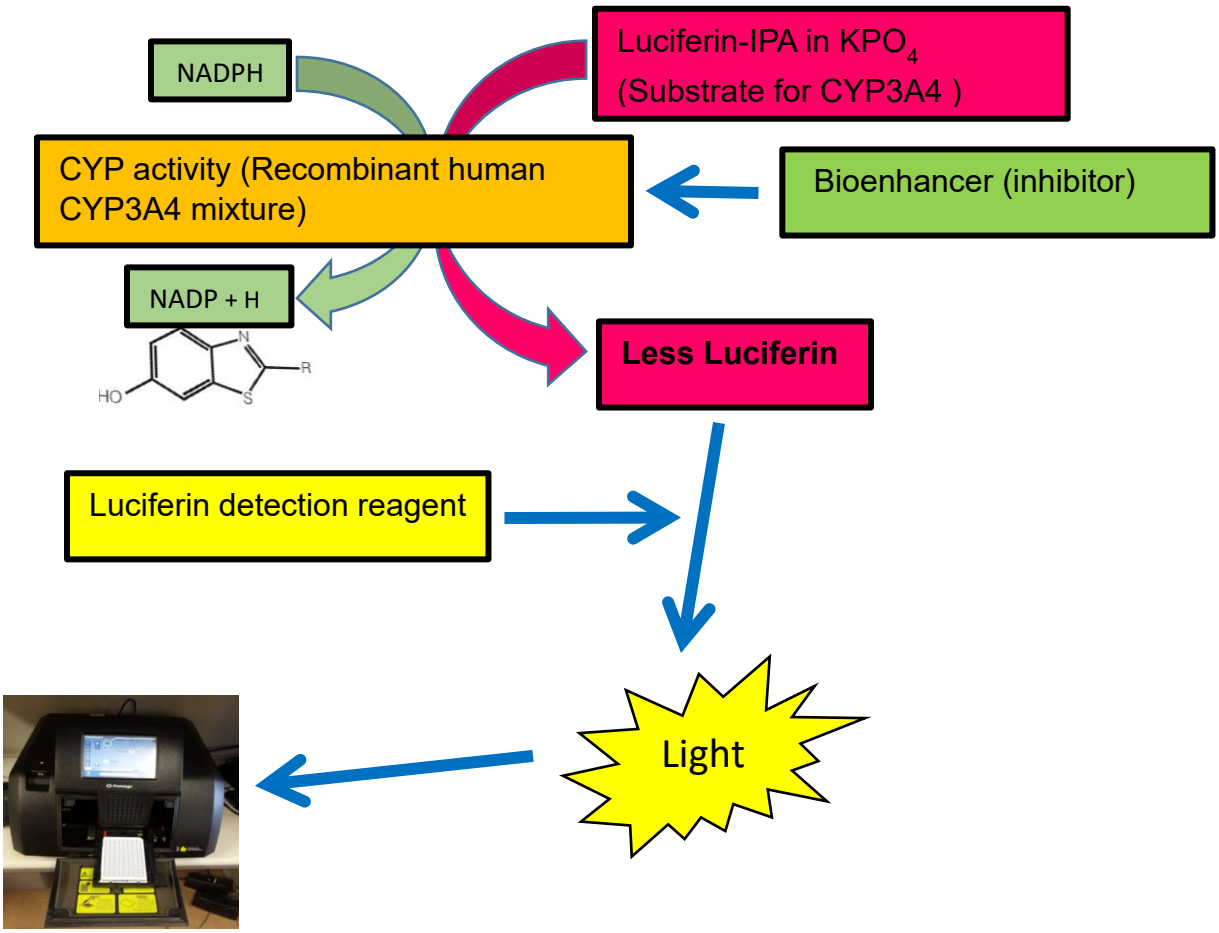

FIGURE 3.2: Schematic illustration of the P450-Glo assay system (adapted from Promega (2014) with some modifications)

the efflux of many drugs and xenobiotics back into the lumen. Therefore, synthetic membranes were used as a model. They are cost-effective, give accurate results, and they are suitable for high-throughput screening assays.

- *1 vial ATP Detection Substrate (lyophilized)*: This substrate measures the amount of ATP left into the reaction mixture after the P-gp reaction.

- *A 10 mL volume of ATP Detection Buffer*: This buffer was used to reconstitute the lyophilized ATP Detection Substrate.

- *A 10 mL volume of Pgp-Glo™ Assay Buffer*: This buffer was used to prepare standards and other components of the system.

- *A 1 mL volume of 50 mM MgATP*: The P-gp ATPase activity utilizes energy in the form of ATP, therefore, the MgATP was used to supply energy into the assay.

- *A 100 µL volume of 10 mM Verapamil*: Verapamil is the P-gp substrate and was used to initiate the reaction of the P-gp ATPase activity. It was also used as a base-line control into the untreated wells.

- *A 250 µL volume of 10 mM Na_3VO_4 (sodium orthovanadate)*: Sodium orthovanadate is a potent P-gp inhibitor. This chemical was used as the reference positive control for the inhibitory effects of test compounds (PDAEs).

The P450-Glo™ CYP3A4 Screening System with Luciferin-IPA was purchased from ANATECH (South Africa). The system contained sufficient reagents for 1,000 assays at 50 µL per assay in 96-well plates.

The components of the P450-Glo™ CYP3A4 Assay included:

- *A 60 µL Luciferin-IPA, 3mM*: A luminogenic substrate appropriate for the CYP enzyme. This luminogenic P450-Glo™ substrate is a derivative of beetle luciferin [(4S)-4,5-dihydro-2- (6-hydroxybenzothiazolyl)-4-thiazolecarboxylic acid or d-luciferin], a substrate of firefly luciferase. It is a proluciferin, which is converted to luciferin by the CYP enzyme. Luciferin-IPA is the most sensitive and selective substrate for all CYP3A4 applications (Promega, 2014:7).

- *1 vial Luciferin Detection Reagent (lyophilized)*: Reacts with the luciferin to produce light (luminescence).

- *A 50 mL Reconstitution Buffer with esterase*: Used to reconstitute the luciferin detection reagent.

- *A 100 µL CYP3A4 (1 pmol/µL) + Reductase + b5*: A membrane preparation containing recombinant human cytochrome P450 (CYP) enzyme.

The membranes are prepared from baculovirus-infected insect cells and contain human CYP enzyme and P450 reductase (and cytochrome b5 for CYP2B6, 2C9, 2C19 and 3A4) (Promega, 2014:7).

- *A 100 µL Control Membranes*: The control membranes are prepared from wild-type baculovirus-infected insect cells and have a total protein concentration of 5 mg/mL. They are the negative control membranes, which are devoid of CYP activity (Promega, 2014:7).

- *A 5.0 mL Potassium Phosphate Buffer, 1 M (pH 7.4)*: Contains a 13.94 g potassium phosphate dibasic, anhydrous and a 2.72 g potassium phosphate monobasic, anhydrous.

- *A 50 mL Luciferin-Free Water*: A contaminant-free supply of water for making necessary dilutions.

- *A 2.75 mL Solution A, NADPH Regeneration System*: Contains a 26 mM NADP+, a 66 mM glucose-6-phosphate, and a 66 mM $MgCl_2$.

- *A 0.6 mL Solution B, NADPH Regeneration System*: A 40 U/mL glucose-6-phosphate dehydrogenase in a 5 mM sodium citrate (pH 5.5).

The phosphate-buffered saline, curcumin, quercetin, sinomenine, naringin, glycyrrhizic acid and propranolol were purchased from Sigma (South Africa). Sodium orthovanadate was purchased from Anatech (South Africa). The intestinal tissues were collected from the R&R abattoir (slaughterhouse) in Pretoria North, South Africa as a donation.

3.2.2 Methods

3.2.2.1 *In vitro* recombinant human p-glycoprotein inhibition by plant-derived absorption enhancers

The Pgp-Glo™ Assay Systems method by Promega (2015:1-11) was utilized for the screening of PDAEs for their effective P-gp inhibition concentrations.

Pgp-Glo™ Assays were performed in two steps: (1) The P-gp reaction and (2) the ATP detection reaction.

*The P-gp reaction***:** In this step, a Recombinant Human P-gp Membrane fraction was incubated in Pgp-Glo™ Assay Buffer with a non-limiting concentration of MgATP (5 mM) for 40 minutes at 37 ºC. Untreated and Na_3VO_4-treated samples (positive control) were included. Verapamil (P-gp substrate) was added in every well of the plate (Promega, 2015:7).

The ATP Detection Reaction: ATP Detection Reagent was added to the P-gp reaction described above. The ATP Detection Reagent stops the P-gp reaction and measures the

ATP remaining in the reaction mixture. This luciferase-based detection reaction provides a linear response to ATP concentration over the range of ATP concentrations found in the Pgp-Glo™ Assay. Thus, any changes in signal directly reflect changes in ATP concentration (Promega, 2015:7).

(1) Preparation of buffers and solutions for Pgp-Glo assay

- *ATP Detection Reagent*: The ATP Detection Buffer was thawed and equilibrated to room temperature. The buffer was mixed briefly to prevent foaming and to resuspend any precipitate that may form after freezing. The entire contents of the 10 mL bottle of ATP Detection Buffer were transferred to the amber bottle containing the lyophilized ATP Detection Substrate. The bottle was mixed by swirling or inverting several times to obtain a homogeneous solution of ATP Detection Reagent.

- *0.5 mM Verapamil*: A 5 µL volume of 10 mM verapamil was mixed with a 95 µL volume of the Pgp-Glo™ Assay Buffer.

- *0.25 mM Na_3VO_4*: A 5 µL volume of 10 mM Na_3VO_4 was mixed with a 195 µL volume of the Pgp-Glo™ Assay Buffer.

- *25mM MgATP*: To prepare enough for a 96-sample assay, a 0.5 mL volume of 50 mM MgATP was mixed with a 0.5 mL volume of the Pgp-Glo™ Assay Buffer.

- *5X concentrated solutions of the test compounds of choice*: A 5X concentration of the test compounds were prepared in phosphate-buffered saline (PBS, pH 7.4) such that the final concentrations of PDAEs ranged from 10 to 200 µM. For example, when the

final concentration was required to be 10 µM, a 50 µM concentration of working solution of a test compound in question was prepared.

(2) The procedure for performing the assay

A 5 µL volume of the Pgp-Glo™ Assay Buffer and a 5 µL volume of the phosphate-buffered saline (PBS, pH 7.4) were added to wells labelled “untreated” and “minus”, a 10 µL volume of 0.25 mM Na_3VO_4 in Pgp-Glo™ Assay Buffer to wells labelled “Na_3VO_4”, and a 10 µL volume of 5X concentrated test compounds (PDAEs) to wells labelled “test compound”. This was followed by the addition of a 10 µL volume of 0.5 mM verapamil in all the wells. Then a 20 µL volume of diluted P-gp membranes was added to each well. The plate was incubated at 37 ºC for 5 minutes. The P-gp reactions was initiated by adding a 10 µL volume of 25 mM MgATP in all the wells. At that point, each P-gp reaction contained 5 mM ATP. The contents of the 96-well microplate were mixed briefly at 37 ºC for 40 minutes using ThemoMixer C (Eppendorf AG, Germany) incubator-shaker. The microplate was removed from the incubator-shaker, the luminescence was initiated by adding a 50 µL volume of the ATP Detection Reagent to all the wells. The plate was mixed briefly on a shaker and then incubated at room temperature for 20 minutes to allow the luminescent signal to develop. Finally, the luminescence was measured on a Glomax Multi$^+$ detection luminometer system (ANATECH, South Africa).

(3) Data analysis

The luminometer data was analysed in Microsoft Excel 2016 office package. An increase in the intensity of the luminescence means the ATP was not consumed in the reaction, thereby implying less P-gp activity or P-gp inhibition. Whereas a decrease in

luminescence the ATP was used up in a reaction indicating more P-gp activity. The luminescence values of the samples were compared to that of the Na_3VO_4 positive control and the percentage inhibition of each sample was calculated using Equation 3.1 below:

$$\%\ Pgp\ inhibition\ = \frac{Luminesence\ of\ control - luminescence\ of\ sample}{Luminescence\ of\ sample} \times 100 \qquad \text{[Equation 3.1]}$$

Statistical analysis of P-gp inhibition data was performed with Microsoft Office Excel 2016 using a one-way analysis of variance (ANOVA, $p < 0.05$) to indicate significant statistical differences in the effects of various PDAEs compared to the control on P-gp inhibition.

3.2.2.2 *In vitro* recombinant human cytochrome P450 3A4 enzyme inhibition by plant-derived absorption enhancers

The P450-Glo™ Assay Systems method by Promega (2014:1-46) was utilized for the screening of PDAEs for their effective P-gp inhibition concentrations.

The P450-Glo™Assays were performed in two steps: (1) The cytochrome P450 reaction and (2) the luciferin detection reaction.

The cytochrome P450 Reaction: The P450-Glo™ substrates are converted by CYP enzymes to a luciferin product (Promega, 2014:8).

The Luciferin Detection Reaction: In this step, the luciferin product produced in Step 1 of the P450-Glo™ Assays is detected as a luminescent signal from a luciferase reaction. Step 2 is initiated by adding an equal volume of Luciferin Detection Reagent (e.g. 50 µL added to a 50 µL CYP reaction in a 96-well plate). This reagent simultaneously stops the

CYP reaction and initiates a luminescent signal that is proportional to the amount of product formed in Step 1 (Promega, 2014:8).

(1) Preparation of buffers and solutions for P450-Glo assay

The CYP3A4 membranes and control membranes were thawed rapidly at 37 ºC and placed on ice. The luciferin-IPA, solutions A and B, the potassium phosphate buffer, and the luciferin-free water were also thawed at stored at room temperature, protected from light.

- *A 4X CYP3A4 reaction mixture with luciferin-IPA*: For the preparation of a 96-well plate 4X CYP3A4 reaction mixture, a 500 µL volume of 1 M potassium phosphate buffer was mixed with a 5 µL volume of 3 mM luciferin-IPA, a 10 µL volume of the CYP3A4 membranes, and a 735 µL volume of the luciferin-free water.

- *A 4X control membranes mixture*: For the preparation of 4 wells of the 4X control mixture, a 20 µL volume of 1 M potassium phosphate buffer was mixed with a 0.2 µL volume of 3 mM luciferin-IPA, a 0.4 µL volume of the control membranes, and a 29.4 µL volume of the luciferin-free water.

- *A 2X NADPH regeneration system for luciferin-IPA reactions*: The NADPH regeneration system reduces NADP+ to NADPH. The NADPH generated serves as the electron source for the CYP oxidative reactions (Promega, 2014:8). For the preparation of 96-well plate assays, A 250 µL volume of the solution A was combined with a 50 µL volume of the solution B and a 2200 µL volume of the luciferin-free water.

- *The luciferin detection reagent*: The entire vial of the luciferin detection reagent was reconstituted with the entire 50 mL volume of the reconstitution buffer with esterase.

- *4X cimetidine*: A 1 mg/mL concentration of cimetidine was prepared in PBS. The final concentration per well of cimetidine positive control was 0.25 mg/mL.

(2) Performing the P450-Glo assay

A 12.5 µL volume of 4X test compound was added to the “test compound” wells of a white opaque 96-well plate, a 12.5 µL volume of the phosphate-buffered saline (PBS, pH 7.4) to the untreated and minus-P450 control wells. This was followed by the addition of a 12.5 µL volume of the 4X control reaction mixture to the minus-P450 control wells and a 12.5 µL volume of the 4X CYP3A4 reaction mixture to all other wells. The contents of the microplate were mixed briefly on a microplate shaker and pre-incubated at room temperature for 10 minutes. The reaction was initiated by adding a 25 µL volume of 2X NADPH regeneration system to all the wells. The contents of the plate were mixed briefly on a plate shaker and incubated at room temperature for 10 minutes. The reaction was terminated by adding a 50 µL volume of reconstituted luciferin detection reagent to all wells and mixed briefly on a microplate shaker. The microplate was incubated at room temperature for 20 minutes to stabilize the luminescent signal. The luminescence was measured using a Glomax Multi^{+} detection luminometer system (ANATECH, South Africa).

(3) Data analysis

The CYP450 inhibition data were analysed using Microsoft Excel 2016. Since the P450-Glo™ substrates are converted by CYP enzymes to a luciferin product (Promega, 2014:1), which generates a luminescence, an increased value of the luminescence indicates enhanced CYP450 activity while a decrease in luminescence value implies CYP450 activity. The luminescence values of the samples were compared to that of the cimetidine positive control and the percentage inhibitions of the samples were calculated using Equation 3.2 below:

$$\%\ CYP\ inhibition\ = \frac{Luminescence\ of\ control - Luminescence\ of\ sample}{Luminescence\ of\ control} \times 100 \qquad \text{[Equation 3.2]}$$

Statistical analysis of CYP inhibition data was performed with Microsoft Office Excel 2016 using a one-way analysis of variance (ANOVA, $p < 0.05$) to indicate significant statistical differences in the effects of various PDAEs compared to the control on CYP inhibition.

3.2.2.3 *Ex vivo* drug permeability studies

(1) Preparation of test mixtures

The phosphate-buffered saline (PBS) at pH 7.4 is an isotonic solution that simulates most of the body fluids. The PBS was used as an isotonic buffer that keeps the model intestinal tissue alive throughout our experiment. It was also used to prepare our test compounds and standards. Propranolol is a P-gp substrate and was used to enhance the P-gp activity in the concentration of 50 µg/mL. Sodium orthovanadate is a potent and selective inhibitor of the P-gp activity. It was used as a positive control in the concentration of 10 mM in PBS

(pH 7.4). Different combinations of PDAEs were prepared in PBS, and their concentrations ranged from 10 to 100 µM.

(2) Collection of the porcine intestinal tissue

Pigs aged between 16-24 weeks old and weighing about 70 kg were selected as sources of intestinal tissues. This was done to keep the properties of our model intestinal tissue as similar to each other as possible. The intestinal tissue was consistent in terms of thickness (1.5 mm) and the diameter (2 cm). Immediately after slaughter, about 60 cm of the small intestine was quickly excised, flushed several times with ice-cold PBS (pH 7.4) to clear the intestinal contents. The intestinal tissue was immersed in ice-cold PBS (pH 7.4) in a cooler box to keep the tissue viable during transportation.

(3) Preparation of everted gut sacs

The effects of PDAEs on p-glycoprotein mediated propranolol efflux were determined using the everted gut sac (Versantvoort, Rompelberg & Sips, 2000:27-28; Han *et al*., 2014:556; Chula *et al*., 2012:138). In the laboratory, the intestinal tissue was mounted on a smooth glass rod, the mesenterium, the outer muscle and the fat tissue were removed. The intestinal tissue was everted gently, over the glass rod so that the mucosal side was toward the outside and the serosal side toward the inside and cut off into small tubes such that the final after mounting and tying is 4 cm (Chula *et al*., 2012:138). One side of the everted gut sac was mounted on the opening of a plastic tube (i.e. 2 cm in diameter) and the other end was tied up with a thread close it completely. Twelve labelled 50 mL plastic centrifuge tubes were mounted on a diffusion chamber apparatus and were connected to an oxygen supply, while the temperature of the diffusion chambers was maintained at 37

ºC (Figure 3.3). Each centrifuge tube was then filled with a 12 mL volume of the appropriate test compound (combination of PDAEs) and the oxygen was bubbled continuously.

(1) The p-glycoprotein inhibition and drug transport assay

The P-gp inhibition assay was carried out according to the procedure explained by Chula et al. (2012:138) with modifications. A 7 mL volume of the PBS fills a 4 cm everted gut sac, therefore, each intestinal sac was filled with a 7 mL volume of 37 ºC PBS (pH 7.4) and initiated the P-gp activity reaction by placing each intestinal sac in the centrifuge tubes containing a 12 mL volume of the appropriate test compound. The volume of 12 mL of a test compound covers the entire apical side of the everted gut sac.

The experimental solution (test compound solution) was continually aerated with 5% CO_2 and 95% O_2 and maintained at 37 ºC (Wang *et al*., 2016:297). The temperature of the diffusion chambers was maintained at 37 ºC to simulate the body temperature and keep the tissue viable. Aliquots of 1 mL serosal solution were taken out from the receiver compartment at different time intervals (0, 30, 60, 90, 120 min) and were immediately replenished with a 1 mL volume of PBS buffer (pH 7.4) at 37 ºC (Chula *et al*., 2012:138).

The 1.5 mL Eppendorf tubes containing each sample were centrifuged at 13000 rpm for 15 minutes using Biocen 22R (Orto Alresa, Spain) to separate the drug solution from other debris of the lumen that could affect the absorbances of the drug (Han *et al*., 2014:556).

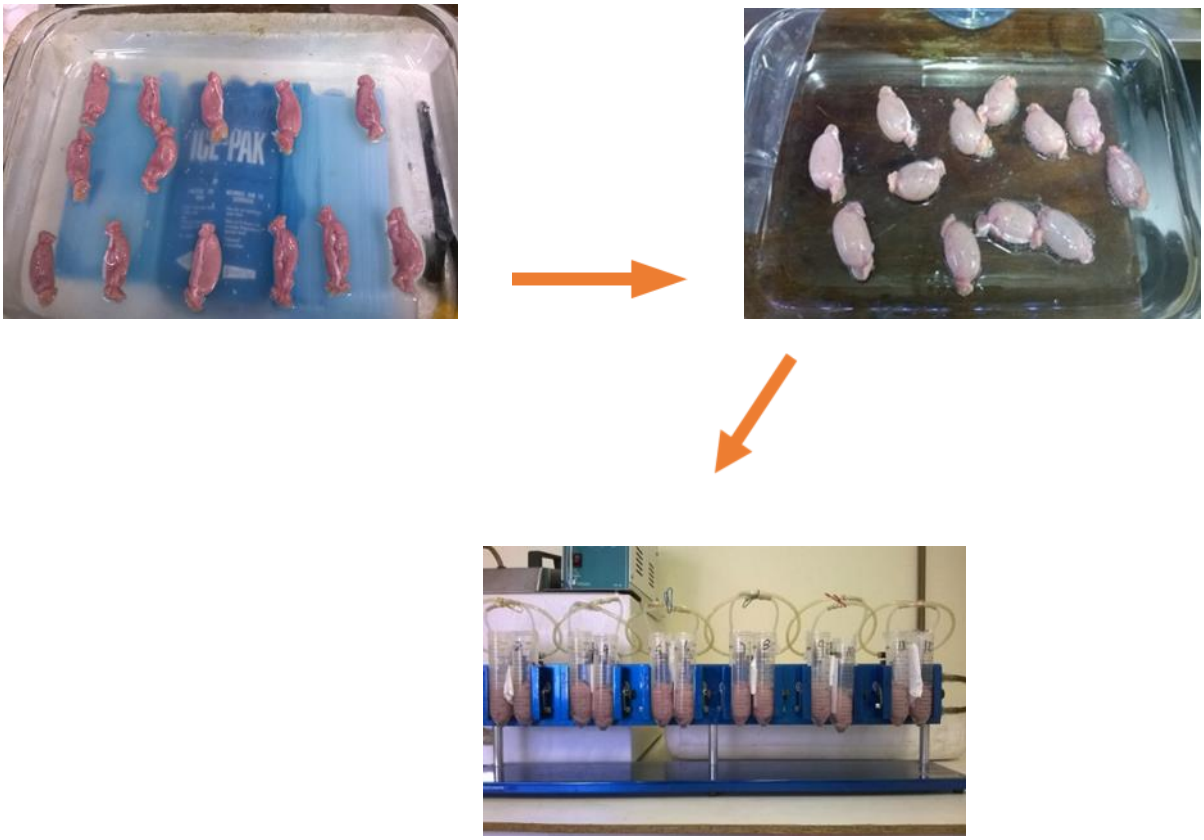

FIGURE 3.3: Everted gut sacs model (Kheoane photo library, 2016)

3.2.2.4 Drug sample and data analysis

The supernatants were plated in a clear 96-well flat and round-bottom UVStar microplate (Lasec, South Africa) in four replicates for each test group. The absorbance of samples was measured with SpectroStar microplate reader (BMG LabTech, Germany) at 319 nm wavelength for propranolol.

The concentration of the drug transported from the apical to the basolateral region of the porcine intestinal tissue was obtained from the absorbances of the samples using the Microsoft Excel 2016. Initially, the standard curve for propranolol (P-gp substrate) was constructed and the concentrations of propranolol alone, in the presence of sodium

orthovanadate positive control and in the presence of the PDAEs over 30 minutes time intervals for 2 hours were calculated from the standard curve. Statistical analysis of the drug transported data was performed with Microsoft Office Excel 2016 using a one-way analysis of variance (ANOVA, $p < 0.05$) to indicate significant statistical differences in the effects of various combinations of PDAEs compared to the control.

3.3 RESULTS

3.3.1 *In vitro* recombinant human p-glycoprotein inhibition by plant-derived absorption enhancers

The effective P-gp inhibitory concentrations of PDAEs are reported in Figure 3.4. Curcumin exhibited higher P-gp inhibitory effects in a concentration-dependent manner, and even in the lowest concentration of 10 µM (24%), with 100 µM concentration of curcumin showing the highest percentage inhibition (95%) of the P-gp activity and the values were statistically significant ($p < 0.05$) when compared to the control. The P-gp inhibition of sinomenine was also concentration-dependent and showed the highest percentage inhibition of the P-gp activity at 50 µM (30%), 75 µM (32%) and 100 µM (75%) concentrations. Quercetin similarly to curcumin and sinomenine showed P-gp inhibitory effects in a concentration-dependent manner with 75 µM and 100 µM concentrations having the highest percentage inhibition (25% and 63% respectively) of the P-gp activity. Naringin on the other hand, showed poor P-gp inhibitory capacity, it reached the P-gp inhibition peak at 50 µM (25%) concentration and thereafter decreased with an increase in concentration. All Glycyrrhizic acid had no P-gp inhibition activity.

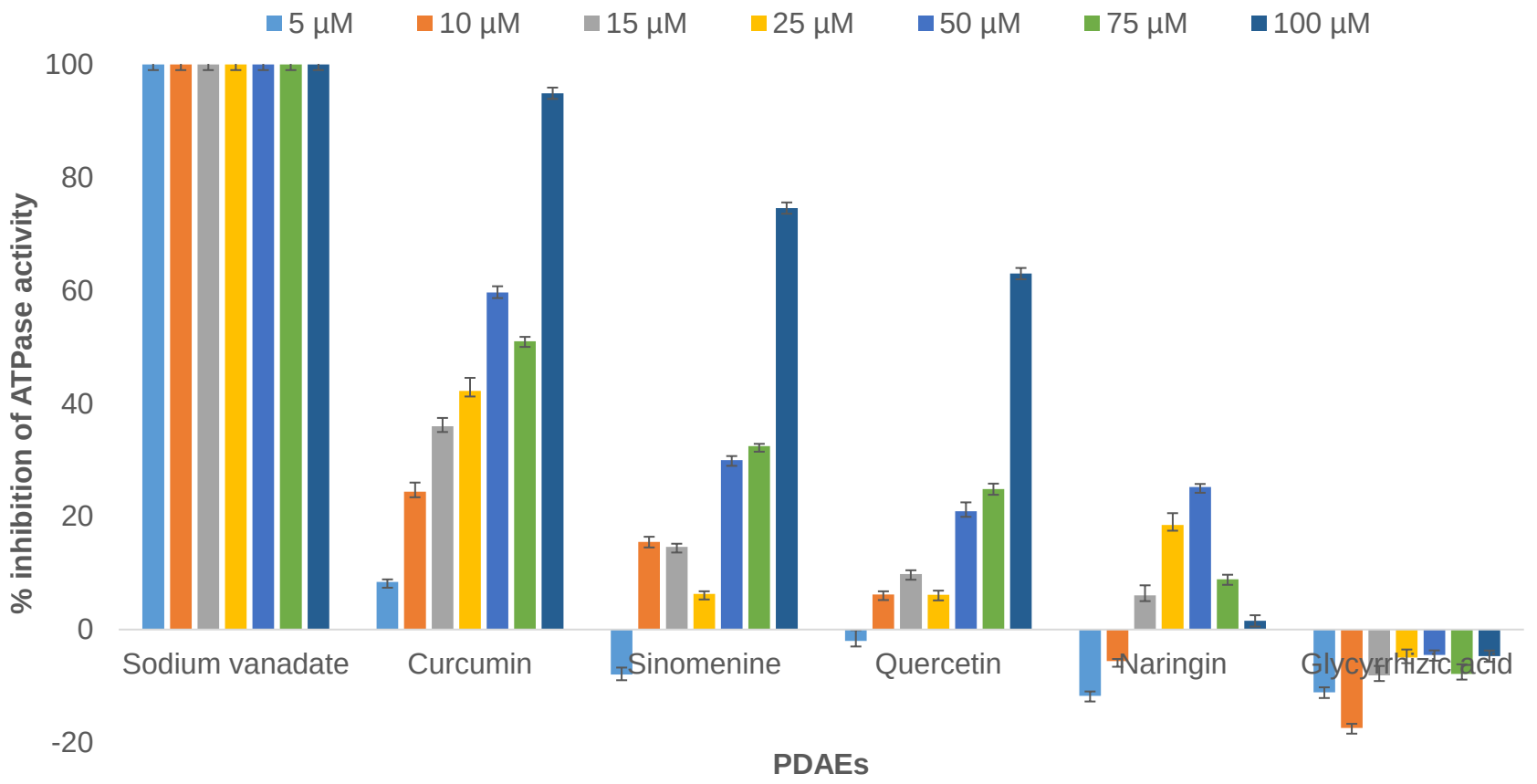

FIGURE 3.4: P-glycoprotein ATPase inhibitory effects of PDAEs (value = mean ± SD, n = 4; percentage inhibition values of test compounds were statistically significant ($p < 0.05$) compared to the control)

3.3.2 *In vitro* recombinant human cytochrome P450 3A4 enzyme inhibition by plant-derived absorption enhancers

CYP3A4 is one of the most important CYP isoforms involved in the metabolism of xenobiotics in the human body (Li, Kaminski & Rasmussen, 1995:1). The effective concentrations of the PDAEs were determined firstly by using different concentrations (i.e. 5 – 200 µM), which were derived from the literature (Volak *et al*., 2008:1594; Liu *et al*., 2011:81; Hou, Lin & Chao, 2012:2307).

The preliminary screening results showed varying CYP3A4 inhibitory effects of PDAEs at different concentrations when compared to cimetidine positive control (Figures 3.5A and 3.5B). For example, curcumin was most effective at 75(75%), 100(80%), 150(79%) and 175(85%) µM concentrations; sinomenine at 10(27%), 50(32%), 125(29%), and 150(32%) µM; quercetin at 75(80%), 100(89%), 175(90%), and 200(92%) µM; naringin at 10(70%), 25(73%), 100(70%), 115(68%), and 175(68%) µM; and glycyrrhizic acid at 10(72%), 15(73%), 50(71%), 105(58%), and 110(66%) µM. However, the overall CYP3A4 inhibitory effects of sinomenine at the concentration ranging from 5 to 200 µM were quite low (below 40%) as compared to other PDAEs screened in this study. On the other hand, quercetin showed the highest CYP3A4 inhibition capacity of more than 50% even at lower concentration of 5 µM. The CYP3A4 inhibitory effects of quercetin were also concentration-dependent, ranging from 51% to 92%. Naringin was most effective at lower concentrations (e.g. 57% at 5 µM), but as opposed to quercetin, naringin lost its CYP3A4 inhibitory capacity when the concentration was increased, it reached the CYP3A4 inhibition peak at 25 µM (73%).

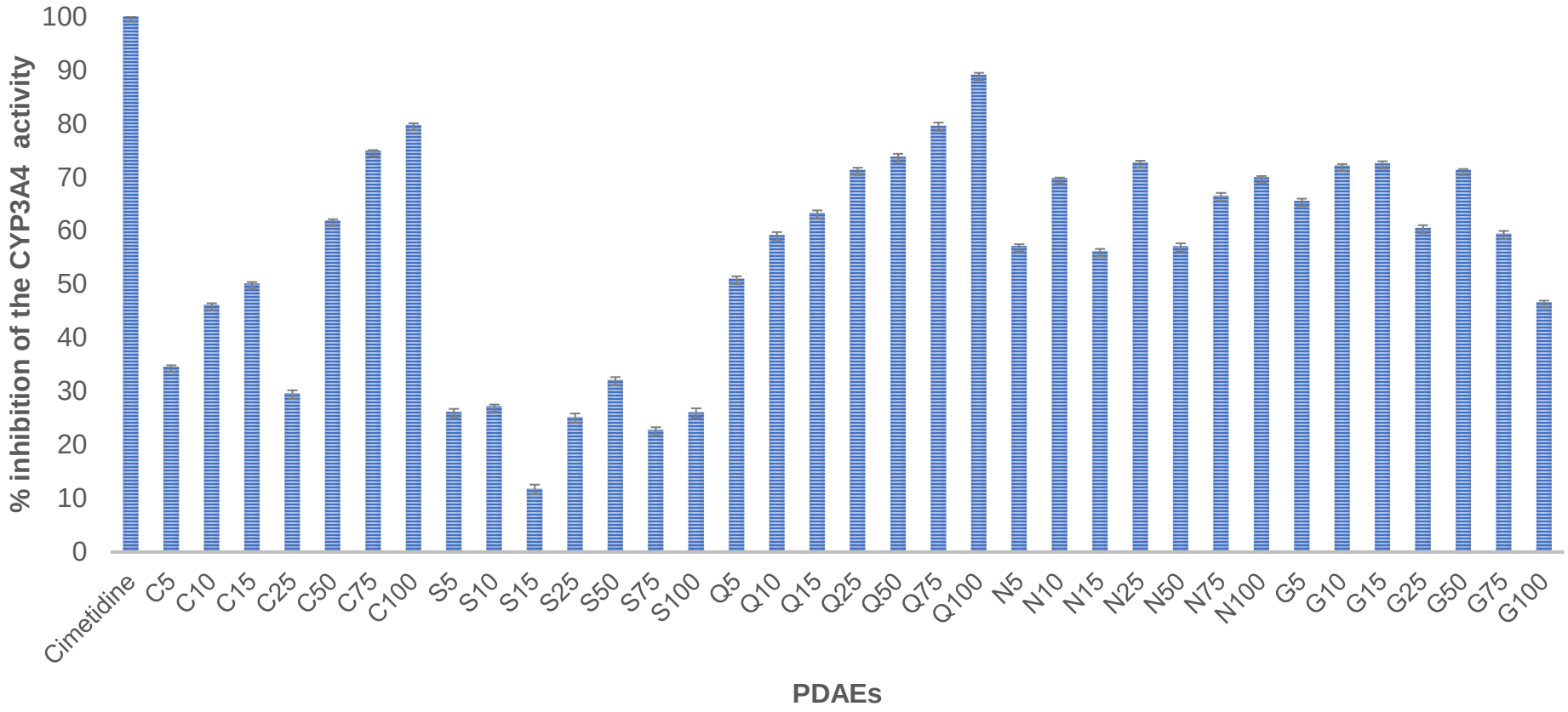

FIGURE 3.5A: Screening of individual PDAEs for effective CYP3A4 inhibitory concentrations (5 – 100 µM: C = Curcumin, S = Sinomenine, Q = Quercetin, N = Naringin; value = mean ± SD, n = 4; percentage inhibition values of test compounds were statistically significant ($p < 0.05$) compared to the control)

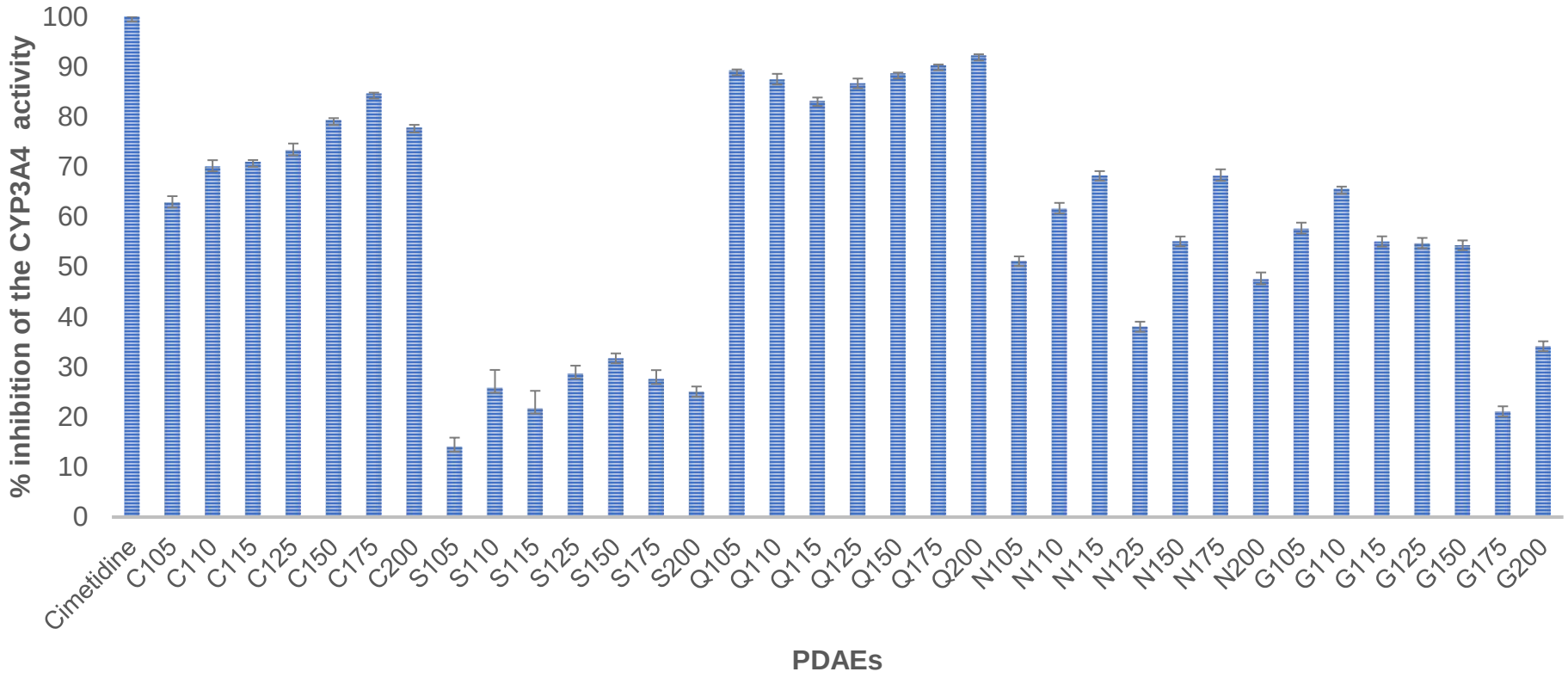

FIGURE 3.5B: Screening of individual PDAEs for effective CYP3A4 inhibitory concentrations (105 – 200 µM: C = Curcumin, S = Sinomenine, Q = Quercetin, N = Naringin; value = mean ± SD, n = 4; percentage inhibition values of test compounds were statistically significant ($p < 0.05$) compared to the control)

Glycyrrhizic acid, same as naringin, was also more effective at lower concentrations (e.g. 66% at 5µM) and reached a peak at 15 µM (73%). It lost its activity when the concentration was increased beyond 15 µM.

Sun et al. (2010:510) reported the possibility of toxicity due to the inhibitory action of P-gp by the mixture of liquorice and Kansui. Similarly, the action of P-gp was also inhibited by co-administration of liquorice and *Daphne genkwa* (Huang *et al*., 2008:2521). This phenomenon highlights the possibility of synergistic effects or toxicity when combining PDAEs. Therefore, after determining the CYP3A4 inhibitory effects of the PDAEs, different concentrations of the PDAEs were combined to assess the possibility of synergy among these phytochemicals. In the present study, 18 combinations of PDAEs were prepared based on the CYP3A4 inhibitory effects capacities of PDAEs from preliminary results in Figures 3.5A and 3.5B. The results for the CYP3A4 inhibition of the combinations of PDAEs (Figure 3.6) revealed synergy between certain PDAEs. Combinations containing quercetin (100 µM) showed the highest CYP3A4 inhibitory effects. For example, the combination of curcumin 100 µM increased the inhibition capacity of quercetin (100 µM) from 89% to 96%; sinomenine 10 µM from 89% to 90%; sinomenine 125 µM from 89% to 90%, sinomenine 100 µM from 89% to 91%; naringin 115 µM from 89% to 95% while glycyrrhizic acid from 89% to 96%.

3.3.3 Effective concentrations of combinations of the plant-derived absorption enhancers *ex vivo*

The lowest effective concentrations of the PDAEs were selected from the P-gp inhibition data (Figure 3.4) and the CYP3A4 inhibition data (Figure 3.5) to form 18 combinations of

PDAEs. This is so because the PDAEs (e.g. curcumin) could inhibit the metabolism of certain drugs by the CYP3A4 enzymes in the intestines (Appiah-Opong *et al*., 2007:83; Hou *et al*., 2007:169) and thus increase the bioavailability of these drugs. Of the 18 combinations, 4 combinations of PDAEs extensively improved the transport of propranolol from the apical to basolateral regions of the porcine intestinal tissue as compared to the basal, but less than sodium orthovanadate (a positive control) (Figure 3.7). For example, quercetin (75 µM) with curcumin (10 µM) increased the basal propranolol from 1.24 ± 0.08 µg/mL to 4.07 ± 0.05 µg/mL after 2 hours; quercetin (75 µM) with curcumin (50 µM) increased the basal propranolol from 1.24 ± 0.08 µg/mL to 3.86 ± 0.04 µg/mL after 2 hours; quercetin (75 µM) with curcumin (75 µM) increased the basal propranolol from 1.24 ± 0.08 µg/mL to 4.17 ± 0.10 µg/mL after 2 hours and quercetin (75 µM) with curcumin (100 µM) increased the basal propranolol from 1.24 µg/mL to 5.19 ± 0.14 µg/mL after 2 hours, which were significantly ($p < 0.05$) different compared to positive control.

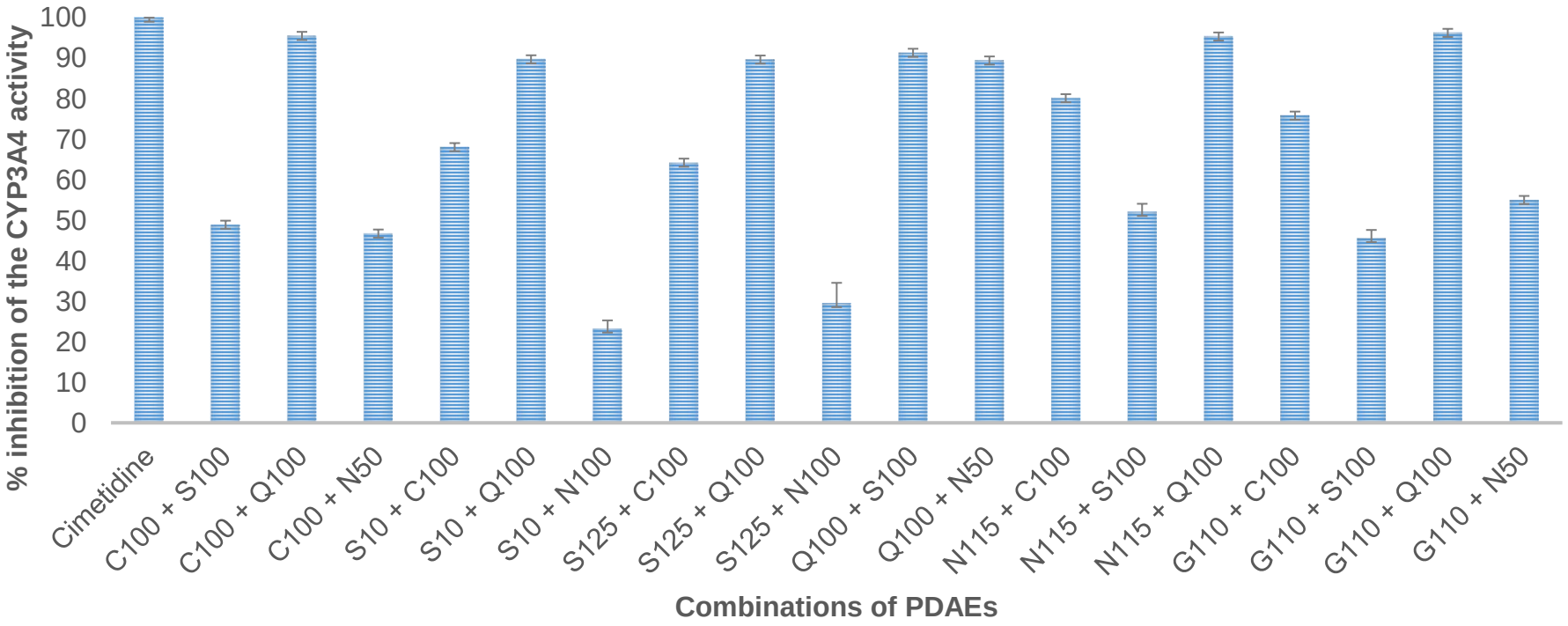

FIGURE 3.6: CYP3A4 inhibitory effects of combinations of PDAEs (C = Curcumin, S = Sinomenine, Q = Quercetin, N = Naringin; value = mean ± SD, n = 4; percentage inhibition values of test compounds were statistically significant ($p < 0.05$) compared to the control)

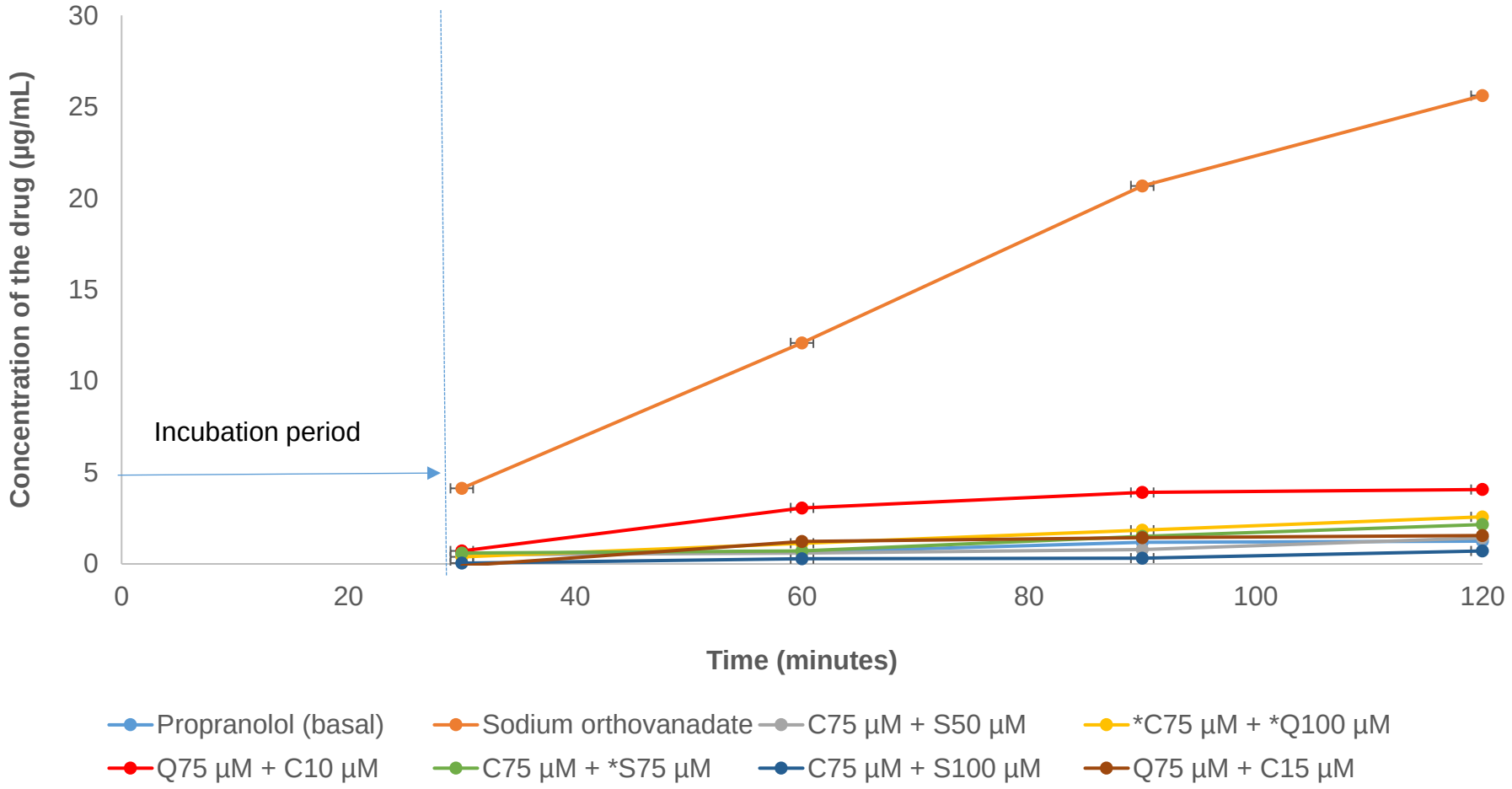

FIGURE 3.7: P-glycoprotein inhibitory effects of the combinations of PDAEs (*C = Curcumin; S = Sinomenine; Q = Quercetin; N = Naringin; value = mean ± SD, n = 4; amount of drug transported values for test compounds were statistically significant ($p < 0.05$) compared to the control)

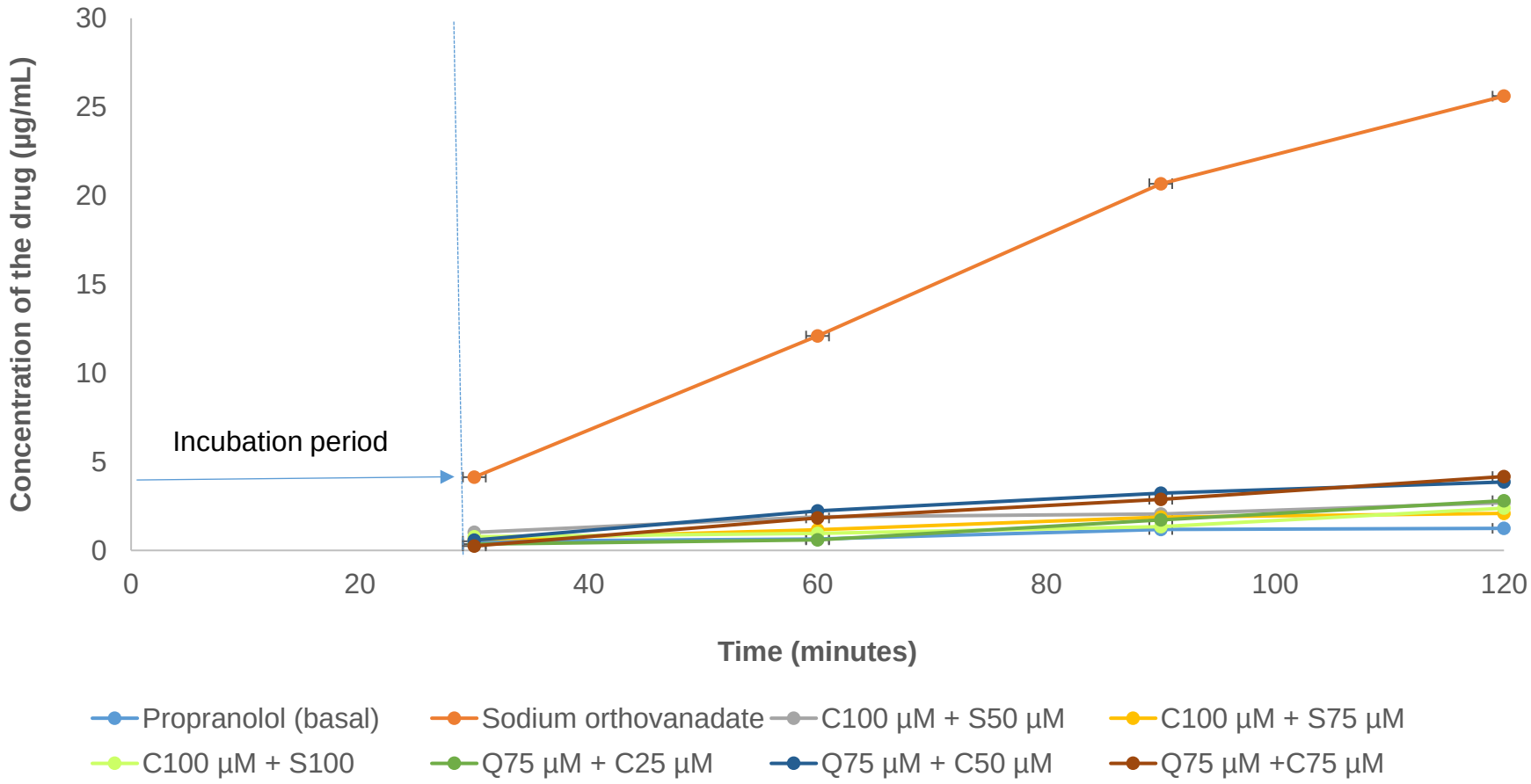

FIGURE 3.7: P-glycoprotein inhibitory effects of the combinations of PDAEs (*C = Curcumin; S = Sinomenine; Q = Quercetin; N = Naringin; value = mean ± SD, n = 4) (continued)

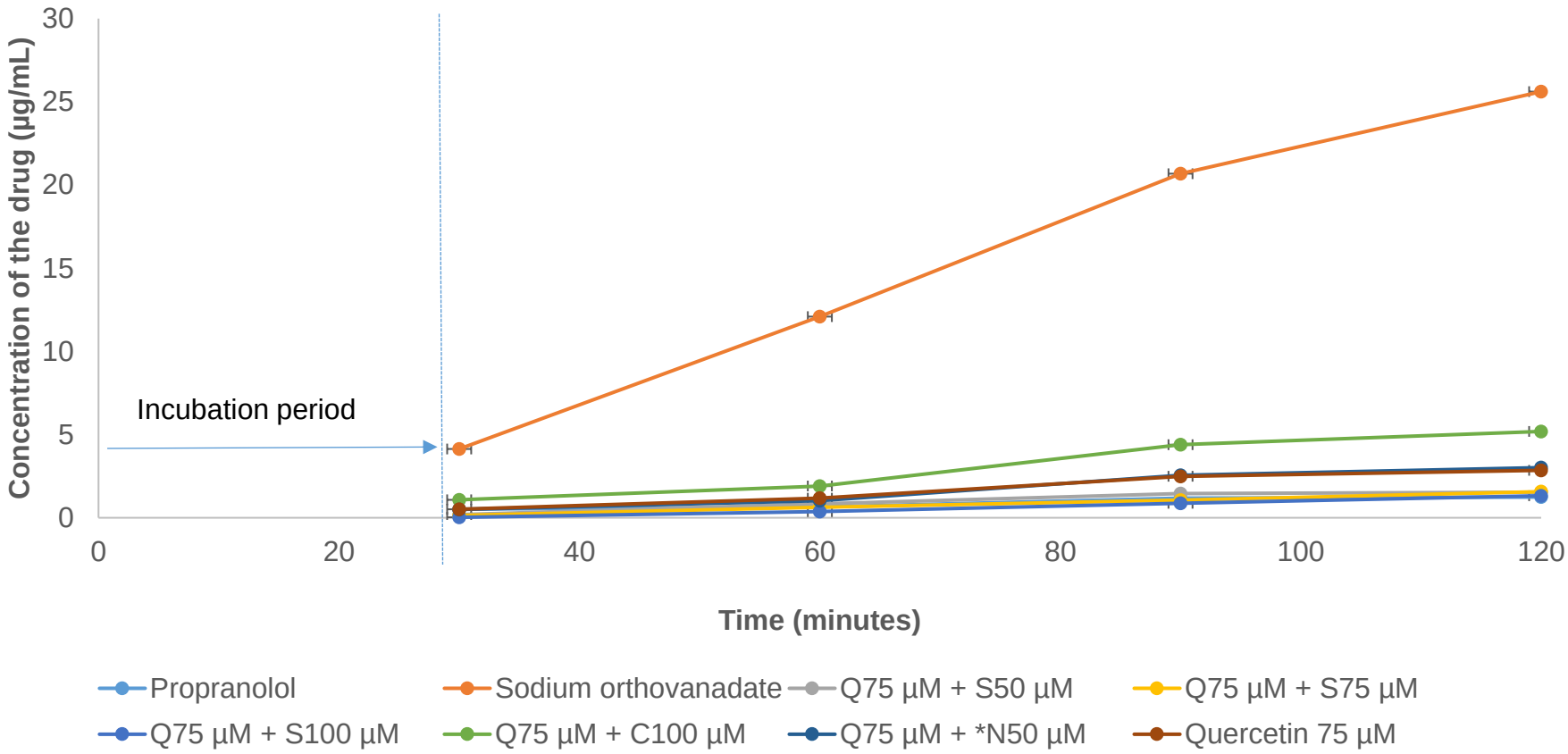

FIGURE 3.7: P-glycoprotein inhibitory effects of the combinations of PDAEs (*C = Curcumin; S = Sinomenine; Q = Quercetin; N = Naringin; value = mean ± SD, n = 4) (continued)

3.4 DISCUSSION

3.4.1 *In vitro* recombinant human p-glycoprotein inhibition by plant-derived absorption enhancers

3.4.1.1 Quercetin

The results of the present study indicated that quercetin was a potent P-gp, for example, 100 µM concentration of quercetin inhibited the P-gp ATPase activity by 63% when compared to the sodium orthovanadate. The same results for quercetin were reported by Aurade et al. (2011:212). Their results reported the inhibition of the insecticide-resistant pest *Helicoverpa armigera* (Ha-P-gp) ATPase activity of 80–90% by quercetin at 100 µM concentration. Similarly, quercetin inhibited P-gp activity, down-regulated P-gp expression and decreased ABCB1 mRNA (in a wide range of concentrations 10 – 100 µM) in different experimental models (cancer cell lines such as HK-2, MCF7, etc.) and thus enhances the sensitivity to anti-tumor agents (cisplatin, tamoxifen, paclitaxel) (Chieli *et al*., 2010:287). Experiments performed on cell lines of human pancreatic carcinoma, exposed to selected concentrations (3, 6 and 12 µM) of quercetin and daunorubicin, confirmed that the polyphenol affects the expression and function of P-gp in a concentration-dependent manner. Moreover, it decreases the expression of ABCB1 (Borska *et al*., 2010:857). The concentration-dependent behaviour of quercetin on both the P-gp inhibition and the CYP3A4 was also observed in the present study. For example, quercetin at 75 µM inhibited the recombinant CYP3A4 enzyme by 80%, 100 µM by 89%, 175 µM by 90% and a 200 µM concentration by 92%.

3.4.1.2 Curcumin

The preliminary data of the present study on the recombinant P-gp revealed that curcumin had P-gp inhibitory effects at all the concentrations used. P-gp inhibitory effects were concentration-dependent. The results also showed that curcumin was also a potent inhibitor of the recombinant P-gp, this is true because the higher percentage inhibition of the P-gp activity even at lower concentration of 10 µM was observed, as compared to other PDAEs, and almost the same as sodium orthovanadate (positive control). The findings of the study by Lu et al. (2013:694) also reported that curcumin at 25 µM concentration inhibited the growth of vincristine-resistant human colon cancer cell line HCT-8/VCR. They further reported that the intracellular Rhodamine123 accumulation was increased ($p < 0.05$), and the expression of the multidrug resistance gene and P-gp were significantly suppressed ($p < 0.05$). Hou et al. (2008:224), in line with our findings, also reported the inhibition of P-gp activity and a decrease in P-gp protein and MDR1 mRNA expression levels in Caco-2 cell monolayers, which were treated with curcumin (30 µM) for 72 hours (Hou *et al*., 2008:224). Romiti et al. (1998:2349) also confirmed that curcumin inhibited the P-gp activity in a dose-dependent manner. They used both freshly plated hepatocytes, containing low levels of P-gp, and 72 hour-cultured hepatocytes, containing high levels of P-gp. Their results revealed that Rhodamine- (R-123) efflux, which represents a specific functional test for P-gp-mediated transport, was inhibited by curcumin. In another study conducted by Aurade, Jayalakshmi and Sreeramulu (2010:271), curcumin mixture inhibited the activity of *Helicoverpa armigera* P-gp (Ha-P-gp) ATPase by 80–90% at 100 µM concentration. Along with curcuminoids I, II and III, it inhibited the verapamil- and ethylparaoxon-stimulated Ha-P-gp ATPase activity. These

findings are similar to the result of 80% that was observed in the present study at a concentration of 100 µM.

3.4.1.3 Naringin

The ATPase activity was not inhibited the by naringin at low concentrations of 5 µM and 10 µM, but some little ATPase inhibition was observed when the concentration was increased to 15 µM and reached a peak ATPase inhibition of only 25% at a 50 µM concentration. These results proved that naringin was a poor P-gp inhibitor, which is in line with the findings of Eagling, Profit and Back. (1999:550), which reported none of the grapefruit juice constituents (e.g. naringin) tested to be markedly inhibited *in vitro* P-gp activity. Similar findings were reported by De Castro et al. (2007:2808) who found the flavonoid aglycone naringenin to be around 10-fold more potent than its glycoside naringin with IC_{50} values of 236 and 2409 µM, respectively. While there is also lack of more literature on the *in vitro* determination of the naringin P-gp inhibition using the same model as in the present study or any other similar models, it was difficult to compare results the present study with a large number of studies following extensive literature search. However, in one *in vivo* study, naringin was reported to have substantial P-gp modulation effects, i.e. P-gp inhibition (Ali *et al*., 2014:109).

3.4.1.4 Sinomenine

Sinomenine seemed to be more effective at the higher concentration of 100 µM demonstrating a concentration dependency or lack of potency, which could potentially cause some toxic effects if large amount of the compound is required for pharmacological effects.

3.4.1.5 Glycyrrhizic acid

Liquorice has been extensively investigated through material basis and interference with CYPs, but investigations of its effect on transporters were very limited, according to the literature (He *et al*., 2019:175). Glycyrrhizic acid inhibited P-gp-mediated efflux of daunorubicin in P-gp-overexpressing KB-C2 cells (Nabekura *et al*., 2008:867). In contrast, GA had no P-gp activity at concentrations ranging from 10 – 100 µM in the present study. These observed differences in inhibitory effects of P-gp could be attributed to the use of different assay methods between these studies. On the other hand, He et al. (2019:179) reported induction of the P-gp by six chemical compounds derived from liquorice. The findings of He et al. (2019:179) explain the negative values that were observed when GA was investigated for the P-gp inhibitory effects.

3.4.2 *In vitro* recombinant human cytochrome P450 3A4 enzyme inhibition by plant-derived absorption enhancers

3.4.2.1 Quercetin

The results of the present study indicated that quercetin was a CYP3A4 inhibitor, for example, 100 µM concentration of quercetin inhibited the CYP3A4 activity by 89% when compared to cimetidine. The same results for quercetin were reported by Aurade et al. (2011:212).

3.4.2.2 Curcumin

The CYP450 inhibition of curcumin using different *in vitro* models is well studied. For example, Volak et al. (2008:1594) and Oetari et al. (1996:39) used the liver microsomes

to study the inhibitory effects of curcumin. The concentrations used range from 0.19 µM to 200 µM. At concentrations of 1, 3, 10, and 30 µM, curcumin inhibited the ethoxyresorufin deethylation (EROD) activity in β-naphthoflavone (βNF)-induced liver microsomes by 36 up to 93%, the pentoxyresorufin depentylation (PROD) activity in phenobarbital (PB)-induced microsomes by 13 up to 88%, and the p-nitrophenol (PNP) hydroxylation activity in pyrazole-induced microsomes only by 0.5 up to 9%, respectively (Oetari *et al*., 1996:39). In the present study, all the curcumin concentrations (5 – 200 µM) inhibited the recombinant CYP3A4 activity and this is in line with the findings of Volak et al. (2008:1594) and Oetari et al. (1996:39). However, the best concentrations our study were 75 µM with 75% inhibition capacity, 100 µM with 80% inhibition and 175 µM with 89% inhibition. Our results also showed a 30% recomb:39inant CYP3A4 inhibition at the concentration of 25 µM, which is closely similar to the findings of Hou et al. (2007:169) on CYP3A4. They reported that a 30 µM curcumin treatment caused a 30–40% decrease in CYP3A4 catalytic activity and a 38% decrease in CYP3A4 protein expression.

Contrary to the findings of other studies, Mach et al. (2010:811) reported that curcumin had minimal inhibition at all concentrations in the CYP450 3A4 or 2D6 *in vitro* studies. These differences in the same plant-derived absorption enhancer could be attributed to the differences in the sensitivity of the *in vitro* models or the methods used. For example, the results obtained through the utilization of recombinant CYP3A4 could be different from those produced from the liver microsomes.

3.4.2.3 Naringin

Naringin inhibited the metabolism of simvastatin in rat hepatocytes (the intrinsic clearance

of simvastatin decreases from 26.2 µL/min/106 cells in the absence naringin to 4.15 µL/min/106 cells in the presence of 50 µM naringin) (Ubeaud *et al*., 1999:1403). However, these effects are not necessarily due to the involvement of the CYP3A4 enzyme alone but could rather be due to the involvement of many CYP450 enzymes. These findings by Ubeaud et al. (1999:1403), could explain the relatively lower CYP3A4 inhibition of naringin as compared to the curcumin and the quercetin in the present study.

3.4.2.4 Sinomenine

The present study results show that sinomenine had the poorest recombinant CYP3A4 inhibition capacities as compared to other PDAEs screened in the present study. The same observation was revealed by the study of Yao et al. (2007:113) where sinomenine (50 µM) had no significant effects on the activities of CYP1A2, CYP3A4, CYP2C9, CYP2E1, and CYP2D6, but decreased the activity of the CYP2C19 by 69% (p=0.012) in human microsomes (Yao *et al*., 2007:113).

When *in vitro* everted rat gut sac model used to investigate the intestinal absorptive behaviour of paeoniflorin influenced by co-administration of sinomenine, sinomenine at 16 and 136 µM concentrations enhance the absorption of paeoniflorin (20 µM) by 1.5- and 2.5-fold, respectively (Chan *et al*., 2006:425). However, this increased paeoniflorin absorption could be due to the inhibition of other CYP450 enzymes, possibly, the CYP2C19 as reported by Yao et al. (2007:113), than the inhibition of the CYP3A4. The P-gp inhibitory effects of sinomenine are not well studied. However, the higher inhibitory capacities were observed at 50, 75 and 100 µM concentrations in the present study.

3.4.2.5 Glycyrrhizic acid

Glycyrrhizic acid (GA) at a concentration of 50 µM inhibited CYP3A4-catalyzed testosterone 6-β-hydroxylation with an IC_{50} of 25.96 µM (Liu *et al*., 2011:81). In the present study, GA at the same concentration inhibited the recombinant human CYP3A4 activity by 71% when compared to cimetidine positive control. Therefore, a 50 µM concentration could be the lowest effective concentration in most CYP3A4 *in vitro* models.

The recent research by Hou, Lin and Chao (2012:2307) had demonstrated that glycyrrhizin (100 µM) and its major metabolite GA (25 µM) increased the CYP3A4 activity by 25.5% and 30.2% individually. However, a 25 µM concentration of GA produced a 61% inhibition of the recombinant human CYP3A4. This is twice the effects reported by Hou, Lin and Chao (2012:2307) and could imply the sensitivity of the recombinant human CYP3A4 model as compared to other CYP3A4 *in vitro* models.

3.4.3 Effective concentrations of combinations of the plant-derived absorption enhancers *ex vivo*

Of the 18 combinations, 4 combinations of PDAEs extensively improved the transport of propranolol from the apical to basolateral regions of the porcine intestinal tissue as compared to the basal (Figure 3.7). The observed increase in propranolol permeability when quercetin (75 µM) is combined with curcumin (10 µM), curcumin (50 µM), curcumin (75 µM) and curcumin (100 µM) than when quercetin 75 µM was used alone indicates the possible synergy between PDAEs. On the other hand, the low propranolol permeability was observed with the combinations of other PDAEs than when they were used

individually. This observation could be due to the toxicity of certain combinations of PDAEs on the intestinal tissue.

3.5 CONCLUSION

The recombinant human P-gp and the recombinant CYP enzyme could be effective approaches for the initial screening of effective concentrations of drugs and phytochemicals. In the present study, these methods were cost-effective because many samples with small volumes were screened at the same time. It was also concluded that the data was inconclusive for PDAEs samples which showed a negative value of the percentage inhibition of the ATPase activity (Figure 3.4). These P-gp effects were observed on sinomenine and quercetin (5 µM), naringin (5 and 10 µM) and glycyrrhizic acid at all concentrations screened. The combination of quercetin at a concentration of 75 µM with curcumin at 10, 50, 75 or 100 µM concentrations improved the permeability and absorption of propranolol through the porcine intestinal tissue. The combinatory approach on the use of the PDAEs improved synergy and thus the efficacy of certain individual PDAEs.

CHAPTER 4

MANUSCRIPT 2

FORMULATION AND CHARACTERISATION OF LIPOSOMES CONTAINING PLANT-DERIVED ABSORPTION ENHANCERS FOR OPTIMIZED ANTI-HIV AND ANTIMALARIAL DRUG DELIVERY

4.1 INTRODUCTION

The effective concentrations of the selected individual plant-derived absorption enhancers (PDAEs) and their combinations were determined in the previous chapter. Now that the effective concentrations were known, the present chapter investigated different combinations of phospholipids for their suitability to prepare liposomes with the best drug entrapment efficiency and release profile. The thin-film hydration technique was used to formulate the liposomes for both hydrophobic and hydrophilic substances. After the selection and optimization of liposomes with the best properties, they were further assessed for entrapment efficiency regarding PDAEs alone, individual drugs alone, and the drug with a combination of PDAEs.

The particle size and zeta potential values of these liposomes were measured, and this was followed by determination of *in vitro* drug release and *in vitro* permeability data. The particle size is an important aspect of colloidal formulations as it describes their nature and may affect their action and interaction with the physiological compartments. For example, nanosized formulations may permeate the gastrointestinal membrane through the paracellular pathway following oral administration. The zeta potential of a particle is

described as a surface charge of that particle and may affect both the pharmacokinetic and pharmacodynamic behaviour of the colloidal dosage form in several ways. For example, if a colloid bears a surface charge, it may remain suspended or deflocculated for a longer time in solution due to repulsive forces of 'like' charges in colloidal systems and this is particularly important in the case of suspensions (Aulton & Taylor, 2013:418). Through the principle of ionization, the surface charge of colloids may also improve their interaction with aqueous gastrointestinal fluids and other body fluids as well as attachment with the highly charged gastrointestinal membrane and the attachment with cells at the site of action (Aulton & Taylor, 2013:416-426).

The *in vitro* drug release profiles of liposomes measure the ability of the liposomes to release the encapsulated drug. Once a liposome reaches the site of action, it is important that it releases the unchanged form of a drug with ease. The *in vitro* permeability studies profiles of liposomes can be obtained using a dialysis membrane to simulate gastrointestinal membrane due to its semi-permeable nature.

After the formulation of liposomes, they were further characterized for their *in vitro* toxicological effects. Bioactive compounds are almost always toxic at high doses (Saleh-e-In *et al*., 2016:2). Therefore, the effective concentration of any phytochemical or drug can pose some toxic effects to the body if it's bioavailable beyond the maximum therapeutic effects (Saleh-e-In *et al*., 2016:2). The determination of toxicological effects is therefore important for the appropriate dosing of phytochemicals or drugs to ensure their safety to the body. Several *in vitro* toxicity models discussed in chapter two are available. However, the liver cellular model was chosen as a toxicity assay model for this study because most of the drug metabolism takes place in the liver, and the liver is the

site where most drug toxicities are best manifested. Furthermore, liver cells are fast-growing due to their high regenerative potential of the liver tissue itself (Michalopoulos, 2007:286).

Apart from PDAEs, both efavirenz (EFV) and mefloquine (MQ) can pose some toxic effects to the living cell on their own and their toxicity may be aggravated by co-administration with the PDAEs. The present study investigated the biocompatibility or toxicity of EFV and MQ alone and when they are combined with the PDAEs. This could help formulators to make informed decisions when formulating these drugs in combination with the PDAEs.

Finally, the *ex vivo* permeability of liposomal formulations across a porcine intestinal tissue was investigated. *Ex vivo* methods can be used to evaluate the intestinal absorption of new drugs. Biological performance can be obtained rapidly and reliably using these *ex vivo* techniques (Luo *et al*., 13:208). The *ex vivo* determination of the permeability of drugs could provide an estimation of how a drug could be transported through the gastrointestinal membrane following oral administration in the *in vivo* studies. Some of the *ex vivo* models that are commonly used in drug absorption studies include everted gut sacs and the intestinal tissue sheets (utilizing Ussing chamber) (Luo *et al*., 13:211; Tambe, Mokashi & Pandita, 2019:66). The everted gut model comprises an intestinal tube, which is everted such that the apical side of the tissue will be an outward part of the intestinal tube while the basolateral side is the inside of the intestinal tube. The intestinal tube is kept immersed in a suitable buffer at pH 7.4, throughout the study, to simulate gastrointestinal fluids.

The intestinal tissue (sheets) model, on the other hand, comprises cut segments of the intestinal tissue, which are first trimmed off the mesenteric fat tissue and the intestinal muscle tissue. Like the everted gut model, the intestinal sheets are kept in a suitable buffer at pH 7.4 throughout the study. The intestinal sheets are usually mounted on inserts that slotted between two halves of the Ussing chambers for drug transport studies. In the present study, the porcine intestinal sheets were used for *ex vivo* permeability studies.

4.2 MATERIALS AND METHODS

4.2.1 Materials

Cholesterol, 1,2-dipalmitoyl-sn-glycero-3-phosphocholine (DPPC), 1,2-distearoyl-sn-glycero-3-phosphocholine (DSPC), l-α-phosphatidylcholine, dioleoyl (DOPC), polyethyleneglycol, chicken egg albumin, efavirenz (EFV), mefloquine (MQ), dialysis bag (MW = 14 kDa), curcumin and quercetin were purchased from Sigma (South Africa). Irradiated fetal bovine serum (FBS) was purchased from Separations (South Africa).

CellTiter-Glo® luminescent cell viability assay kit was purchase from Anatech (South Africa). Norvegicus liver hepatoma cells (H-4-II-E, ATCC® CRL-1548™), 1640 RPMI media 200 mM (with L-glutamine), penicillin-streptomycin (Pen-Strep) (10 000 units penicillin, 10 mg/mL streptomycin) were purchased from Sigma Aldrich (South Africa).

The phosphate-buffered saline (PBS) at pH 7.4 is an isotonic solution that simulates most of the body fluids and was purchased from Sigma (South Africa). The intestinal tissues were collected as a donation from the R&R abattoir (slaughterhouse) in Pretoria North, South Africa. Other chemicals used were of analytical grade.

4.2.2 Methods

Thermosensitive liposomes (TSLs) and non-thermosensitive liposomes (NTSLs) loaded with the anti-HIV drug (EFV) and the antimalarial (MQ) were prepared by thin-film lipid hydration and sonication methods (Achim *et al*., 2009:703; Xiao *et al*., 2016:83; Perez *et al*., 2016:190; Sauvage *et al*., 2016:101; Chen *et al*., 2016:74; Zhang *et al*., 2014:2177). Preparation of TSLs needs an increase in temperature to above ambient (e.g. around 55 ºC) whereas NTSLs can be prepared without the need to increase the temperature above room temperature (Achim *et al*., 2009:705). TSLs were based on dipalmitoylphosphatidylcholine (DPPC), distearoylphosphatidylcholine (DSPC) and cholesterol (CHOL) and non-thermosensitive liposomes (NTSL) were based on L-α-phosphatidylcholine, dioleoyl (DOPC) and CHOL. To select liposomal platforms with best entrapment efficiency, different molar ratios of phospholipids were used, and their albumin entrapment efficiencies were assessed. The TSL were prepared in the following molar ratios: (1) DPPC: CHOL (1:1, mol/mol) and (2:1, mol/mol) (Yucel, Degim & Yilmaz, 2013:460) and (2) DSPC:CHOL:DPPC (4:6:26, mol/mol/mol) (Achim *et al*., 2009:705). The molar ratios for the preparation of non-thermosensitive liposomes were DOPC:CHOL (30:6, mol/mol) and (1:1, mol/mol) (Salva *et al*., 2015:148).

4.2.2.1 Preparation of small unilamellar vesicles (SUVs)/liposomes

(1) Thin-film preparation

A 5 mg/mL stock solution of each lipid was prepared by dissolving a 50 mg lyophilized lipid powder in a 10 mL volume of chloroform in a 20 mL scintillation vial to form a lipid solution. A suitable volume (µL) determined based on pre-determined molar ratios of

lipids, from each lipid stock solution was mixed with a volume of another lipid in a separate 20 mL scintillation vial to form a lipid mixture of the desired molar ratio such that the final volume was 225 µL.

(i) Lipid films for hydrophilic substances

After the lipid solutions were thoroughly mixed, chloroform was evaporated in the fume-hood at room temperature over 24 hours. The residual chloroform was removed by briefly maintaining the film under a nitrogen gas flow until a dry film was formed at the base of the vial (Achim *et al*., 2009:705). These lipid films were used for most PDAEs since these substances were hydrophilic in nature.

(ii) Lipid films for hydrophobic substances

EFV is a hydrophobic anti-HIV drug and because of its lipid-loving nature, it was insoluble in water, but dissolved well in chloroform. *In vivo* study involving rats administered EFV in a 20 mg/kg concentration (Moller, Fourie & Harvey, 2018:2), which is around 500 µg/mL concentration according to the average body weight of mice. Therefore, a 200 µL volume of a 500 µg/mL concentration of EFV solution in chloroform was mixed with the lipid mixture prior to the drying step. Chloroform was evaporated from the mixture under the fume-hood at room temperature over 24 hours, followed by removal of residual organic solved using nitrogen gas.

Mefloquine is a hydrophobic antimalarial drug, which is practically insoluble in water, sparingly soluble in ethanol, and freely soluble in methanol. A 500 µg/mL MQ solution was prepared in methanol. A 200 µL volume of this solution was mixed with the lipid

mixture prior to the thin-film formation. Chloroform and methanol were evaporated from the mixture in the fume-hood at room temperature over 24 hours, followed by removal of residual organic solvent using nitrogen gas.

The PDAE curcumin was insoluble in water and dissolved well in methanol. Preliminary *in vitro* and *ex vivo* studies suggested that curcumin at the concentration of 100 µM in combination with quercetin at a concentration of 75 µM were more effective as PDAE. At least 50% entrapment efficiency of these PDAEs was anticipated, therefore, a 200 µM and 150 µM of curcumin and quercetin, respectively, were initially loaded into the liposomes.

Curcumin is a hydrophobic PDAE, which is practically insoluble in water, and freely soluble in methanol. A 200 µM curcumin solution was prepared in methanol. A 200 µL volume of this solution was mixed with the lipid mixture prior to the thin-film formation. Chloroform and methanol were evaporated from the mixture in the fume-hood at room temperature over 24 hours, followed by removal of residual organic solvent using nitrogen gas.

The PDAE quercetin dissolved better in ethanol. Therefore, a thin film lipid mixture for quercetin-loaded liposomes was prepared by mixing the film lipid mixture with a 200 µL volume of a 150 µM quercetin in ethanol. Chloroform and ethanol were removed from the mixture under the fume-hood at room temperature using the fan for 24 hours, followed by removal of residual organic solved with nitrogen gas.

(2) Thin-film hydration

(i) Preparation of liposome blank/placebos

The dried lipid film was hydrated by adding a 200 µL volume of phosphate-buffered saline (PBS) solution. The vial was sealed, mixed on a vortex mixer for 10 seconds intervals up to 7 times to form a lipid-PBS emulsion.

(ii) Preparation of drug-loaded liposomes

- *For hydrophilic molecules (e.g. chicken egg albumin):* A drug was dissolved in PBS (pH 7.4) to form a drug solution. The dried lipid film was hydrated by adding a 200 µL volume of drug solution. The vial was sealed, mixed on a vortex mixer for 10 seconds intervals up to 7 times to form a lipid-drug emulsion.

- *For hydrophobic drugs (e.g. EFV, MQ, and PDAEs curcumin and quercetin*: The dried lipid film containing either a drug or PDAE was rehydrated by adding a 200 µL volume of PBS (pH 7.4) solution. The vial was sealed, mixed on a vortex mixer for 10 seconds intervals up to 7 times to form a lipid-drug emulsion.

(3) Size reduction

Liposomes size reduction was carried out by using sonication technique (Forbes *et al*., 2019:70). After rehydration step, the lipid-drug/PBS emulsion was transferred from the scintillation vial into an Eppendorf tube, placed on ice, and was sonicated for 5 min at 10% amplitude using the Omni Sonic Ruptor 400 sonicator (OMNI International, USA) to obtain liposomes of the desired size range.

4.2.2.2 Characterisation of liposomes

(1) Entrapment efficiency

After the sonication step of SUVs, the non-encapsulated drug was removed by centrifugation at 30,000 xg for 1 hour at 4 ºC, followed by centrifugal rinsing with a 200 µL volume of distilled water at 30,000 xg for 1 hour at 4 ºC using Biocen 22R (Orto Alresa, Spain). For example, after the rehydration and sonication steps, Eppendorf tubes containing liposomal particles were centrifuged and the supernatant was placed in a separate Eppendorf tube and labelled “first wash.” The particles were then mixed with a 200 µL volume of distilled water and centrifuged; the supernatant for this step was labelled “second wash.” After the washing step, the supernatants were analysed using UV/Vis spectroscopy method to quantify the non-encapsulated drug (e.g. the absorbances of supernatants were measured with Spectrostar (BMG LabTech, Germany) microplate reader at a 280 nm wavelength for the chicken egg albumin, at a 248 nm for EFV, MQ at 221 nm, curcumin at a 423 nm, and quercetin at a 374 nm). The pellet (Figure 4.1) was suspended in a 200 µL volume of PBS and stored at 4 ºC until used.

(2) Particle size and zeta potential

Mean particle diameter (z-average) and zeta potential (surface charge) of liposomes were measured in a folded capillary cell using Malvern Zetasizer Nano ZS (Malvern, UK). The measurements were made at 25 ºC in triplicate. For both measurements, a 10 mL volume of liposomes was pipetted into a 1.5 mL Eppendorf tube and suspended in a 90 mL volume of filtered phosphate-buffered saline (PBS) at pH 7.4 (Salva *et al*., 2015:149).

FIGURE 4.1: Liposome pellet (Kheoane Photo Library, 2017)

The samples were ultrasonicated in a water bath for 60 seconds and topped to 1 mL with 0.9 mL filtered PBS and gently mixed. The folded capillary cell was rinsed with filter PBS before use and filled slowly in an inverted position using a 1 mL syringe then flipped upright when the sample front reached the U-base of the cell to avoid air bubbles from being retained. Once the sample began to emerge from second sample port, a stopper was inserted, and the syringe was removed and placed with a second stopper. The cell was checked for bubbles within the clear capillary area and any liquid that spilt onto the electrode was wiped off. The cell was placed into the apparatus and the particle size (nm) and zeta potential (mV) were measured using a predefined zeta sizer software protocol results were recorded.

(3) *In vitro* drug release from the dosage forms

An *in vitro* drug release of liposomes was carried out to determine the rate and extent, at which the entrapped drug was released from the liposomal vesicles. A solution containing 0.1% tween 20 and 10% fetal bovine serum (FBS) was prepared in PBS. Tween 20 was used as a surfactant, therefore, helps with the release of entrapped drug.

Tween 20 was used to simulate the conditions of the gastrointestinal tract where natural surfactants (i.e. surfactants in gastric juice and bile) are present and responsible for enhancing drug absorption through increasing the rate and extent of drug dissolution through micellar solubilization (Aulton & Taylor, 2013:315). A 50 µL volume of particles were mixed with a 50 µL volume of 10% FBS-0.1% tween 20 solution in the Eppendorf tube. The mixture was incubated in a ThemoMixer C incubator (Eppendorf AG, Germany), at 37 ºC. After incubation, the mixture was centrifuged at 30000 xg at 4 ºC for 15 minutes. A 20 µL volume of the resultant supernatant was withdrawn and placed in a 96-well microplate and diluted with 80 µL volume of 10% FBS-0.1% tween 20 solution to 100 µL sample for each microplate well. A 20 µL volume of supernatant taken from the experimental Eppendorf tube was replaced with a 20 µL volume of 10% FBS-0.1% tween 20 solution. These steps were repeated in 30 minutes time interval for the first 2 hours (i.e., 30, 60, 90, 120 min), then after 3 hours and finally after 24 hours. The absorbances of the contents of the microplate were measured at 248 nm for EFV and 221 nm for MQ.

(4) *In vitro* drug permeability studies

A dialysis bag (14 kDa) was used as a semi-permeable membrane allowing drug molecules to pass through its pores while retaining the liposomal vesicles. A donor compartment was created using a dialysis membrane tube (9 cm), which was sealed on one end. A 5 mL volume of sample (e.g., EFV 20 µg/mL, MQ 18.4 µg/mL) was placed into the membrane tube and the second end of the membrane opening was sealed. A receiver compartment (i.e., release medium) was created by placing a 50 mL volume of PBS into a 50 mL conical tube. A dialysis bag containing a sample (donor compartment) was submerged completely into the release medium to initiate the drug transport process.

The conical tube and its contents were incubated at 37 ºC and 100 rpm in the Scientific incubator shaker (Labotec, South Africa). A 1 mL volume of sample was withdrawn after every 30 minutes for 2 hours then after 3 hours and finally after 24 hours. The withdrawn sample was replaced with a 1 mL volume of PBS after each withdrawal. The absorbance of EFV was measured at 248 nm and MQ at 221 nm.

4.2.2.3 *In vitro* toxicological effects of optimised liposomes

(1) Preparation of the 1640 RPMI culture media

A 500 mL volume of the 1640 RPMI culture media containing 10% FBS, 2% L-glutamine and 1% penicillin – streptomycin (Pen-Strep) was prepared. Briefly, a 440 mL of 1640 RPMI solution was pipetted into a sterile conical tube using a sterile pipette tip. Into this solution, a 50 mL volume of FBS, a 5 mL volume of the L-glutamine solution and a 5 mL volume of the Pen-Strep were pipetted. All the preparation steps of the 1640 RPMI culture media were done under the laminar flow to maintain aseptic conditions and ensure sterility. The Pen-Strep is a combination of penicillin and streptomycin broad-spectrum antibiotics and was added into the media as prophylaxis against bacterial contamination during the incubation period of the cells. Both the FBS and L-glutamine were used as sources of nutrition and essential amino acids for the cells.

(1) Revival and cultivation of H-4-II-E cells

The lyophilized H-4-II-E cells were aseptically revived in the prepared 1640 RPMI culture media. A 10 mL volume of 1640 RPMI culture media was used to hydrate the entire vial of lyophilized H-4-II-E cells. The mixture was then transferred into a 50 mL sterile conical

tube, the cap of the tube was partially closed and incubated at 37 ºC, 5% CO2 and humidified atmosphere for 5 days.

(2) Seeding of H-4-II-E cells

The revived and cultivated H-4-II-E cells were enumerated using the BIO-RAD Automated Cell Counter (Model: TC20TM). A 150 µL volume (6.6 x 104 cells) were seeded in triplicates into a sterile, 96-well opaque luminescence microplate under aseptic conditions. The microplate was then covered and incubated at 37 ºC, 5% CO2 and humidified atmosphere for 3 days. After 3 days, the microplate was treated with either liposome loaded with test compounds or blank liposomes or 1640 RPMI culture media and was further incubated for 24 hours under the same atmospheric conditions. The same procedure was repeated three times to assess the reproducibility of results.

(3) Performing CellTiter-Glo luminescent cell viability assay

The CellTiter-Glo® Luminescent Cell Viability Assay is a homogeneous method to determine the number of viable cells in culture based on quantitation of the ATP present, which signals the presence of metabolically active cells. The amount of ATP is directly proportional to the number of cells present in culture in agreement with previous reports (Promega, 2015:1; Crouch *et al.*, 1993:81).

(i) Preparation of CellTiter-Glo® reagent

The lyophilized CellTiter-Glo® substrate and the frozen CellTiter-Glo® buffer were equilibrated to room temperature prior to use. A 10 mL volume of CellTiter-Glo® buffer was transferred into the amber bottle containing CellTiter-Glo® substrate to reconstitute

the lyophilized enzyme/substrate mixture. This formed the CellTiter-Glo® reagent. The reagent was mixed by gentle vortexing to obtain a homogeneous solution.

(ii) Preparation of the adenosine triphosphate (ATP) standard solution

The ATP stock solution (40 µM) was prepared in 1640 RPMI culture media. For ATP standard curve determination, the serial dilution was performed from the stock solution such that the final concentrations were 0.0313, 0.0625, 0.125, 0.25, 0.5, 1, 2, and 4 µM.

(iii) Treatment of the H-4-II-E cells with test compounds

A 150 µL volume or less (i.e. where the volume of the test compound was less than 150 µL, the volume was made up to 150 µL by adding the CellTiter-Glo® buffer), of either drug-based liposomes or placebo liposomes was injected into a 96-well opaque microplate containing live cells such that two different concentrations (i.e. a 123 µg/mL and 74 µg/mL) for EFV and EFV-PDAEs liposomes and two different concentrations (i.e. 105 µg/mL and 63 µg/mL) for MQ and MQ-PDAEs were achieved. The microplate was then incubated for another 24 hours prior to the cell viability assay step.

(iv) Performing cell viability assay

The 96-well opaque plate containing treated and untreated H-4-II-E cells was equilibrated

at room temperature for 30 minutes. After incubation, a 150 µL volume of the CellTiter-Glo® reagent was placed into each well of the plate. The contents of the plate were mixed for 2 minutes on an orbital shaker to induce cell lysis. The plate with its contents was then incubated at room temperature for 10 minutes to stabilize the luminescent signal. After

the incubation, the luminescence was measured using the luminometer set at an integration time of 0.25 to 1 second per well. The control wells containing 1640 RPMI culture media without cells and/or blank liposomes were used to obtain a value for background luminescence.

(v) Performing the ATP assay for standard curve for ATP standard curve

A 150 µL volume of different concentrations (0.0313, 0.0625, 0.125, 0.25, 0.5, 1, 2, and 4 µM) of the ATP solution were plated in triplicates in the 96-well opaque microplate. The 1640 RPMI media was added instead of the ATP solution for the untreated wells to obtain the background luminescence. A 150 µL volume of the CellTiter-Glo® reagent was added to every well. The contents of the plate were then mixed on an orbital shaker for 2 minutes. The plate with its contents was then incubated at room temperature for 10 minutes to stabilize the luminescence signal. The luminescence was then measured using the luminometer.

4.2.2.4 *Ex vivo* drug permeability studies using optimised liposomes

(1) Preparation of test mixtures

A 200 µL volume of liposomal formulation was mixed with a 6.8 mL of PBS (pH 7.4) such that the final concentration of DOPC:CHOL-based EFV and EFV-PDAEs liposomal test mixtures was 13.4 µg/mL while the final concentration of the DSPC:CHOL:DPPC-based MQ liposomal test mixture was 12.0 µg/mL and that of the DSPC:CHOL:DPPC-based MQ-PDAEs liposomal test mixture was 13 µg/mL. Both EFV and MQ standards (positive controls) were prepared at a concentration of 500 µg/mL.

(2) Collection of porcine intestinal tissue

The porcine intestinal tissue was collected from the R&R abattoir in Pretoria North, South Africa following the procedure described in chapter three.

(3) Preparation of porcine intestinal tissue for Ussing chambers

In the laboratory, the jejunum tissue was pulled over a test tube. The serosal, overlaying longitudinal and circular muscles were stripped off with blunt dissection (Legen & Salobir, 2005:185). A piece of jejunum tissue was cut along the mesenteric border to form a jejunum sheet, which was repeatedly washed off from the glass tube to remove any intestinal contents and the excess mucus. The tissue was then washed off onto a sheet of filter paper in a glass dish. The jejunum sheet was cut into smaller pieces, which were mounted on the diffusion chamber inserts. The inserts were clamped between two diffusion chamber half cells linked to the heating block of a Sweetana-Grass diffusion chamber (Tarirai *et al*., 2012:254).

(4) Drug permeability studies across excised porcine jejunum tissue

At the beginning of the experiments, the Ussing chamber system/diffusion chambers, Figure 4.2, with the tissue were pre-incubated with 7.0 mL of PBS (pH 7.4) at 37 ºC for 20 minutes to equilibrate the contents (Neuhoff *et al*., 2003:1142). A mixture of 5% carbon dioxide and 95% oxygen was bubbled into the chambers to stir the contents and prevent stagnant layer formation. A 7 mL volume of liposomal test mixture or the standard test compound was introduced into the donor chamber followed by 20 min incubation.

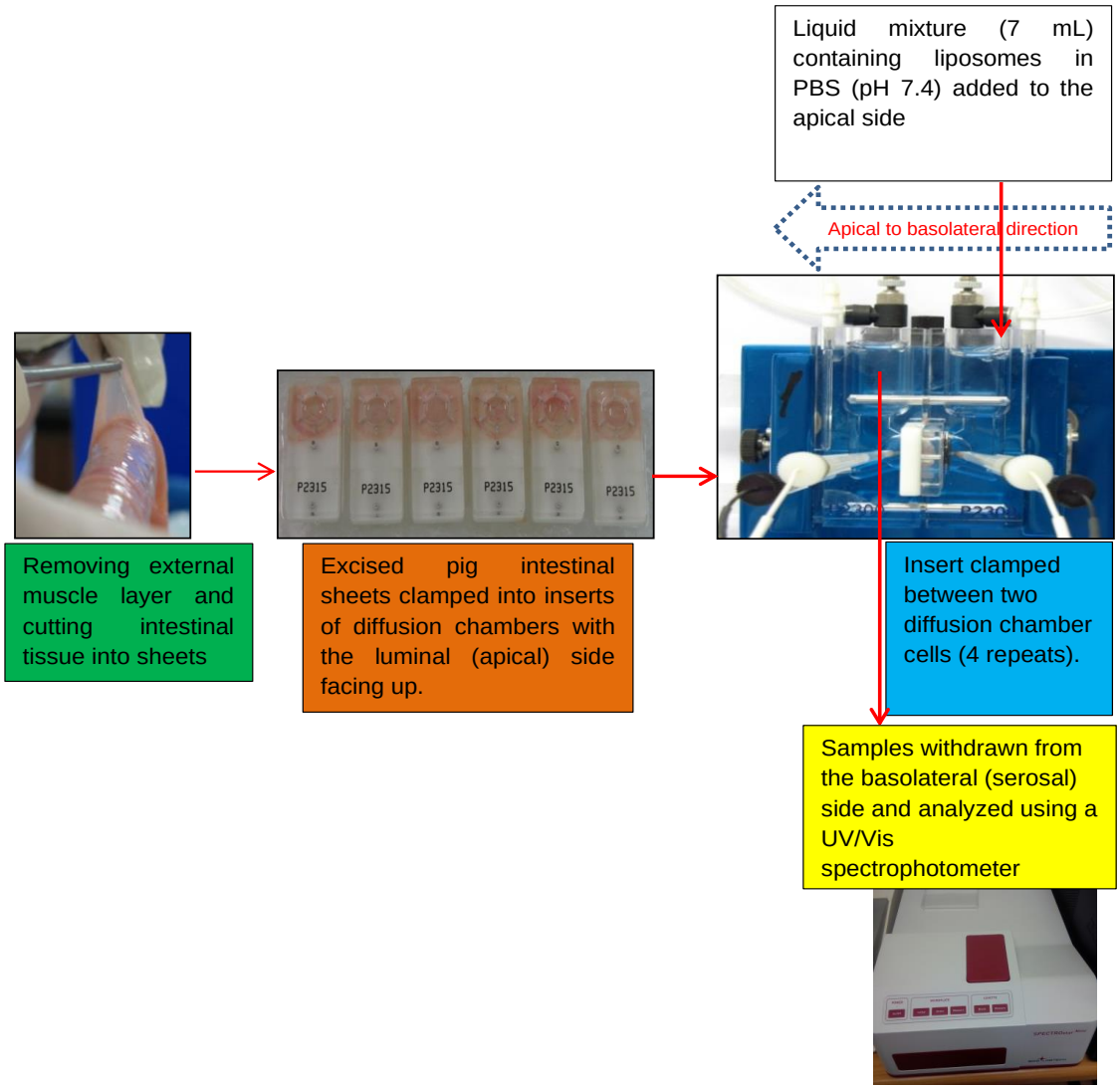

FIGURE 4.2: Ussing chamber system (Kheoane Photo Library, 2020)

Samples of 200 µL were withdrawn from the receiver chamber every 20 min up to 2 h and were immediately replaced by a 200 µL volume of pre-warmed PBS (pH 7.4) into the receiver chamber to maintain ionic equilibrium. The drug permeability studies were performed in both the apical-to-basolateral (A-B) and basolateral-to-apical (B-A) directions across the excised pig jejunum tissue. Drug permeability experiments were conducted in four replicates (Tararai *et al*., 2012:254).

(i) Drug sample analysis

Drug analysis was performed according to the method developed by De Sa Viana et al. (2011:98-99) with some modifications, using the high-performance liquid chromatography (HPLC) system, which was composed of the Waters 717 plus Autosampler, Waters 1525 Binary HPLC Pump, and Waters 2487 Dual Absorbance Detector. The HPLC chromatographic conditions were as follows:

- *Column*: C18 reverse-phase HPLC column, (250 x 3.9 mm, 10 µm).
- *Mobile phase*: Acetonitrile with 1% formic acid – the elution mode was isocratic.
- *Flow rate*: 1.5 mL/min
- *Injection volume*: 20 µL
- *Column temperature*: Ambient
- *Run time*: 10 minutes
- *Retention time*: 7.5 minutes
- *Detection wavelength*: 248 nm.

4.2.3 Data analysis

4.2.3.1 Entrapment efficiency

The amount of the drug retained in the washes after sonication and centrifugation of liposomes was measured on UV/Vis spectrophotometer. The standard curve of curcumin, quercetin, albumin, EFV and MQ was constructed using the Microsoft Excel 2016. The amount of the drug in the washes was calculated using the standard curve equation. The percentage entrapment efficiency (EE%) of liposomes was calculated using Equation 4.1:

$$EE\% = \frac{Di - Dw}{Di} \times 100 \qquad \text{[Equation 4.1]}$$

Where D_i is the initial amount of drug-loaded in the liposomes and D_w is the amount of drug retained in the washes.

4.2.3.2 Particle size and zeta potential

The data from Malvern Zetasizer Nano ZS (Malvern, UK) was analysed in Microsoft Excel 2016 to obtain average particle size and zeta potential and standard deviations.

4.2.3.3 *In vitro* drug release

The UV/Vis spectrophotometer data of the *in vitro* drug release study was analysed in Microsoft Excel 2016. The amount of the drug release from the liposomes over 24-hour period was calculated from the standard curve and the percentage drug release (DR%) was calculated using Equation 4.2:

$$DR\% = \frac{D_{rm}}{D_{LPs}} \times 100 \qquad \text{[Equation 4.2]}$$

Where D_{rm} was the concentration of the drug in the release medium over a predefined time interval and D_{LPs} was the initial concentration of liposomes.

4.2.3.4 *In vitro* drug permeability

The UV/vis spectrophotometer data was analysed in Microsoft Excel 2016 to quantify the amount of the drug transported from the donor compartment into the receiver compartment through a semi-permeable dialysis membrane over 24-hour period. The amount of drug transported was calculated from the standard curve and the percentage of drug transported (DT%) was calculated using Equation 4.3:

$$DT\% = \frac{D_{receiver}}{D_{donor}} \times 100 \qquad \text{[Equation 4.3]}$$

Where $D_{receiver}$ was the concentration of the drug in the receiver compartment (release medium) and D_{donor} was the concentration of the drug in the donor compartment.

4.2.3.5 *In vitro* toxicological effects of liposomes

The luminometer data was analysed in Microsoft Excel 2016. The increased value of the luminescence indicated the high amount ATP present and the increased number of H-4-II-E cells in the culture medium. The amount of ATPs present in every well of a 96-well plate containing both test compound treated, and untreated H-4-II-E cells were calculated from the ATP standard curve. The obtained values of the ATP from the ATP standard curve were then expressed as percentage cell viability.

Statistical analysis of the toxicological effects of liposomes data was performed with Microsoft Office Excel 2016 using a one-way analysis of variance (ANOVA, $p < 0.05$) to

indicate significant statistical differences in the cytotoxic effects of various liposomal formulations containing PDAEs compared to the control on live H-4-II-E cells.

4.2.3.6 *Ex vivo* drug permeability studies of liposomes

The samples were analysed using HPLC and there were no usable values. The same samples were measured using UV/Vis spectrophotometer for confirmation. However, there were still no usable values for analysis. The possible reasons for this observation were discussed under the discussion section of this chapter.

4.3 RESULTS

4.3.1 Entrapment efficiency

Liposomes loaded with albumin were prepared to acquire the preliminary data for screening the phospholipid combinations with potentially better entrapment efficiency (EE%). Preliminary data of albumin-loaded liposomes showed that DPPC and CHOL-based liposomes in 1:1 mol/mol molar ratio had the best EE% of 86% than DPPC:CHOL (2:1 mol/mol) (Table 4.1). DOPC:CHOL (1:1 mol/mol) also produced better EE% of 70% than DOPC:CHOL (30:6 mol/mol) while DSPC:CHOL:DPPC (4:6:26 mol/mol/mol) had the EE% of 47% (Table 4.1). Therefore, DPPC:CHOL (1:1 mol/mol), DOPC:CHOL (1:1 mol/mol) and DSPC:CHOL:DPPC (4:6:26 mol/mol/mol) liposomal platforms were selected for further studies.

The selected liposomal platforms were loaded with curcumin, quercetin, EFV, MQ, EFV-curcumin-quercetin, and MQ-curcumin-quercetin. All three liposomal platforms showed best EFV and EFV-curcumin-quercetin EE% of more than 90% with DOPC:CHOL

liposomes having the highest entrapment efficiency of 94% for both EFV samples (Table 4.2). DSPC:CHOL:DPPC liposomes had better EE% of curcumin (67%), quercetin (88%), MQ (84%), and MQ-curcumin-quercetin (91%) than DPPC:CHOL and DOPC:CHOL liposomes.

4.3.2 Particle size and zeta potential

The particle size and surface charge of liposomes were measured using Zetasizer Nano-ZS (Malvern, UK) and the results are presented in Table 4.3. The particle size of all types of liposomes (i.e. DPPC:CHOL, DOPC:CHOL and DSPC:CHOL:DPPC liposomes) ranged from 96.0 ± 1.6 nm to 230.0 ± 1.8 nm and varied between and within liposome types, while the zeta potential ranged from -14.1 ± 0.5 mV to -3.0 ± 1.1 mV. Quercetin-loaded DPPC:CHOL liposomes had the largest particle size while MQ-loaded DPPC:CHOL liposomes (MQ-DPPC:CHOL:DPPC-LPs) had the smallest particle size. In terms of the zeta potential, MQ-loaded DSPC:CHOL:DPPC liposomes (MQ-DSPC:CHOL:DPPC-LPs) had the highest zeta potential than all other types of liposomes while EFV-loaded DOPC:CHOL liposomes (EFV-DOPC:CHOL-LPs) had the lowest zeta potential. In general, DSPC:CHOL:DPPC liposomes had the highest surface charge than other types of liposomes, followed by DPPC:CHOL liposomes while DOPC:CHOL liposomes had the lowest surface charge than the former liposome types.

TABLE 4.1: Entrapment efficiencies of different albumin-loaded liposomes

Albumin-loaded liposomes	***EE%**
DPPC:CHOL (1:1 mol/mol)	86.0 ± 6.0
DPPC:CHOL (2:1 mol/mol)	14.0 ± 2.0
DOPC:CHOL (1:1 mol/mol)	70.0 ± 1.0
DOPC:CHOL (30:6 mol/mol)	51.0 ± 4.0
DSPC:CHOL:DPPC (4:6:26 mol/mol/mol)	47.0 ± 4.0

*Value = mean ± SD, n = 4

TABLE 4.2: Entrapment efficiencies for different liposomes loaded with PDAEs alone and/or the drug

Nanocarrier	**EE%**					
	[a]Cur	**[b]Quer**	**[c]EFV**	**[d]MQ**	**[e]EFV-Bio**	**[f]MQ-Bio**
DPPC:CHOL	41.0 ± 0.2	61.0 ± 1.4	92.0 ± 0.1	23.0 ± 1.8	92.0 ± 0.2	47.0 ± 2.0
DOPC: CHOL	39.0 ± 0.6	67.0 ± 3.4	94.0 ± 1.3	42.0 ± 2.2	94.0 ± 0.3	68.0 ± 2.2
DSPC: CHOL:DPPC	67.0 ± 1.9	88.0 ± 4.1	91.0 ± 0.7	84.0 ± 0.8	91.0 ± 0.8	91.0 ± 0.5

Abbreviations: [a]Cur = Curcumin alone; [b]Quer = Quercetin alone; [c]EFV = Efavirenz alone; [d]MQ = Mefloquine alone; Bio = Bioenhancer/Plant-derived absorption enhancer (i.e. curcumin and quercetin combination); [e]EFV-Bio = Efavirenz- curcumin + quercetin combination; [f]MQ-Bio = Mefloquine- curcumin + quercetin combination (value = mean ± SD, n = 4)

TABLE 4.3: Particle size and zeta potential values of different drug-loaded liposomes

	DPPC:CHOL-LPs		**DOPC:CHOL-LPs**		**DSPC:CHOL:DPPC-LPs**	
	Particle size (d. nm)	Zeta potential (mV)	Particle size (d. nm)	Zeta potential (mV)	Particle size (d. nm)	Zeta potential (mV)
Blank	110.0 ± 1.2	-7.2 ± 1.0	102.0 ± 1.8	-10.1 ± 1.0	118.0 ± 2.4	-4.2 ± 0.4
Cur	135.0 ± 2.6	-9.4 ± 0.1	166.0 ± 4.3	-10.6 ± 0.9	165.0 ± 5.0	-5.0 ± 0.1
Quer	230.0 ± 8.7	-6.6 ± 0.5	139.0 ± 0.8	-11.1 ± 1.0	103.0 ± 3.1	-5.3 ± 0.6
EFV	177.0 ± 5.1	-8.0 ± 0.9	131.0 ± 2.5	-14.1 ± 0.5	160.0 ± 2.8	-4.7 ± 0.3
MQ	96.0 ± 1.6	-7.8 ± 1.7	121.0 ± 2.1	-10.4 ± 0.6	120.0 ± 4.0	-3.0 ± 1.1
EFV-Bio	138.0 ± 2.4	-8.2 ± 0.6	194.0 ± 2.4	-12.0 ± 1.2	174.0 ± 9.8	-7.0 ± 0.7
MQ-Bio	182.0 ± 3.1	-7.2 ± 1.3	168.0 ± 3.2	-11.8 ± 1.6	188.0 ± 2.4	-5.7 ± 0.9

Abbreviations: Cur = Curcumin alone; Quer = Quercetin alone; EFV = Efavirenz alone; MQ = Mefloquine alone; Bio = Curcumin and quercetin combination; EFV-Bio = Efavirenz-curcumin + quercetin combination; MQ-Bio = Mefloquine-curcumin + quercetin combination, Blank = Unloaded liposomes or placebos (value = mean ± SD, n = 4)

4.3.3 *In vitro* drug release

In vitro drug release study was conducted to quantify the rate and extent of drug release (e.g. EFV and MQ in the presence and absence of PDAEs (also referred to as bioenhancers (Bio) in the present study) from selected liposomal platforms. Drug release was observed over a 24-hour period. Results for DPPC:CHOL liposomes showed an immediate release behaviour (i.e. a maximum amount of the drug released was observed within 30 minutes of the study) of the drug for EFV-based formulations (i.e. EFV and EFV-PDAE liposomes) and a sustained release pattern of the drug was observed in MQ-based formulations (Figure 4.3) where most of the drug was released for the first 3 hours.

Drug release was more in the presence of PDAEs for EFV-based formulations (14%) while the opposite was the case with MQ-based formulations. DOPC:CHOL liposomes produced a controlled release of the drug with a peak drug release at 3 hours for EFV, 90 minutes for EFV-PDAEs, and 2 hours MQ-PDAEs (Figure 4.4). For DOPC:CHOL liposomes, more drug was released in the presence of PDAEs for both EFV and MQ-based formulations while MQ-loaded liposomes retained the drug throughout the study period.

The DSPC:CHOL:DPPC liposomes like DPPC:CHOL liposomes released a drug optimally (17%) within the first 30 minutes of the study for both EFV-based formulations (Figure 4.5). A sustained release behaviour was also observed for MQ-based formulations. Amongst the three liposomal platforms compared for *in vitro* drug release of EFV, EFV-PDAEs, MQ, and MQ-PDAEs, DSPC:CHOL:DPPC liposomes released EFV-based formulations better than DPPC:CHOL plats for immediate release behaviour.

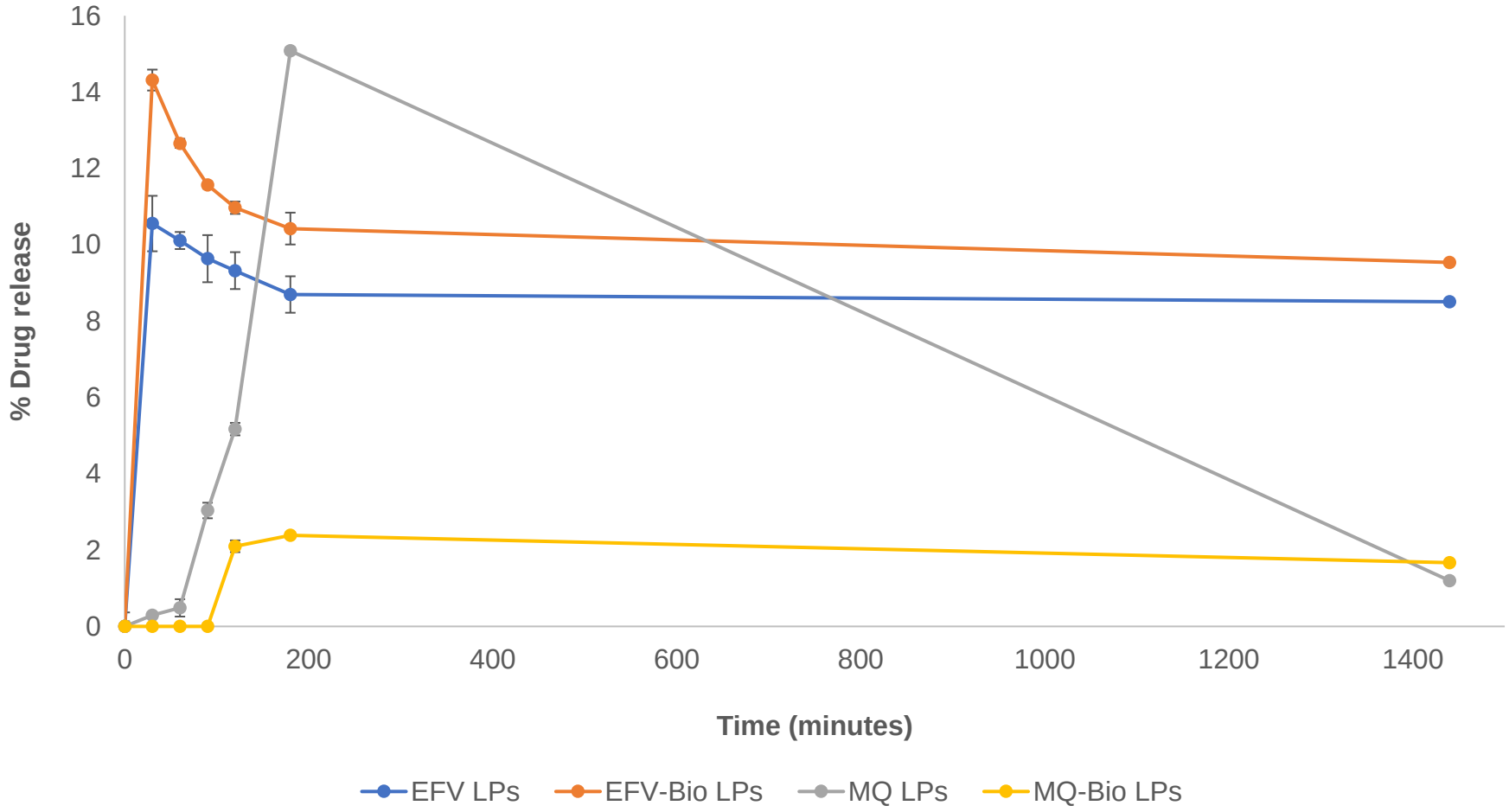

FIGURE 4.3: *In vitro* drug release from the DPPC:CHOL-based liposomes (value = mean ± SD, n = 4)

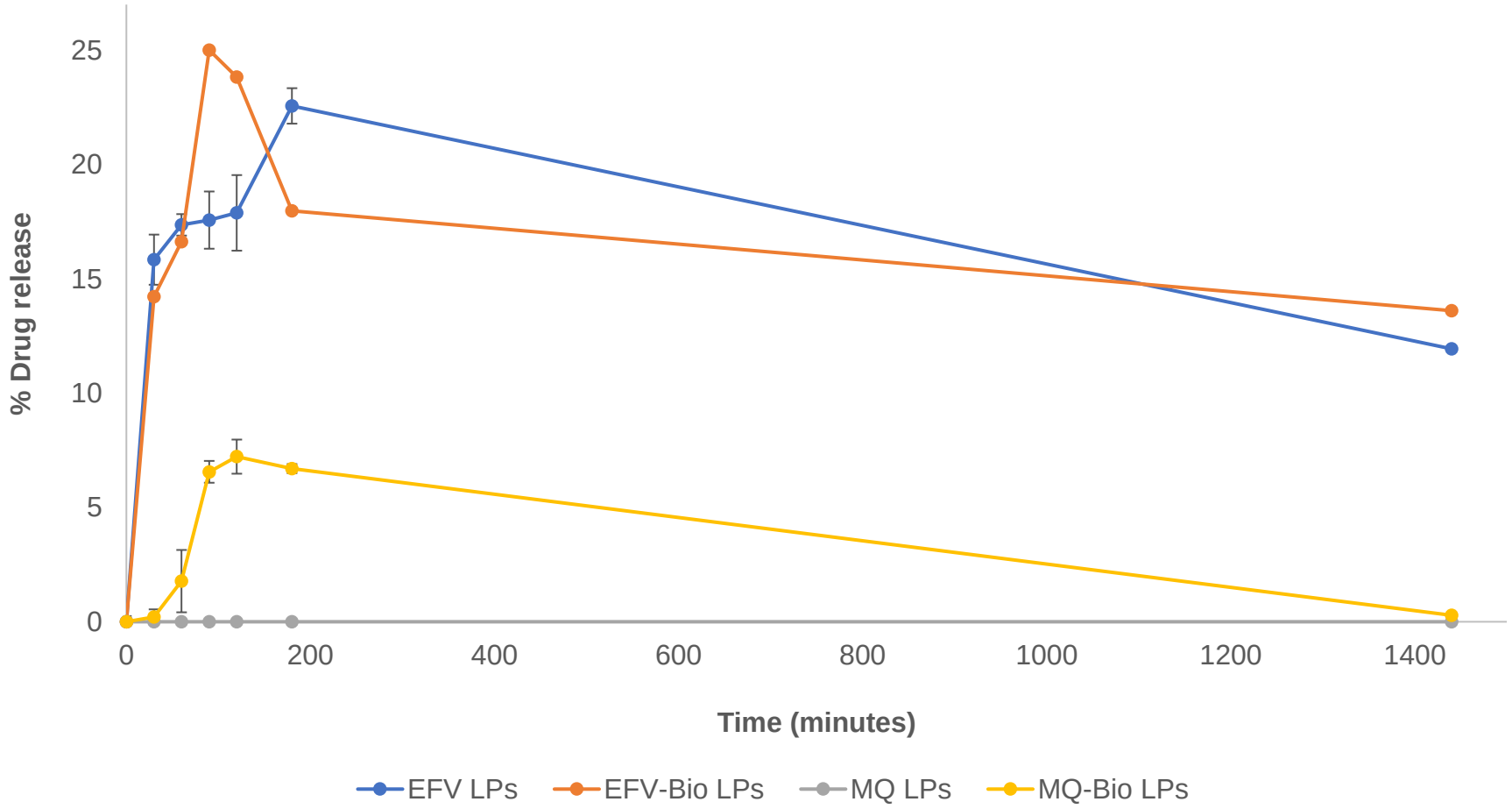

FIGURE 4.4: *In vitro* drug release from the DOPC:CHOL-based liposomes (value = mean ± SD, n = 4)

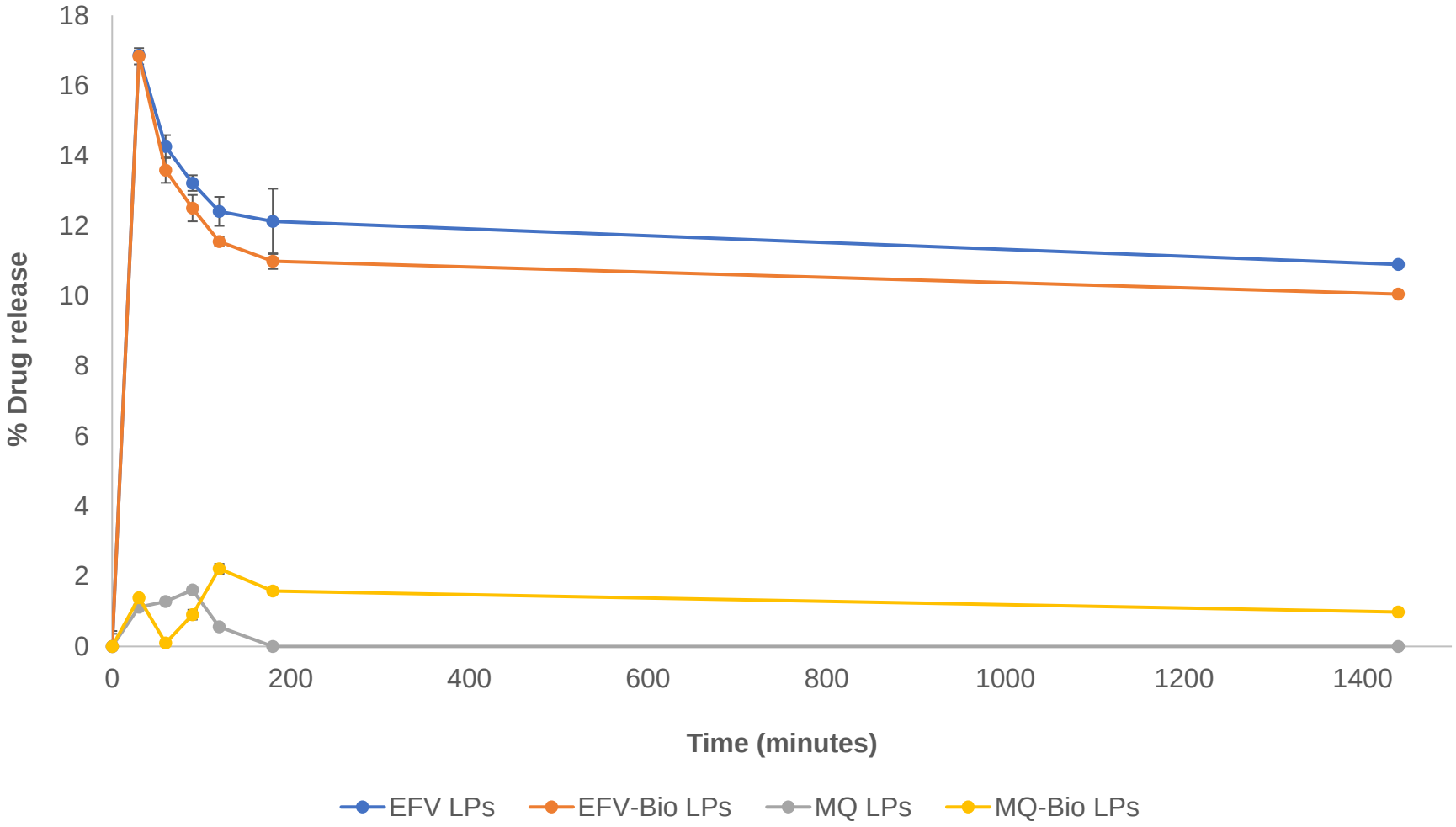

FIGURE 4.5: *In vitro* drug release from the DSPC:CHOL:DPPC-based liposomes (value = mean ± SD, n = 4)

DOPC:CHOL liposomes were best for a sustained release pattern of EFV-based formulations. DPPC:CHOL liposomes released MQ better than both DOPC:CHOL and DSPC:CHOL:DPPC liposomes. On the other hand, DOPC:CHOL liposomes showed better drug release results than DPPC:CHOL and DSPC:CHOL:DPPC liposomes for MQ-PDAEs formulations.

4.3.4 *In vitro* drug permeability

In vitro drug transport studies of EFV, EFV-PDAEs, MQ, and MQ-PDAEs-loaded liposomes were determined using a 14 kDa dialysis membrane. The PBS (pH 7.4) and incubator shaker at 37 ºC were used to simulate the environment and peristaltic movement of the gastrointestinal tract. The movement of the drug was observed over a 24-hour period.

A 70% of EFV was transported through the membrane into a receiver compartment after 24 hours for EFV free drug (positive control) while a 28% MQ control was transported after the same period (Figure 4.6). All liposomes released the drug into a release medium (receiver compartment) in a controlled and sustained manner throughout a 24 hours drug transport study period as compared to EFV and MQ controls. The concentration of the release medium was increasing or cumulative as the time increases. Amongst the three types of liposomes loaded with EFV or EFV-PDAEs, EFV-loaded and EFV-PDAEs-loaded DSPC:CHOL:DPPC liposomes (EFV-Bio-DSPC:CHOL:DPPC-LPs) had higher amount of EFV transport after 24 hours (Figure 4.8) than any other types of liposomes.

There was also slight increase in the amount of EFV transported for EFV-Bio-DSPC:CHOL:DPPC-LPs as compared to EFV-DSPC:CHOL:DPPC-LPs. For MQ-loaded

liposomes, MQ-DOPC:CHOL-LPs had the highest amount of drug transported after 24 hours (Figure 4.7), but had slow onset of drug transport (i.e. a small amount of drug (2%) was measured after 2 hours). MQ-DPPC:CHOL-LPs had slightly lower value of drug transport after 24 hours, but the onset of drug transport was observed after 30 minutes and was consistent throughout 24-hour period (Figure 4.6). The drug transport for MQ-PDAEs liposomes was generally lower for all types of liposomes.

4.3.5 *In vitro* toxicological effects of liposomes

The previous chapter reported the entrapment efficiencies of different types of liposomal platforms and stated varying entrapment efficiencies and thus different concentrations. Based on the entrapment efficiency, *in vitro* drug release kinetics and the *in vitro* permeability studies data, the previous chapter concluded that the DOPC:CHOL-based EFV and EFV-PDAEs were best formulations when compared to other types of liposomal platforms. Similarly, MQ and MQ-PDAEs produced liposomes when formulated in DSPC:CHOL:DPPC platforms. Therefore, the present chapter determined the biocompatibility of the DOPC:CHOL based EFV and EFV-PDAEs liposomes as well as the DSPC:CHOL:DPPC-based MQ and MQ-PDAEs liposomes. Based on the above deducations, DPPC:CHOL formulations were therefore not evaluated for cytotoxicity.

The obtained toxicity data showed higher toxicities of more concentrated samples (i.e. 123 µg/mL and 105 µg/mL) for EFV or EFV-PDAEs and MQ or MQ-PDAEs, respectively, when compared with a less concentrated samples (i.e. 74 µg/mL and 63 µg/mL, respectively) of the same material (Figure 4.9 and Figure 4.10). Higher cell viabilities were observed for untreated cells and when the cells are treated with the placebo liposomes.

The incorporation of PDAEs to EFV liposomes did not change the cell viability at low concentration of EFV (74 µg/mL), but at a higher concentration of EFV (123 µg/mL), PDAEs potentiated EFV toxicity (Figure 4.9).

The incorporation of PDAEs to the MQ liposomes posed some toxic effects to the H-4-II-E cells when both concentrations (105 µg/mL and 63 µg/mL) of MQ were used (Figure 4.10).

4.3.6 *Ex vivo* drug permeability studies of liposomes

The *ex vivo* drug permeability studies data revealed less or no drug permeability through the intestinal tissue for both A-B and B-A directions. This was observed when liposomal formulations and free drug were used for both efavirenz and mefloquine**.**

4.4 DISCUSSION

4.4.1 Entrapment efficiency

The entrapment efficiency of liposomal formulation measures the ability of the liposomal platform to encapsulate a drug. In the present study, different combinations and ratios of phospholipids were screened for better entrapment efficiency by loading them with the chicken egg albumin. The obtained data revealed that the DPPC:CHOL (1:1 mol/mol), DOPC:CHOL (1:1 mol/mol) and DSPC:CHOL:DPPC (4:6:26 mol/mol/mol) had the best entrapment efficiency, and were therefore, selected for the subsequent studies. When loaded with curcumin, quercetin, EFV, MQ, EFV-curcumin-quercetin, and MQ-curcumin-quercetin, these three liposomal platforms showed best EFV and EFV-curcumin-quercetin EE% of more than 90% with DOPC:CHOL liposomes having the highest

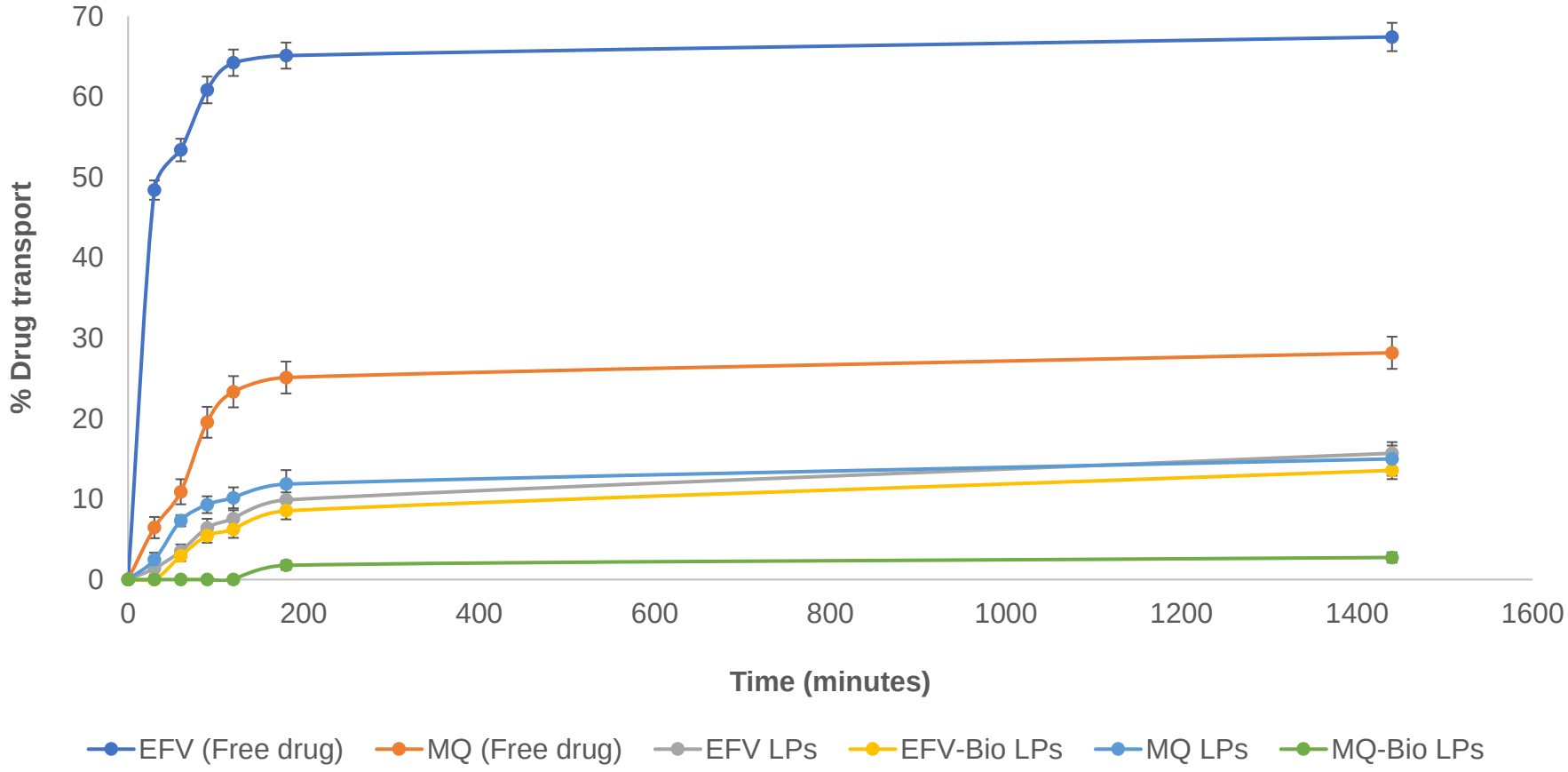

FIGURE 4.6: *In vitro* drug permeability from DPPC:CHOL-based liposomes (EFV = Efavirenz; MQ = Mefloquine; LPs = Liposomes; Bio = combination of curcumin and quercetin; value = mean ± SD, n = 4)

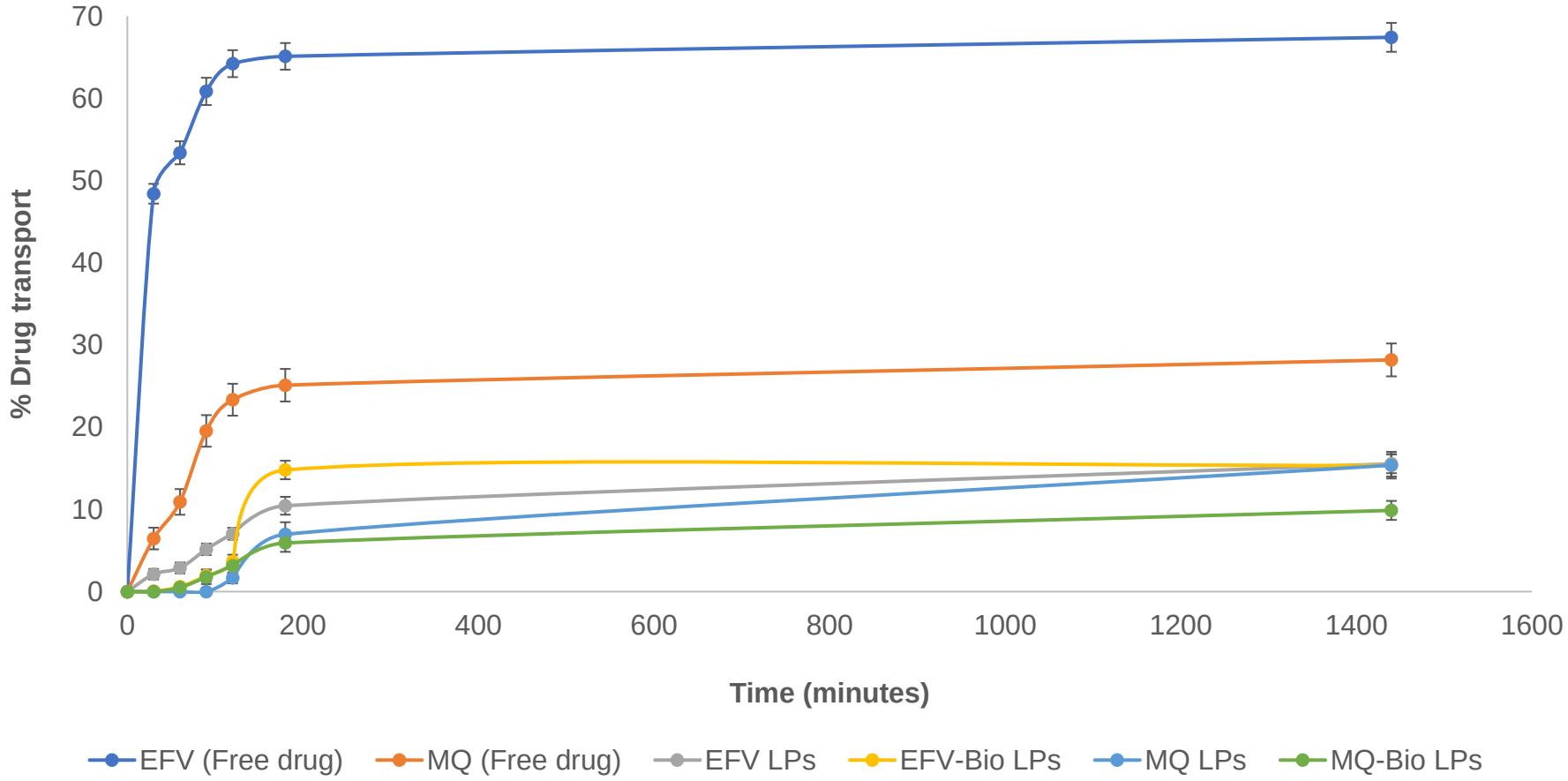

FIGURE 4.7: *In vitro* drug permeability from DOPC:CHOL-based liposomes (EFV = Efavirenz; MQ = Mefloquine; LPs = Liposomes; Bio = combination of curcumin and quercetin; value = mean ± SD, n = 4)

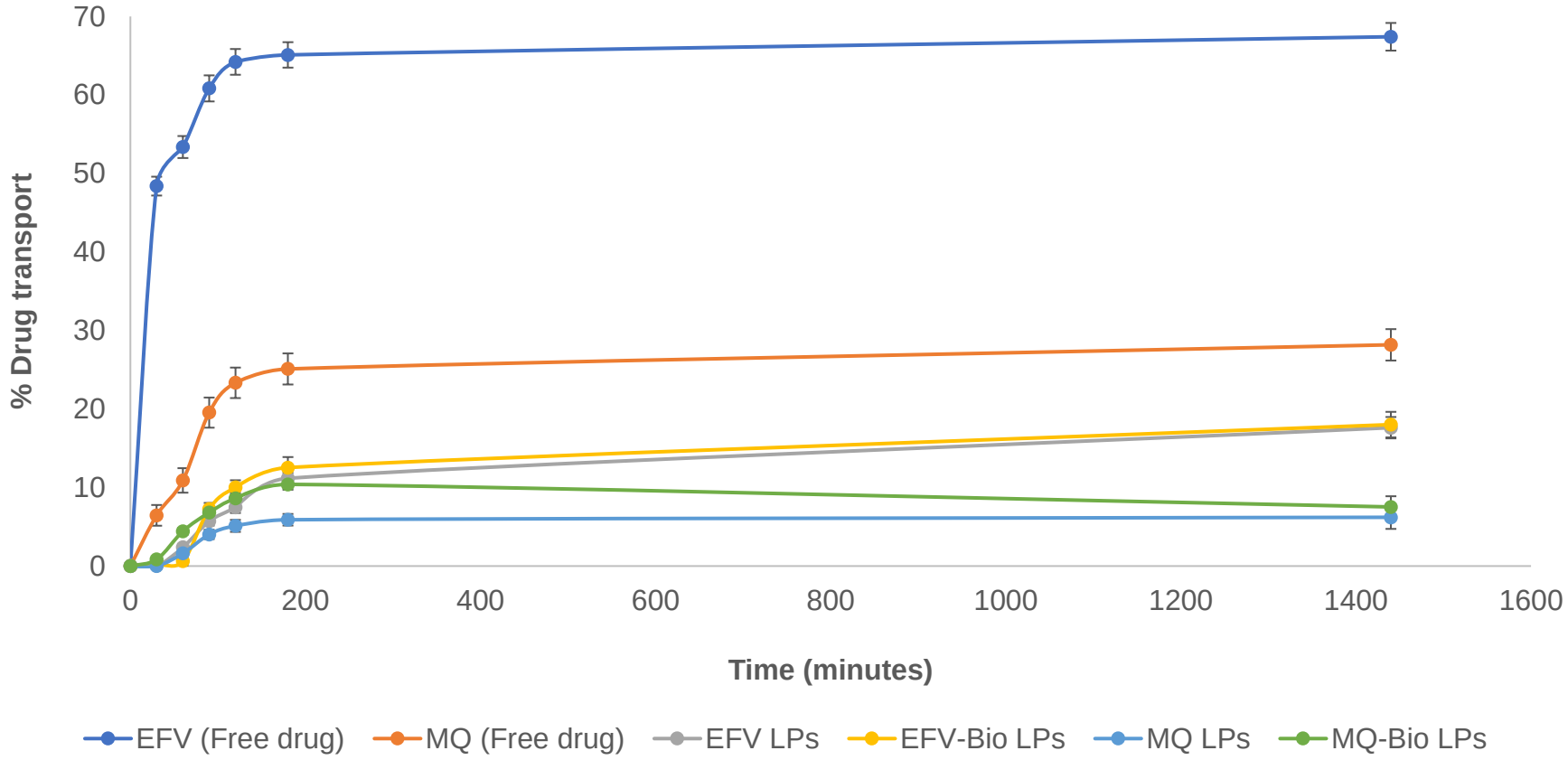

FIGURE 4.8: *In vitro* drug permeability from DSPC:CHOL:DPPC-based liposomes (EFV = Efavirenz; MQ = Mefloquine; LPs = Liposomes; Bio = combination of curcumin and quercetin; value = mean ± SD, n = 4)

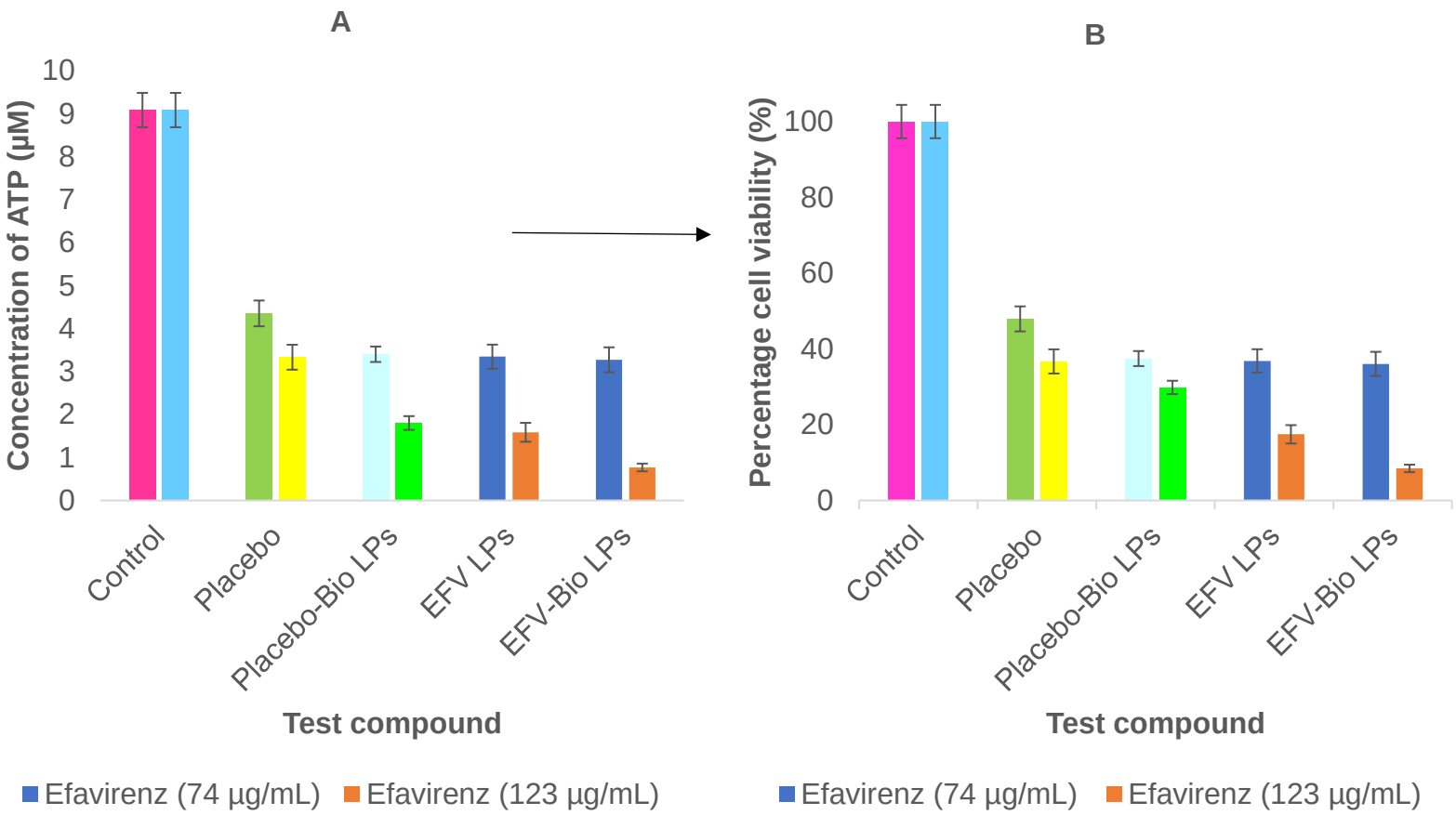

FIGURE 4.9: The amount of ATP (µM) present (A) and the percentage cell viability (B) following the DOPC:CHOL liposomes treatment to the H-4-II-E cells (value = mean ± SD, n = 4; percentage viability values are statistically significant ($p < 0.05$) compared to the control)

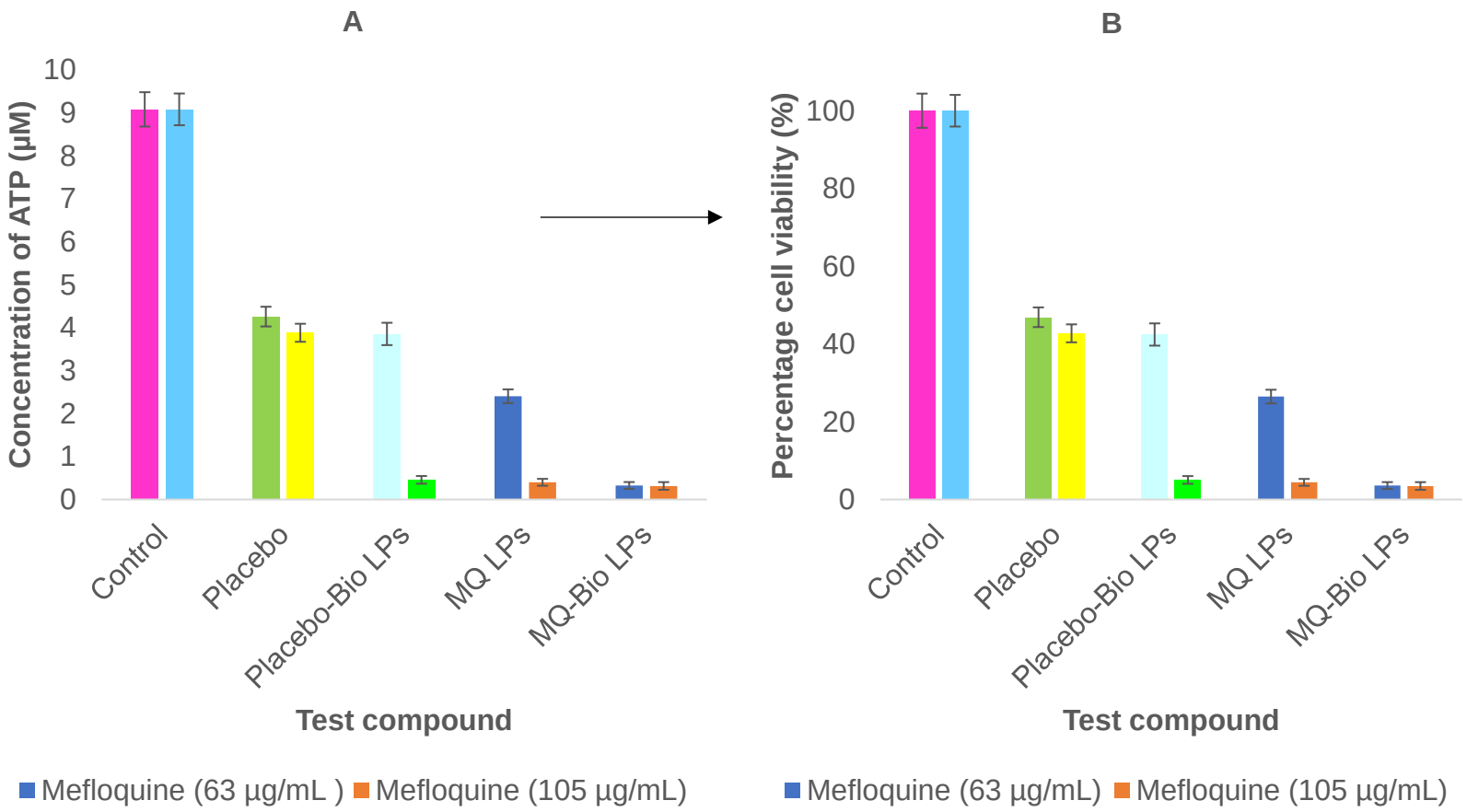

FIGURE 4.10: The amount of ATP (µM) present (A) and the percentage cell viability (B) following the DSPC:CHOL:DPPC liposomes treatment to the H-4-II-E cells (value = mean ± SD, n = 4; percentage viability values are statistically significant ($p < 0.05$) compared to the control)

entrapment efficiency of 94% (i.e. 470 µg/mL) for both EFV samples. DSPC:CHOL:DPPC liposomes had the better EE% of curcumin (67%, 134 µM), quercetin (88%, 132 µM), MQ (84%, 420 µg/mL), and MQ-curcumin-quercetin (91%, 455 µg/mL) than DPPC:CHOL and DOPC:CHOL liposomes. EFV is assigned to BCS II/IV (Cristofoletti *et al*., 2013:328). BCS II drugs are poorly soluble, but highly permeable, whereas BCS IV drugs are poorly soluble and poorly permeable.

Therefore, EFV is more lipid loving. In the present study, EFV entrapment efficiency was more than 90% for all liposomal platforms, and this high loading efficiency was expected for lipophilic drugs due to the amphiphilic nature of phospholipids. For lipophilic drugs, the concentration of the drug is expected to be more within the lipid bilayer where the hydrophobic fatty acids “tails” are located. Curcumin had poor aqueous solubility and could not dissolve in PBS, as such, its solubility was enhanced by adding methanol as a cosolvent. Therefore, curcumin experienced poor entrapment efficiency as compared to quercetin. Because phospholipids dissolve in methanol, enough liposomal platforms were possibly not formed in the presence of methanol as co-solvent in curcumin solution. Loading EFV with the combination of PDAEs could not either decrease or increase the entrapment efficiency of EFV in all three types of liposomal platforms. On the other hand, the entrapment efficiency of MQ was improved by co-loading with the combination of PDAEs (curcumin-quercetin) as compared when it was loaded alone. While it is not clear why the entrapment efficiency suddenly improved, this could be attributed to the interaction between MQ molecules with the molecules of PDAEs curcumin and quercetin, possibly through non-covalent attachment of functional groups of these molecules.

4.4.2 Particle size and zeta potential

As highlighted in the introduction of this chapter, the particle size is an important aspect of colloidal formulations as it describes their nature and may affect their action and interaction with the physiological compartments, for example, nanosized formulations may permeate the gastrointestinal membrane through the paracellular pathway following oral administration. Nanosized materials are described by Aulton and Taylor (2013:778) as structures and products that have one or more dimension between approximately 1 and 100 nm and even up to 1000 nm. In the present study, all the liposomal platforms fell within the prescribed size range of nanosized materials, from 96 ± 1.6 nm to 230 ± 1.8 nm as presented in Table 4.3. The best liposomal particle size range was controlled by setting the probe sonicator to the appropriate amplitude based on the volume the liposomal emulsion. Increasing the amplitude of the sonicator to more than 10% for a 200 µL volume of the liposomal emulsion created a lot of heat that seemed to melt the phospholipids or disrupt the liposomes, therefore the amplitude was maintained at around 10% for that reason.

Zeta potential of a particle is described as a surface charge of the particle and may affect both the pharmacokinetic and pharmacodynamic behaviour of the colloidal dosage form in several ways. For example, if a colloid bears a surface charge, it may remain suspended or deflocculated for a longer time in solution and this is particularly important in the case of suspensions (Aulton & Taylor, 2013:418). In the present study, the surface charges of all types of liposomal platforms were electronegative. The surface charge of these liposomes could improve drug delivery of both the anti-HIV and antimalarial drugs through improved bioavailability and improved affinity at the site of action. The

bioavailability of anti-HIV (e.g. EFV) and antimalarial (e.g. MQ) liposomal formulations following oral administration may be improved in several ways: (1) through improved interaction with aqueous gastrointestinal (GIT) fluid (because they are ionized) i.e. the hydrophilic heads constituting the liposomes will interact with the GIT fluid while hiding the lipophilic drug within its lipophilic tails; (2) through improved absorption due to liposomal formulation attachment to the highly charged GIT membrane i.e. an electronegative liposome has high affinity to the positive charges of the GIT membrane, therefore once bound, it will release an encapsulated unbound form of EFV or MQ, which will immediately permeate through the lipophilic GIT membrane to the basolateral region this membrane.

Similarly, if these liposomal formulations are to be administered through an intravenous route (IV), because of their surface charge, they would interact well with the blood and would be well distributed to their sites of action through the blood circulation.

Once at the site of action, these liposomal formulations would have a greater affinity with the binding sites due to difference in charges. This would imply increase in residence time and prolonged drug release at the site of action and thereby improving pharmacological effects of the drug.

4.4.3 *In vitro* drug release

The *in vitro* drug release study was performed to study the release behaviour of EFV and MQ alone or in the presence of the PDAEs from the liposomal platforms. The observed *in vitro* drug release data for DPPC:CHOL whereby EFV was immediately released in a burst for the first 30 minutes followed by the controlled release of the drug over a period

of 24 hours, suggests the suitability of this formulation for HIV treatment where oral multiple dosing is not needed for improved patient compliance. That is, if a drug is released in a burst manner immediately after administration, it would provide a loading dose of the drug, which could possibly be enough to suppress the virus.

The subsequent drug releases in a controlled manner would provide the maintenance dose of the drug, thereby ensuring constant plasma concentrations of the drug for a prolonged period. HIV infection is a typical example where a sustained action of the anti-HIV drug is desired. This is because a patient takes a medical treatment for life, and patient compliance is therefore, necessary to keep the virus suppressed. On the other hand, the DPPC:CHOL platform released MQ in a different manner as opposed to the EFV release, whereby a drug release increased over time and reached its peak at 3 hours. This release pattern for MQ could similarly be beneficial in malaria treatment because the incubation period exhibited by the malaria-causing agent (plasmodium), i.e. in the case where MQ is given as a prophylaxis to travellers, a DPPC:CHOL based MQ formulation may be given at the beginning of the journey and will be released in a controlled, but slow manner such that when a patient gets exposed to the malaria-causing agent, a drug would be released in sufficient amount in the body.

The presence of PDAEs did not change the release pattern of both EFV and MQ for this platform, but the changes in the extent of release were observed in both situations, i.e. the release of EFV was enhanced while that of MQ was reduced in the presence of PDAEs. These difference in the release pattern of EFV versus MQ in the presence of PDAEs could be attributed to the interaction of functional groups of EFV or MQ and PDAEs. For example, if the bonding between a drug and the plant-derived absorption

enhancer is very strong, drug release from drug-PDAE complex will be slow and vice versa. Similarly, the interaction between the drug-PDAE complex and the nanocarrier itself may have an impact on drug release. The sudden drop in drug release at 1400 minutes suggests that DPPC:CHOL is not suitable nanoplatform for sustained release, but could be improved by combining this drug with PDAEs.

The DOPC:CHOL-based platforms released both drugs in a controlled and cumulative manner with a peak drug release at 3 hours. However, MQ was retained within the platform throughout the study period indicating the strong interaction between MQ and the DOPC:CHOL-based platform, which could be attributed to the nature of both entities. This makes DOPC:CHOL-based platform not suitable, as a dosage form, for MQ. Interestingly, the *in vitro* drug release of MQ from this platform was enhanced by the incorporation of the PDAEs in the platform, which could possibly change the extent of interaction between the DOPC:CHOL platform and MQ leading to MQ release.

The observed similarity between the drug release patterns of both the DPPC:CHOL-based platforms and the DSPC:CHOL:DPPC-based platforms as opposed to the DOPC:CHOL-based platform could be due to the fact that both liposomes are thermo-sensitive types of liposomes (Achim *et al*., 2009:705).

4.4.4 *In vitro* drug permeability

The dialysis bag method was adopted for this study, whereby, a semi-permeable, 14 kDa dialysis membrane and the PBS (pH 7.4) were used to assess the movement of the encapsulated drug from the membrane sac (donor compartment) into the rest of the solution (receiver compartment) over a 24-hour period.

The concentration of the permeated drug was higher when a free drug was used when compared to the liposomes indicating the potential of liposomes to provide a controlled release of the drug and thus a sustained action. This observed behaviour of the liposomes is suitable in the case of HIV treatment where multiple dosing of the drug may not be desired so that patient compliance may be improved. Similarly, in the case of malaria prophylaxis, a sustained drug release may be desired such that a patient who is not ill can only take a medication once.

4.4.5 *In vitro* toxicological effects of liposomes

The obtained toxicity data of the placebo liposomes versus drug-loaded liposomes seemed to be logical with what was expected. For example, the percentage cell viabilities of the placebos versus drug-loaded liposomes were of the order placebo > placebo-PDAEs > drug-loaded liposomes. This simply means that the phospholipids used in the present study are more biocompatible with the liver cells as compared to drug-loaded and drug-PDAEs-loaded liposomes.

In contrast to previous reports, which regarded phospholipids as biocompatible with the human body (Singh, Gangadharappa & Mruthunjaya, 2017:166; Cullis & De Kruijff, 1979:399), the phospholipid-cholesterol placebos were not completely biocompatible with the liver cells (percentage cell viability < 50%) when compared to the untreated cells (control). Therefore, the observed lack of complete biocompatibility of the placebos could be attributed to some traces of organic solvent used (i.e. chloroform) that may be left within the phospholipids during the preparation of liposomes. Furthermore, the used molar ratios could potentially cause the observed level of toxicity.

Efavirenz-loaded liposomes were safe at low concentrations of 74 µg/mL (Figure 4.8). Interestingly, when the same concentration was prepared in combination with PDAEs, its toxicity could not increase tremendously making it the best combinatory dosage form that could enhance the bioavailability of efavirenz, at the same time giving a sustained release of a drug. Mefloquine-loaded liposomes were also safe at a low concentration of 63 µg/mL but became toxic when prepared in combination with PDAEs. The addition of PDAEs was toxic to liver cells when loaded in DSPC:CHOL:DPPC platforms at every instance of the study, making them incompatible with this nanocarrier.

4.4.6 *Ex vivo* drug permeability from liposomes

Based on the results of the drug permeability studies reported in chapter three of the present study, it became interesting to explore the possible causes of the obtained data as the same model was successfully used with propranolol (P-gp substrate) in chapter three. It was therefore evident that the problem could not be the *ex vivo* model itself, but the drug or liposomal formulation. However, the liposomal formulations were also excluded because free drugs were also not transported through the porcine intestinal tissue. Although the *ex vivo* model was successfully used in chapter three, the final concentrations of liposomes were very low because the final working volume of 7 mL was required while the final volume of liposomal formulations was 0.2 mL, implying high cost for using this model if liposome concentrations were to be maintained.

The pharmacokinetics of both efavirenz and mefloquine were reviewed against the obtained data and any similarities between the two drugs were sought. The pharmacokinetic parameters that were of interest included the relationship between

efavirenz and/or mefloquine and CYP450 metabolizing enzymes and the P-gp, and protein binding of these drugs was also concluded to be crucial. Although both the CYP450 and the P-gp may affect absorption of many drugs, their involvement in this study could not be verified because the same results were obtained even when both efavirenz and mefloquine were co-formulated with the combination of curcumin and quercetin, which are known CYP450 and P-gp inhibitors.

The inhibitory effects of combination of PDAEs on both CYP450 and P-gp could have been affected by dilution of liposomal formulations from 0.2 mL to make a working volume of 7 mL, which reduced the concentrations of encapsulated curcumin and quercetin from 134 µM and 132 µM to 3.9 µM and 3.7 µM, respectively. It is important to note that chapter three reported the effective concentrations for curcumin to be 100 µM while that one of quercetin to be 75 µM. The high entrapment efficiency of liposomes is another possible factor that might have contributed to low permeability of drugs. This was revealed by the *in vitro* drug release data, which showed a sustained drug release behaviour of liposomes. Since the *ex vivo* experiment is limited to run for up to 2 hours, most of the drug would not have been released from the liposomes within this time.

Plasma protein binding could be another possible avenue, in which the bioavailability of drugs may be hindered. Albumin is the major drug-binding protein in the serum, although other proteins, such as α_1 acid glycoprotein, lipoproteins, and globulins are also capable of binding drugs (Johnson-Davis, & Dasgupta, 2016:245). The porcine intestinal tissue contains a network of mesenteric blood supply vessels, in which a drug may be held temporarily and then washed away to the rest of systemic circulation by the constant supply of fresh blood through the process called sink condition.

If a drug is highly protein-bound, it is less bioavailable as only unbound (free drug) form of a drug can elicit pharmacological effects (Aulton, 2016). Similarly, the bound form of a drug may not be detected through spectrometric or chromatographic drug analysis methods. Of great interest, when the protein binding of both efavirenz and mefloquine were observed, it turned out that efavirenz has 99% protein binding capacity while mefloquine has 98% protein binding capacity, but propranolol has 85% - 95% protein binding capacity.

4.5 CONCLUSION

Different liposomal formulations containing an anti-HIV or antimalarial agent were formulated and characterized. The characterisation data revealed some differences in different liposomal formulations based on their entrapment efficiency, particle size and surface charge, *in vitro* drug release and the permeability through a semi-permeable membrane. These differences enabled the researcher to be aware of the best and novel dosage form, which could improve drug delivery in HIV/AIDS and malaria diseases. In terms of all liposomal characterisation parameters applied in the current study, the DSPC:CHOL:DPPC-based liposomal formulations performed better than other formulations.

Most orally administered drugs are extensively metabolized in the liver and their toxicity may manifest first at that site; thus, the liver cells create the best model to measure the toxicity of many drugs. Phospholipids were not completely biocompatible with the liver cells and their molar ratios need be taken into consideration when formulating liposomes. The toxicity of certain liposomes is potentiated by the incorporation of the PDAEs into

such liposomes thereby making a combination therapy less feasible. Formulation of a low concentration (74 µg/mL) and thus less toxic combination dosage form based on EFV and PDAEs (DOPC:CHOL-EFV-PDAEs) was achieved. On the other hand, MQ at low concentration, was best as monotherapy as it became toxic when co-formulated with the PDAEs.

The everted gut sac method may not be suitable for assessment of permeability studies of liposomal formulation of highly protein-bound drugs such as efavirenz and mefloquine due to its short experimental runtime. The determination of the transport studies of liposomes formulated in this study may best be achieved through the *in vivo* studies as they may require prolonged time intervals who may not be possible with the *ex vivo* studies.

CHAPTER 5

FINAL CONCLUSION AND RECOMMENDATIONS

5.1 INTRODUCTION

Different PDAEs were identified, and their literature was reviewed. The effective concentrations of the selected PDAEs were successfully determined in chapter three. chapter four successfully formulated liposomes of different compositions using various combinations of phospholipids and cholesterol at different molar ratios. From these liposomes, the best liposomal formulations were successfully selected based on their particle size, zeta potential, entrapment efficiency, *in vitro* drug release, and *in vitro* drug permeability studies. The selected liposomal formulations were further assessed for their biocompatibility capacities to the liver in chapter five, and chapter six determined the *ex vivo* drug transport studies of the selected liposomal formulations.

5.2 FINAL CONCLUSION

Curcumin and quercetin provide the best inhibitory effects on both the P-gp and CYP3A4 at the concentrations of 100 µM and 75 µM, respectively. The liposomal formulations based on l-α-phosphatidylcholine, dioleoyl with cholesterol (1:1 mol/mol), and 1,2-distearoyl-sn-glycero-3-phosphocholine with cholesterol and 1-2-dipalmitoyl-sn-glycero-3-phosphocholine (4:6:26 mol/mol/mol) could be used as novel anti-HIV and antimalarial dosage forms, which could load sufficient amount of a drug and provide a controlled and sustained release of the drug. However, these liposomal formulations are not completely biocompatible to the liver cells. The *ex vivo* permeability studies based on porcine

intestinal tissue model is not suitable for liposomal formulation of highly protein-bound drugs. Therefore, the drug transport studies and thus the bioavailability of liposomal formulations could not be achieved using this *ex vivo* model and therefore need further investigation possibly using *in vivo* models.

5.3 RECOMMENDATIONS FOR FUTURE STUDIES

The present study revealed the potential of the combinations of PDAEs to inhibit both the CYP450 enzymes and the P-gp thus improving the bioavailability of anti-HIV drug EFV and antimalaria drug MQ *in vitro*. However, the higher entrapment efficiency, sustained drug release behaviour and possibly higher protein binding profile of these drugs gave inconclusive results in *ex vivo* studies. Therefore, future studies need to further expand on the findings of the present study using an optimized *ex vivo* models utilizing microplates (or small volumes) and *in vivo* models, which provide prolonged experimental runtimes. Formulation of these drugs as liposomes gave a modified release pattern of the drug, which could reduce the frequency of dosing of both anti-HIV drug and antimalaria drug thereby improving patient compliance. Future studies may further explore other forms of nanocarriers to further improve drug loading and release of these drugs.

5.4 LIMITATIONS OF THE STUDY

The utilization of H-4-II-E cells to assess the biocompatibility of liposomes was the limitation of this study. The H-4-II-E cells are hepatoma liver cells that are normally used to investigate the cytotoxicity of compounds in cancer treatment studies. Although this type of cells can provide reliable results, normal liver cells could be more suitable for biocompatibility studies. Furthermore, there was less cell viability, particularly where

drugs were incorporated with bioenhancers into liposomal nanocarriers. This could be due to the cytotoxic effects possessed by curcumin (Amanlou *et al*., 2019:151).

The *ex vivo* model used in this study gave inconclusive results for liposomal formulations of high protein binding drugs and was, therefore, a limitation for this study. The other primary reason for failure of this model could be large volume of working solutions (i.e. 7 mL) required to run this method, which could not be achieved without dilution of liposomes.

The concentration of drugs contained in liposomal formulations analysed using the HPLC method was also a limitation of this study as they were unable to be detected. The reason behind this encounter could be due to low limit of detection (LOD) and the sensitivity of this method.

REFERENCES

ABDEL-HAFEZ, S.M., HATHOUT, R.M. & SAMMOUR, O.A. 2018. Curcumin-loaded ultra-deformable nanovesicles as a potential delivery system for breast cancer therapy. *Colloids and Surfaces B: Biointerfaces*, 167:63-72.

ABSORPTION SYSTEMS. 2016. Efflux transporters. [Online]. Available from: https://www.absorption.com/kc/efflux-transporters/ [Accessed: 30/07/2019].

ACHIM, M., PRECUP, C., GONGANAUNITU, D., BARBU-TUDORAN, L., PORFIRE, A.S., SCURTU, R. & CIUCE, C. 2009. Thermosensitive liposomes containing doxorubicin. Preparation and *in vitro* evaluation. *Farmacia*, 57(6):703-710.

ADHIKARI, C., MISHRA, A., NAYAK, D. & CHAKRABORTY, A. 2018. Drug delivery system composed of mesoporous silica and hollow mesoporous silica nanospheres for chemotherapeutic drug delivery. *Journal of Drug Delivery Science and Technology*, 45:303-314.

AGHAPOUR, F., MOGHADAMNIA, A.A., NICOLINI, A., KANI, S.N.M., BARARI, L., MORAKABATI, P., REZAZADEH, L. & KAZEMI, S. 2018. Quercetin conjugated with silica nanoparticles inhibits tumour growth in MCF-7 breast cancer cell lines. *Biochemical and Biophysical Research Communications*, 500:860-865.

AKAL, Z.U., ALPSOY, L. & BAYKAL, A. 2016. Biomedical applications of SPION@APTES@PEG-folicacid@carboxylated quercetin nano-drug on various cancer cells. *Applied Surface Science*, 378:572-581.

ALEXIS, F., RHEE, J.W., RICHIE, J.P., RADOVIC-MORENO, A.F., LANGER, R. & FAROKHZAD, O.C. 2008. New frontiers in nanotechnology for cancer treatment. *Urologic Oncology*, 26(1):74-85.

ALIA, M.M., AGHAB, F.G., EL-SAMMADA, N.M. & HASSANA, S.K. 2014. Modulation of anticancer drug-induced p-glycoprotein expression by naringin. *Zeitschrift für Naturforschung C*, 64(1-2):109-116.

AMANLOU, N., PARSA, M., ROSTAMIZADEH, K., SADIGHIAN, S. & MOGHADDAM, F. 2019. Enhanced cytotoxic activity of curcumin on cancer cell lines by incorporating into gold/chitosan nanogels. *Materials Chemistry and Physics*, 226:151-157.

AMBUDKAR, S.V., DEY, S., HRYCYNA, C.A., RAMACHANDRA, M., PASTAN, I. & GOTTESMAN, M.M. 1999. Biochemical, cellular, and pharmacological aspects of the multidrug transporter. *Annual Review of Pharmacology and Toxicology*, 39:361-398.

ANTÔNIO, E., JUNIOR, O.R.A., ARAÚJO, I.S., KHALIL, N.M. & MAINARDES, R.M. 2017. Poly(lactic acid) nanoparticles loaded with ursolic acid: Characterisation and *in vitro* evaluation of radical scavenging activity and cytotoxicity. *Materials Science and Engineering C*, 71:156-166.

APPIAH-OPONG, R., COMMANDEUR, J.N.M., VAN VUGT-LUSSENBURG, B. & VERMEULEN, N.P.E. 2007. Inhibition of human recombinant cytochrome P450s by curcumin and curcumin decomposition products. *Toxicology*, 235:83-91.

APPIAH-OPONG, R., COMMANDEUR, J.N.M., VAN VUGT-LUSSENBURG, B. & VERMEULEN, N.P.E. 2007. Inhibition of human recombinant cytochrome P450s by curcumin and curcumin decomposition products. *Toxicology*, 235:83-91.

APPIAH-OPONG, R., DE ESCH, I., COMMANDEUR, J.N.M., ANDARINI, M. & VERMEULEN, N.P.E. 2008. Structure-activity relationships for the inhibition of recombinant human cytochromes P450 by curcumin analogues. *European Journal of Medicinal Chemistry*, 43:1621-1631.

AULTON, M.E. & TAYLOR, K.M.G. 2013. Aulton's pharmaceutics: The design and manufacture of medicines. 4th ed. Churchill Livingstone: Elsevier.

AURADE, R.M., AKBAR, S.M.D., GOUD, H., JAYALAKSHMI, S.K. & SREERAMULU, K. 2011. Inhibition of p-glycoprotein ATPase and its transport function of *Helicoverpa armigera* by morin, quercetin and phloroglucinol. *Pesticide Biochemistry and Physiology*, 101:212-219.

AURADE, R.M., JAYALAKSHMI, S.K. & SREERAMULU, K. 2010. Modulatory effects of natural curcuminoids on p-glycoprotein ATPase of insecticide-resistant pest *Helicoverpa armigera* (Lepidopetera: Noctuidae). *Journal of Membrane Biology*, 236:271-278.

BAKER, I. 2018. Magnetic nanoparticle synthesis. In: Narayan, R. *Nanobiomaterials*: *Nanostructured Materials for Biomedical Applications*. USA: Elsevier Science:197-229.

BARENHOLZ, Y. 2012. Doxil® - The first FDA-approved nano-drug: Lessons learned. *Journal of Controlled Release*, 160:117-134.

BERZINA, T., PUCCI, A., RUGGERI, G., EROKHIN, V. & FONTANA, M.P. 2011. Gold nanoparticles–polyaniline composite material: Synthesis, structure and electrical properties. *Synthetic Metals*, 161(13-14):1408-1413.

BHARDWAJ, R.K., GLAESER, H., BECQUEMONT, L., KLOTZ, U., GUPTA, S.K. & FROMM, M.F. 2002. Piperine, a major constituent of black pepper, inhibits human p-glycoprotein and CYP3A4**.** *Journal of Pharmacology and Experimental Therapeutics*, 302(2):645-650.

BLANCO, A. & BLANCO, G. 2017. Chapter 5: Lipids. In: Blanco, A. & Blanco G. *Medical Biochemistry*. USA. Elsevier Science: 99-119.

BLUMENTHAL, M. 2000. Interactions between herbs and conventional drugs: Introductory considerations. *Herbal Gram*, 49:52-63.

BOBO, D., ROBINSON, K.J., ISLAM, J., THURECHT, K.J. & CORRIE, S.R. 2016. Nanoparticle-based medicines: A review of FDA-approved materials and clinical trials to date. *Pharmaceutical Research*, 33(10):2373-2387.

BOLLU, V.S., BARUI, A.K., MONDAL, S.K., PRASHAR, S., FAJARDO, M., BRIONES, D., RODRÍGUEZ-DIÉGUEZ, A., PATRA, C.P. & GÓMEZ-RUIZ, S. 2016. Curcumin-loaded silica-based mesoporous materials: Synthesis, characterisation and cytotoxic properties against cancer cells. *Materials Science and Engineering C*, 63:393-410.

BORSKA, S., SOPEL, M., CHMIELEWSKA, M., ZABEL, M. & DZIEGIEL, P. 2010. Quercetin as a potential modulator of p-glycoprotein expression and function in cells of human pancreatic carcinoma line resistant to daunorubicin. *Molecules*, 15:857-870.

BOUMENDJEL, A., PIETRO, A., DUMONTET, C. & BARRON, D. 2002. Recent advances in the discovery of flavonoids and analogs with high-affinity binding to p-glycoprotein responsible for cancer cell multidrug resistance. *Medicinal Research Reviews*, 22:512-29.

BRISTOL-MYERS SQUIBB. 2005. Sustiva® (efavirenz) capsules and tablets. *The FDA* [Online]. Available from: https://www.accessdata.fda.gov/drugsatfda_docs/label/2005/020972s026,021360s013lbl.pdf [Accessed: 03/08/2019].

BROWN, L., HEYNEKE, O., BROWN, D., VAN WYK, J.P.H. & HAMMAN, J.H. 2008. Impact of traditional medicinal plant extracts on antiretroviral drug absorption. *Journal of Ethnopharmacology*, 119:588-592.

BULL, E., MADANI, S.Y., SHETH, R., SEIFALIAN, A., GREEN, M. & SEIFALIAN, A.M. 2014. Stem cell tracking using iron oxide nanoparticles. *International Journal of Nanomedicine*, 9:1641-1653.

CALDERA, F., ARGENZIANO, M., TROTTA, F., DIANZANI, C., GIGLIOTTI, L., TANNOUS, M., PASTERO, L., AQUILANO, D., NISHIMOTOE, T., HIGASHIYAMA, T. & CAVALLI, R. 2018. Cyclic nigerosyl-1,6-nigerose-based nanosponges: An innovative pH and time-controlled nanocarrier for improving cancer treatment. *Carbohydrate Polymers*, 194:111-121.

CHAN, K., LIU, Z.Q., JIANG, Z.H., ZHOU, H., WONG, Y.F., XU, H. & LIU, L. 2006. The effects of sinomenine on intestinal absorption of paeoniflorin by the everted rat gut sac model. *Journal of ethnopharmacology*, 103:425-32.

CHAN, K., LIU, Z.Q., JIANG, Z.H., ZHOU, H., WONG, Y.F., XU, H.X. & LIU, L. 2006. The effects of sinomenine on intestinal absorption of paeoniflorin by the everted rat gut sac model. *Journal of Ethnopharmacology*, 103:425-432.

CHANG, M., LU, S., ZHANG, F., ZUO, T., GUAN, Y., WEI, T., SHAO, W. & LIN, G. 2015. RGD-modified pH-sensitive liposomes for docetaxel tumour targeting. *Colloids and Surfaces B: Biointerfaces*, 129:175-182.

CHEN, C., SUN, W., WANG, X., WANG, Y. & WANG, P. 2018. Rational design of curcumin loaded multifunctional mesoporous silica nanoparticles to enhance the cytotoxicity for targeted and controlled drug release. *Materials Science and Engineering C*, 85:88-96.

CHEN, Q., ZHENG, J., YUAN, X., WANG, J. & ZHANG, L. 2018. Folic acid grafted and tertiary amino based pH-responsive pentablock polymeric micelles for targeting anticancer drug delivery. *Materials Science & Engineering C*, 82:1-9.

CHEN, Y., MINH, L.V., LIU, J., ANGELOV, B., DRECHSLER, M., GARAMUS, V.M., WILLUMEIT-ROMER, R. & ZOU, A. 2016. Baicalin loaded in folate-PEG modified liposomes for enhanced stability and tumour targeting. *Colloids and Surfaces B: Biointerfaces*, 140:74-82.

CHENG, S.S., FU, S.X., LI, Y.S. & WANG, N.C. 1964. The pharmacology of sinomenine I: The analgesic and anti-phlogistic actions and acute toxicity. *Acta Pharmacologica Sinica*, 4: 177-180.

CHIELI, E., ROMITI, N., RODEIRO, I. & GARRIDO, G. 2010. *In vitro* modulation of ABCB1/p-glycoprotein expression by polyphenols from Mangifera indica. *Chemico Biological Interactions*, 186(3):287-94.

CHO, Y.A., LEE, W. & CHOI, J.S. 2012. Effects of curcumin on the pharmacokinetics of tamoxifen and its active metabolite, 4-hydroxytamoxifen, in rats: Possible role of CYP3A4 and p-glycoprotein inhibition by curcumin. *Pharmazie*, 67(2):124-130.

CHOI, J.S. & HAN, H.K. 2005. Enhanced oral exposure of diltiazem by concomitant use of naringin in rats. *International Journal of Pharmaceutics*, 305(1-2):122-128.

CHOI, J.S. & LI, X. 2005. Enhanced diltiazem bioavailability after oral administration of diltiazem with quercetin to rabbits. *International Journal of Pharmaceutics*, 297(1-2):1-8.

CHOI, J.S., JO, B.W. & KIM, Y.C. 2004. Enhanced paclitaxel bioavailability after oral administration of paclitaxel or prodrug to rats pretreated with quercetin. *European Journal Pharmaceutics and Biopharmaceutics*, 57:313-318.

CHULA, S., HANG, L., YINYING, B., JIANNING, S. & RENBING, S. 2012. The effects of notoginsenoside R1 on the intestinal absorption of geniposide by the everted rat gut sac model. *Journal of Ethnopharmacology*, 142:136-143.

CIPOLLA, D., WU, H., EASTMAN, S., REDELMEIER, T., GONDA, I. & CHAN, H. 2014. Development and characterisation of an *in vitro* release assay for liposomal ciprofloxacin for inhalation. *Journal of Pharmaceutical Sciences*, 103:314-327.

CRISTOFOLETTI, R., NAIR, A., ABRAHAMSSON, B., GROOT, D.W., KOPP, S., LANGGUTH, P., POLLI, J.E., SHAH, V.P. & DRESSMAN, J.B. 2013. Biowaiver monographs for immediate release solid oral dosage forms: Efavirenz. *Journal of Pharmaceutical Sciences*, 102(2):318-329.

CROUCH, S.P.M., KOZLOWSKI, R., SLATER, K.J. & FLETCHER, J. 1993. The use of ATP bioluminescence as a measure of cell proliferation and cytotoxicity. *Journal of Immunological Methods*, 160(1):81-88.

CULLIS, P.R. & DE KRUIJFF, B. 1979. Lipid polymorphism and the functional roles of lipidsin biological membranes. *Biochimica et Biophysica Acta (BBA) - Reviews on Biomembranes*. 559(4):399-420.

CURCIO, M., MAURO, L., NAIMO, G.D., AMANTEA, D., CIRILLO, G., TAVANO, L., CASABURI, I., NICOLETTA, F.P., ALVAREZ-LORENZO, C. & IEMMA, F. 2018. Facile synthesis of pH-responsive polymersomes based on lipidized PEG for intracellular co-delivery of curcumin and methotrexate. *Colloids and Surfaces B: Biointerfaces*, 167:568-576.

D'SOUZA, S. 2014. A review of *in vitro* drug release test methods for nano-sized dosage forms. *Advances in Pharmaceutics*, 2014:1-12.

DALWADI, D.A., KIM, S., AMDANI, S.M., CHEN, Z., HUANG, R. & SCHETZ, J.A. 2016. Molecular mechanisms of serotonergic action of the HIV-1 antiretroviral efavirenz. *Pharmacological Research*, 110:10-24.

DE CASTO, W.V., MERTENS-TALCOTT, S., DERENDORF, H. & BUTTERWECK, V. 2007. Grapefruit juice-drug interactions: Grapefruit juice and its components inhibit p-glycoprotein (ABCB1) mediated transport of talinolol in Caco-2 cells. *Journal of Pharmaceutical Sciences*, 96(10):2808-2817.

DE LIMA, H.H.C., KUPFER, V.L., MOISES, M.P., GUILHERME, M.R., RINALDI, J.C., FELISBINO, S.L., RUBIRA, A.F. & RINALDI, A.W. 2018. Bionanocomposites based on mesoporous silica and alginate for enhanced drug delivery. *Carbohydrate Polymers*, 196:126-134.

DE SA VIANA, O., MEDEIROS, F.P.M., GRANGEIRO-JUNIOR, S., ALBUQUERQUE, M.M. LA ROCA SOARES, M.F., SOARES-SOBRINHO, J.L., ALVES, L.D.S., ROLIM, L.A., DA SILVA, K.E.R. & ROLIM-NETO, P.J. 2011. Development and validation of a HPLC analytical assay method for efavirenz tablets: a medicine for HIV infections. *Brazilian Journal of Pharmaceutical Sciences*, 47(1):97-102.

DELL'ALBANI, P., DI MARCO, B., GRASSO, S., ROCCO, C. & FOTI, M.C. 2017. Quercetin derivatives as potent inducers of selective cytotoxicity in glioma cells. *European Journal of Pharmaceutical Sciences*, 101:56-65.

DHIVYA, R., RANJANI, J., BOWEN, P.K., RAJENDHRAN, J., MAYANDI, J. & ANNARAJ, J. 2017. Biocompatible curcumin loaded PMMA-PEG/ZnO nanocomposite induce

apoptosis and cytotoxicity in human gastric cancer cells. *Materials Science and Engineering C*, 80:59-68.

DHIVYA, R., RANJANI, J., RAJENDHRAN, J., MAYANDI, J. & ANNARAJ, J. 2018. Enhancing the anti-gastric cancer activity of curcumin with biocompatible and pH-sensitive PMMA-AA/ZnO nanoparticles. *Materials Science and Engineering C*, 82:182-189.

DIAS, M.F., DE FIGUEIREDO, B.C.P., TEIXEIRA-NETO, J., GUERRA, M.C.A., FIALHO, S.L. & CUNHA, A.S. 2018. *In vivo* evaluation of antitumoral and antiangiogenic effect of imiquimod-loaded polymeric nanoparticles. *Biomedicine & Pharmacotherapy*, 103:1107-1114.

DOYLE, L. & ROSS, D.D. 2003. Multidrug resistance mediated by the breast cancer resistance protein BCRP (ABCG2). *Oncogene*, 22(47):7340-7358.

DUPUY, J., LARRIEU, G., SUTRA, J.F., LESPINE, A. & ALVINERIE, M. 2003. Enhancement of moxidectin bioavailability in lamb by a natural flavonoid: Quercetin. *Verterinary Parasitology*, 112(4):337-347.

EAGLING, V. A., PROFIT, L. & BACK, D.J. 1999. Inhibition of the CYP3A4-mediated metabolism and p-glycoprotein-mediated transport of the HIV-1 protease inhibitor saquinavir by grapefruit juice components. *British Journal of Clinical Pharmacology*, 48(4):543-552.

ELAHI, N., KAMALI, M. & BAGHERSAD, M.H. 2018. Recent biomedical applications of gold nanoparticles: A review. *Talanta*, 184:537-556.

EL-HABIT, O.H. & AL-KHAMASH, H.S. 2012. Testing the cytotoxicity and genotoxicity of the antimalarial drug mefloquine. *Journal of King Saud University – Science*, 24:277-284.

ENGELKING, L.R. 2015. Chapter 57: Triglycerides and Glycerophospholipids. In: Englking, L.R. *Textbook of Veterinary Physiological Chemistry*. USA. Elsevier Science: 365-371.

ENGEN, A., MAEDA, J., WOZNIAK, D.E., BRENTS, C.A., BELL, J.J., UESAKA, M., AIZAWA, Y. & KATO, T.A. 2015. Induction of cytotoxic and genotoxic responses by natural and novel quercetin glycosides. *Mutation Research*, 784-785:15-22.

FACCHI, S.P., SCARIOT, D.B., BUENO, P.V.A., SOUZA, P.R., FIGUEIREDO, L.C., FOLLMANN, H.D.M., NUNES, C.S., MONTEIRO, J.P., BONAFÉ, E.G., NAKAMURA, C.V., MUNIZ, E.C. & MARTINS, A.F. 2016. Preparation and cytotoxicity of N-modified chitosan nanoparticles applied in curcumin delivery. *International Journal of Biological Macromolecules*, 87:237-245.

FARAZUDDIN, M., DUA, B., ZIA, Q., KHAN, A.A., JOSHI, B. & OWAIS, M. 2014. Chemotherapeutic potential of curcumin-bearing microcells against hepatocellular carcinoma in model animals. *International Journal of Nanomedicine*, 9:1139-1152.

FORBES, N., HUSSAIN, M.T., BRIUGLIA, M.L., EDWARDS, D.P., TER HORST, J.H. SZITA, N. & PERRIE, Y. 2019. Rapid and scale-independent microfluidic manufacture of liposomes entrapping protein incorporating in-line purification and at-line size monitoring. *International Journal of Pharmaceutics*, 556:68-81.

FREITAS, L.B.O., CORGOSINHO, L.M., FARIA, J.A.Q.A., SANTOS, V.M., RESENDE, J.M., LEAL, A.S., GOMES, D.A. & SOUSA, E.M.B. 2017. Multifunctional mesoporous silica nanoparticles for cancer-targeted, controlled drug delivery and imaging. *Microporous and Mesoporous Materials*, 242:271-283.

FUGH-BERMAN, A. & ERNST, E. 2001. Herb–drug interactions: Review and assessment of report reliability. *British Journal of Clinical Pharmacology*, 52(5):587-595.

FUGH-BERMAN, A. 2000. Herb-drug interactions. *Lancet*, 355(9198):1020.

GAIKWAD, D., SHEWALE, R., PATIL, V., MALI, D., GAIKWAD, U. & JADHAV, N. 2017. Enhancement in *in vitro* anti-angiogenesis activity and cytotoxicity in lung cancer cell by pectin-PVP based curcumin particulates. *International Journal of Biological Macromolecules*, 104:656-664.

GANGADHARAPPA, H.V., PRASAD, S.M.C. & SINGH, R.P. 2017. Formulation, *in vitro* and *in vivo* evaluation of celecoxib nanosponge hydrogels for topical application. *Journal of Drug Delivery Science and Technology*, 41:488-501.

GANTA, S., DEVALAPALLY, H. & AMIJI, M. 2010. Curcumin enhances oral bioavailability and anti-tumour therapeutic efficacy of paclitaxel upon administration in nanoemulsion formulation. *Journal of Pharmaceutical Sciences*, 99(11):4630-4641.

GAO, M., PENG, Y., JIANG, L. & QIU, L. 2018. Effective intracellular delivery and Th1 immune response induced by ovalbumin loaded in pH-responsive polyphosphazene polymersomes. *Nanomedicine: Nanotechnology, Biology, and Medicine,*14:1609-1618.

GARCIA, M.C., ALOISIO, C., ONNAINTY, R. & ULLIO-GAMBOA, G. 2017. Self-assembled nanomaterials. In: Narayan, R (comp). Nanobiomaterials. Elsevier: Woodhead Publishing: 41-94.

GHOSH, S., MALLICK, S., DAS, U., VERMA, A., PAL, U., CHATTERJEE, S., NANDY, A., SAHA, K.D., MAITI, N.C., BAISHYA, B., KUMAR, G.S. & GMEINER, W.H. 2018. Curcumin stably interacts with DNA hairpin through minor groove binding and demonstrates enhanced cytotoxicity in combination with FdU nucleotides. *BBA - General Subjects*, 1862:485-494.

GOMEZ-SUCERQUIA, L.J., BLAS-GARCIA, A., MARTI-CABRERA, M., ESPLUGUES, J.V. & APOSTOLOVA, N. 2012. Profile of stress and toxicity gene expression in human hepatic cells treated with Efavirenz. *Antiviral Research*, 94:232-241.

GUORGUI, J., WANG, R., MATTHEOLABAKIS, G. & MACKENZIE, G.G. 2018. Curcumin formulated in solid lipid nanoparticles has enhanced efficacy in Hodgkin's lymphoma in mice. *Archives of Biochemistry and Biophysics*, 648:12-19.

HALDER, A., DAS, S., OJHA, D., CHATTOPADHYAY, D. & MUKHERJEE, A. 2018. Highly monodispersed gold nanoparticles synthesis and inhibition of herpes simplex virus infections. *Materials Science and Engineering C*, 89:413-421.

HALDER, A., MUKHERJEE, P., GHOSH, S., MANDAL, S., CHATTERJI, U. & MUKHERJEE, A. 2018. Smart PLGA nanoparticles loaded with Quercetin: Cellular uptake and in-vitro anticancer study. *Materials Today: Proceedings*, 5:9698-9705.

HAN, Y.Q., WANG, J., CUI, Q.X., WANG, L.Q., CHENG, B.F., ZHAO, H.Z., JIANG, M., BAI, G. & LUO, G.A. 2014. Absorption, metabolism and effect of compatibility on absorption of qishenyiqi dropping pill. *Biomedical Chromatography*, 28:554–563.

HE, Y., CI, X., XI, Y., YI, X., ZENG, Y., LI, Y. & LIU, C. 2019. Potential detoxification effect of active ingredients in liquorice by upregulating efflux transporter. *Phytomedicine*, 56:175-182.

HECHT, M., ERBER, S., HARRER, T., KLINKER, H., ROTH, T., PARSCH, H., FIEBIG, N., FIETKAU, R. & DISTEL, L.V. 2015. Efavirenz has the highest anti-proliferative effect of non-nucleoside reverse transcriptase inhibitors against pancreatic cancer cells. *PLoS ONE*,10(6):e0130277.

HLA, T. & DANNENBERG, A.J. 2012. Sphingolipid signaling in metabolic disorders. *Cell Metabolism*, 16:420-434.

HOI, J.S. & LI, X. 2005. Enhanced diltiazem bioavailability after oral administration of diltiazem with quercetin to rabbits. *International Journal of Pharmaceutics*, 297:1-8.

HOLTHUIS, J.C., POMORSKI, T., RAGGERS, R.J., SPRONG, H. & VAN MEER, G. 2001. The organizing potential of sphingolipids in intracellular membrane transport. *Physiological Reviews*, 81:1689-1723.

HONARY, S. & ZAHIR, F. 2013. Effect of Zeta Potential on the Properties of Nano-Drug Delivery Systems - A Review (Part 1). *Tropical Journal of Pharmaceutical Research*, 12(2):255-264.

HOU, X.L., TAKAHASHI, K., KINOSHITA, N., QIU, F., TANAKA, K., KOMATSU, K., TAKAHASHI, K. & AZUMA, J. 2007. Possible inhibitory mechanism of curcuma drugs on CYP3A4 in 1α,25 dihydroxyvitamin D3 treated Caco-2 cells. *International Journal of Pharmaceutics*, 337:169-177.

HOU, X.L., TAKAHASHI, K., TANAKA, K., TOUGOU, K., QIU, F., KOMATSU, K., TAKAHASHI, K. & AZUMA, J. 2008. Curcuma drugs and curcumin regulate the expression and function of P-gp in Caco-2 cells in completely opposite ways. *International Journal of Pharmaceutics*, 358:224-229.

HOU, Y.C., LIN, S.P. & CHAO, P.D.L. 2012. Liquorice reduced cyclosporine bioavailability by activating p-glycoprotein and CYP3A. *Food Chemistry*, 135(4):2307-2312.

HUANG, B.B., LI, G.F., REN, F., TANG, Z.K., MA, H.F., SUN, Y.B., CHEN, L.J. & YANG, L. 2008. Effect of *Glycyrrhiza inflata* and *Daphne genkwa* on permeabilities of rhodamine 123, a p-glycoprotein substrate across rat jejunum membranes *in vitro*. *China Journal of Chinese Materia Medica*, 33:2521–2526.

HUISMAN, M.T., CHHATTA, A.A., VAN TELLINGEN, O., BEIJNEN, J.H. & SCHINKEL, A.H. 2005. MRP2 (ABCC2) transports taxanes and confers paclitaxel resistance and both processes are stimulated by probenecid. *International Journal of Cancer*, 116:824-829.

HWANG, J.Y. & LOH, X.J. 2016. Small molecule therapeutic-loaded liposomes as therapeutic carriers: From development to clinical applications. *RSC Advances*, 6:70592-70615.

IBRAHIM, S., TAGAMI, T., KISHI, T. & OZEKI, T. 2018. Curcumin marinosomes as promising nano-drug delivery system for lung cancer. *International Journal of Pharmaceutics*, 540:40-49.

JIANG, L., LI, L., HE, X., YI, Q., HE, B., CAO, J., PAN, W. & GU, Z. 2015. Overcoming drug-resistant lung cancer by paclitaxel loaded dual-functional liposomes with mitochondria targeting and pH-response. *Biomaterials*, 52:126-139.

JIANG, T., ZHANG, Z., ZHANG, Y., LV, H., ZHOU, J., LI, C., HOU, L. & ZHANG, Q. 2012. Dual-functional liposomes based on pH-responsive cell-penetrating peptide and hyaluronic acid for tumour-targeted anticancer drug delivery. *Biomaterials*, 33:9246-9258.

JOHNSON-DAVIS, K.L. & DASGUPTA, A. 2016. Special issues in therapeutic drug monitoring in patients with uremia, liver disease, and in critically ill patients. In: Clarke, W & Dasgupta, A. (Ed.). *Clinical challenges in therapeutic drug monitoring: Special populations, physiological conditions and pharmacogenomics*. Elsevier: 245-260.

JOSHY, K.S., SHARMA, C.P., KALARIKKAL, N., SANDEEP, K., THOMAS, S. & POTHEN, L.A. 2016. Evaluation of *in vitro* cytotoxicity and cellular uptake efficiency of zidovudine-loaded solid lipid nanoparticles modified with aloe vera in glioma cells. *Materials Science and Engineering C*, 66:40-50.

KANG, M.H., PARK, M.J., YOO, H.J., HYUK, K.Y., LEE, S.G., KIM, S.R., YEOM, D.W., KANG, M.J. & CHOI, Y.W. 2014. RIPL peptide (IPLVVPLRRRRRRRRC)-conjugated liposomes for enhanced intracellular drug delivery to hepsin-expressing cancer cells. *European Journal of Pharmaceutics and Biopharmaceutics*, 87:489-499.

KENT, U.M., AVIRAM, M., ROSENBLAT, M. & HOLLENBERG, P.F. 2002. The licorice root derived isoflavan glabridin inhibits the activities of human cytochrome P450s: 3A4, 2B6, and 2C9. *Drug Metabolism and Disposition*, 30:709-715.

KESARWANI, K. & GUPTA, R. 2013. Bioavailability enhancers of herbal origin: An overview. *Asian Pacific Journal of Tropical Biomedicine*, 3(4):253-266.

KHWAJA, S., FATIMA, K., HASANAIN, M., BEHERA, C., KOUR, A., SINGH, A., LUQMAN, S., SARKAR, J., CHANDA, D., SHANKER, K., GUPTA, A.K., MONDHE, D.M. & NEGI, A.S. 2018. Antiproliferative efficacy of curcumin mimics through microtubule destabilization. *European Journal of Medicinal Chemistry*, 151:51-61.

KOLBLE, K. 1993. Regional mapping of short tandem repeats on human chromosome 10: Cytochrome P450 gene CYP2E, D10S 196, D10S 220, and D10S 225. *Genomics*, 18:702-704.

KOO, O.M., RUBINSTEIN, I. & ONYUKSEL, H. 2005. Role of nanotechnology in targeted drug delivery and imaging: a concise review. *Nanomedicine*, 1(3):193-212.

KOTTA, S., KHANA, A.W., ANSARIB, S.H., SHARMAC, R.K. & ALI, J. 2014. Anti-HIV nanoemulsion formulation: Optimization and *in vitro–in vivo* evaluation. *International Journal of Pharmaceutics*, 462:129-134.

KUBOTA, T., KURODA, S., KANAYA, N., MORIHIRO, T., AOYAMA, K., KAKIUCHI, Y., KIKUCHI, S., NISHIZAKI, M., KAGAWA, S., TAZAWA, H. & FUJIWARA, T. 2018. HER2-targeted gold nanoparticles potentially overcome resistance to trastuzumab in gastric cancer. *Nanomedicine: Nanotechnology, Biology, and Medicine*, 14:1919-1929.

LEE, J.S. & FEIJEN, J. 2012. Review polymersomes for drug delivery: Design, formation and characterisation. *Journal of Controlled Release*, 161:473-483.

LI, A.P., KAMINSKI, D.L. & RASMUSSEN, A. 1995. Substrates of human hepatic cytochrome P450 3A4. *Toxicology*, 104(1-3):1-8.

LI, R., DENG, L., CAI, Z., ZHANG, S., WANG, K., LI, L., DING, S. & ZHOU, C. 2017. Liposomes coated with thiolated chitosan as drug carriers of curcumin. *Materials Science and Engineering C*, 80:156-164.

LI, Y., DUAN, Z., TIAN, Y., LIU, Z. & WANG, Q. 2013. A novel perspective and approach to intestinal octreotide absorption: Sinomenine mediated reversible tight junction opening and its molecular mechanism. *International Journal of Molecular Sciences*, 14:12873-12892.

LI, J., WANG, X., ZHANG, T., WANG, C., HUANG, Z., LUO, X. & DENG, Y. 2015. A review on phospholipids and their main applications in drug delivery systems. *Asian Journal of Pharmaceutical Sciences*, 10:81-98.

LIM, L.L. & LIM, L.Y. 2006. Effects of citrus fruit juices on cytotoxicity and drug transport pathways of Caco-2 cell monolayers. *International Journal of Pharmaceutics*, 307:42-50.

LIM, L.L. & LIM, L.Y. 2006. Effects of citrus fruit juices on cytotoxicity and drug transport pathways of Caco-2 cell monolayers. *International Journal of Pharmaceutics*, 307:42-50.

LIM, S.C. & CHOI, J.S. 2006. Effects of naringin on the pharmacokinetics of intravenous paclitaxel in rats. *Biopharmaceutics and Drug Disposition*, 27:443-447.

LIN, J., CAI, Q., TANG, Y., XU, Y., WANG, Q., LI, T., XU, H., WANG, S., FAN, K., LIU, Z., JIN, Y. & LIN, D. 2018. PEGylated Lipid bilayer coated mesoporous silica nanoparticles for codelivery of paclitaxel and curcumin: Design, characterisation and its cytotoxic effect. *International Journal of Pharmaceutics*, 536:272-282.

LIN, W., YEUNG, C., LIANG, C., HUANG, Y., LIU, C. & HOU, S. 2018. A colorimetric sensor for the detection of hydrogen peroxide using DNA-modified gold nanoparticles. *Journal of the Taiwan Institute of Chemical Engineers*, 89:49-55.

LIU, L., XIAO, J., PENG, Z. & CHEN, Y. 2011. *In vitro* metabolism of glycyrrhetic acid by human cytochrome P450. *Acta Pharmaceutica Sinica*, 46:81-87.

LIU, Y., TANG, Z., LIN, Y., QU, X., LV, W., WANG, G. & LI, C. 2017. Effects of quercetin on proliferation and migration of human glioblastoma U251 cells. *Biomedicine and Pharmacotherapy*, 92:33-38.

LIU, Z.Q., ZHOU, H., LIU, L., JIANG, Z.H., WONG, Y.F., CAI, X., XU, H.X. & CHAN, K. 2005. Influence of co-administrated sinomenine on pharmacokinetic fate of paeoniflorin in unrestrained conscious rats. *Journal of Ethnopharmacology*, 99(1):61-67.

LOCKHART, J.N., STEVENS, D.M., BEEZER, D.B., KRAVITZ, A. & HARTH, E. 2015. Dual drug delivery of tamoxifen and quercetin: Regulated metabolism for anticancer treatment with nanosponges. *Journal of Controlled Release*, 220:751-757.

LU, W.D., QIN, Y., YANG, C., LI, L. & FU, Z.X. 2013. Effect of curcumin on human colon cancer multidrug resistance *in vitro* and *in vivo*. *Clinics*, 68(5):694-701.

LUO, Z., LIU, Y., ZHAO, B., TANG, M., DONG, H., ZHANG, L., LV, B. & WEI, L. 2013. *Ex vivo* and *in situ* approaches used to study intestinal absorption. *Journal of Pharmacological and Toxicological Methods*, 68:208-216.

LV, Q., WANG, G., CHEN, S., HU, L., ZHANG, X., YING, G., QIN, C. & ZHOU, H. 2016. *In vitro* and *in vivo* inhibitory effects of glycyrrhetinic acid in mice and human cytochrome P450 3A4. *International Journal of Environmental Research and Public Health*, 13(84):1-8.

LV, Y., HE, H., QI, J., LU, Y., ZHAO, W., DONG, X. & WU, W. 2018. Visual validation of the measurement of entrapment efficiency of drug nanocarriers. *International Journal of Pharmaceutics*, 547:395-403.

MACH, C.M., CHEN, J.H., MOSLEY, S.A., KURZROCK, R. & SMITH, J.A. 2010. Evaluation of liposomal curcumin cytochrome P450 metabolism. *Anticancer Research*, 30:811-814.

MADHUSUDHAN, A., REDDY, G.B., VENKATESHAM, M., VENKATESHAM, M. & VEERABHADRAM, G. 2012. Design and evaluation of efavirenz loaded solid lipid nanoparticles to improve the oral bioavailability. *International Journal of Pharmacy and Pharmaceutical Science Research*, 2(4):84-89.

MALLICK, S. & CHOI, J.S. 2014. Liposomes: Versatile and biocompatible nanovesicles for efficient biomolecules delivery. *Journal of Nanoscience and Nanotechnology*, 14:755-765.

MANNECK, T., HAGGENMÜLLER, Y. & KEISER, J. 2010. Morphological effects and tegumental alterations induced by mefloquine on Schistosomula and adult flukes of *Schistosoma mansoni*. *Parasitology*, 137:85-98.

MENDES, C., MEIRELLES, G.C., BARP, C.G., ASSREUY, J., SILVA, M.A.S. & PONCHEL, G. 2018. Cyclodextrin based nanosponge of norfloxacin: Intestinal permeation enhancement and improved antibacterial activity. *Carbohydrate Polymers*, 195:586-592.

MICHALOPOULOS, G.K. 2007. Liver regeneration. *Journal of Cell Physiology*, 213(2): 286-300.

MICHLEWSKA, S., IONOV, M., MAROTO-DÍAZ, M., SZWED, A., IHNATSYEU-KACHAN, A., LOZNIKOVA, S., SHCHARBIN, D., MALY, M., RAMIREZ, R.G., DE LA MATA, F.J. & BRYSZEWSKA, M. 2018. Ruthenium dendrimers as carriers for anticancer siRNA. *Journal of Inorganic Biochemistry*, 181:18-27.

MISHRA, B., PATEL, B.B. & TIWARI, S. 2010. Colloidal nanocarriers: A review on formulation technology, types and applications toward targeted drug delivery. *Nanomedicine: Nanotechnology, Biology, and Medicine*, 6:9-24.

MITSUTAKE, S. & IGARASHI, Y. 2013. Sphingolipids in lipid microdomains and obesity. *Vitamins and Hormones,* 91:271-284.

MIZUTANI, Y., MITSUTAKE, S., TSUJI, K., KIHARA, A. & IGARASHI, Y. 2009.Ceramide biosynthesis in keratinocyte and its role in skin function. *Biochimie*, 91:784-790.

MOLAVI, O., XIONG, X., DOUGLAS, D., KNETEMAN, N., NAGATA, S., PASTAN, I., CHU, Q., LAVASANIFAR, A. & LAI, R. 2013. Anti-CD30 antibody conjugated liposomal doxorubicin with significantly improved therapeutic efficacy against anaplastic large cell lymphoma. *Biomaterials*, 34:8718-8725.

MOLLER, M., FOURIE, J. & HARVEY, B.H. 2018. Efavirenz exposure, alone and in combination with known drugs of abuse, engenders addictive-like bio-behavioural changes in rats. *Scientific Reports*, 8(12837):1-13.

MYTHILI, R., SELVANKUMAR, T., SRINIVASAN, P., SENGOTTAIYAN, A., SABASTINRAJ, J., AMEEN, F., AL-SABRI, A., KAMALA-KANNAN, S., GOVARTHANAN, M. & KIM, H. 2018. Biogenic synthesis, characterisation and antibacterial activity of gold nanoparticles synthesised from vegetable waste. *Journal of Molecular Liquids*, 262:318-321.

NABEKURA, T., YAMAKI, T., UENO, K. & KITAGAWA, S. 2008. Inhibition of p-glycoprotein and multidrug resistance protein 1 by dietary phytochemicals. *Cancer Chemotherapy and Pharmacology*, 62(5):867-873.

NANOTRANSMED. 2019. *Dendrimer* [Online]. Available from: http://nanotransmed.u-strasbg.fr/activities/circulating-materials/dendrimers/ [Accessed: 06/08/2019].

NORUZI, M. 2015. Biosynthesis of gold nanoparticles using plant extracts. *Bioprocess Biosystems Engineering*, 38:1-14.

NOUNOU, M.M., EL-KHORDAGUI, L.K., KHALAFALLAH, N.A. & KHALIL, S.A. 2006. *In vitro* release of hydrophilic and hydrophobic drugs from liposomal dispersions and gels. *Acta Pharmaceutica*, 56:311-324.

OSONWA, U.E., MAJEKODUNMI, S.O., OSEGBO, E. & UDOBRE, A. 2017. Enhancement of antimalaria effect of mefloquine by chlorpheniramine. *American Journal of Medicine and Medical Sciences*, 7(6):248-264.

OERLEMANS, C., BULT, W., BOS, M., STORM, G., NIJSEN, J.F. & HENNINK, W.E. 2010. Polymeric micelles in anticancer therapy: Targeting, imaging and triggered release. *Pharmaceutical Research*, 27(12):2569-2589.

OETARI, S., SUDIBYO, M., COMMANDEUR, J.N.M., SAMHOEDI, R. & VERMEULEN, N.P.E. 1996. Effects of curcumin on cytochrome P450 and glutathione s-transferase activities in rat liver. *Biochemical Pharmacology*, 51:39-45.

OLIVEIRA, L.S., MARCAL, L., ROCHA, L.A., DE FARIA, E.H., CIUFFI, K.J., NASSAR, E.J. & CORREA, I.C. 2018. Photoinitiator and anesthetic incorporation into mesoporous silica. *Powder Technology*, 326:62-68.

PAL, S.L., JANA, U., MANNA, P.K., MOHANTA, G.P. & MANAVALAN. R. 2011. Nanoparticle: An overview of preparation and characterisation. *Journal of Applied Pharmaceutical Science*, 1(6):228-234.

PAN, D., DAS, A., LIU, D., VEAZEY, R.S. & PAHAR, B. 2012. Isolation and characterisation of intestinal epithelial cells from normal and SIV-infected rhesus macaques. *PLoS ONE*, 7(1):e30247.

PANWAR, P., PANDEY, B., LAKHERA, P.C. & SINGH, K.P. 2010. Preparation, characterisation, and *in vitro* release study of albendazole-encapsulated nanosize liposomes. *International Journal of Nanomedicine*, 5:101-108.

PEER, D.K., JEFFREY, M., HONG, S. & FAROKHZAD, O.C. 2007. Nanocarriers as an emerging platform for cancer therapy. *Nature Nanotechnology*, 2(12):751-760.

PEGORARO, C., CECCHIN, D., GRACIA, L.S., WARREN, N., MADSEN, J., ARMES, S.P., LEWIS, A., MACNEIL, S. & BATTAGLIA, G. 2013. Enhanced drug delivery to melanoma cells using PMPC-PDPA polymersomes. *Cancer Letters*, 334:328-337.

PEREZ, A.P., ALTUBE, M.J., SCHILRREFF, P., APEZTEGUIA, G., CELES, F.S., ZACCHINO, S., DE OLIVEIRA, C.I., ROMERO, E.L. MORILLA, M.J. 2016. Topical amphotericin B in ultradeformable liposomes: Formulation, skin penetration study, antifungal and antileishmanial activity *in vitro*. *Colloids and Surfaces B: Biointerfaces*, 139:190-198.

PHARMA EXCIPIENTS. 2019. *Delivery of Poorly Soluble Drugs via Mesoporous Silica: Impact of Drug Overloading on Release and Thermal Profiles* [Online]. Available from: https://www.pharmaexcipients.com/oral-excipients/mesoporous-silica-drug-delivery/ [Accessed: 06/08/2019].

POLLARD, T.D., LIPPINCOTT-SCHWARTZ, J., EARNSHAW, W.C. & JOHNSON, G.T. 2017. Chapter 13: Amino acid sequences identify candidate transmembrane segments. In: Pollard, T.D., Lippincott-Schwartz, J., Earnshaw, W.C. & Johnson, G.T. *Cell Biology*. USA. Elsevier Science: 227-239.

PONTIER, S.M & SCHWEISGUTH, F. 2012. Glycosphingolipids in signaling and development: From liposomes to model organisms. *Developmental Dynamics*, 241:92-106.

PROMEGA. 2014. P450-Glo Screening Systems: Instructions for Use of Products V9770, V9781, V9790, V9800, V9880, V9890 and V9920. Technical bulletin. Madison, USA. Promega Corporation.

PROMEGA. 2015. CellTiter-Glo® Luminescent Cell Viability Assay: Instructions for Use of Products G7570, G7571, G7572 and G7573. Technical Bulletin. Madison, USA. Promega Corporation.

PROMEGA. 2015. Pgp-Glo Assay Systems: Instructions for Use of Products V3591 and V3601. Technical Bulletin. Madison, USA. Promega Corporation.

PUSHPALATHA, R., SELVAMUTHUKUMAR, S. & KILIMOZHI, D. 2017. Nanocarrier mediated combination drug delivery for chemotherapy - A review. *Journal of Drug Delivery Science and Technology*, 39:362-371.

PUSHPALATHA, R., SELVAMUTHUKUMAR, S. & KILIMOZHI, D. 2018. Cross-linked, cyclodextrin-based nanosponges for curcumin delivery: Physicochemical characterisation, drug release, stability and cytotoxicity. *Journal of Drug Delivery Science and Technology*, 45:45-53.

QIAN, W.Y., SUN, D.M., ZHU, R.R., DU, X.L., LIU, H. & WANG, S.L. 2012. pH-sensitive strontium carbonate nanoparticles as new anticancer vehicles for controlled etoposide release. *International Journal of Nanomedicine*, 7:5781-5792.

RAJA, S.B., RAJENDIRAN, V., KASINATHAN, N.K., AMRITHALAKSHMI, P., VENKATABALASUBRAMANIAN, S., MURALI, M.R., DEVARAJ, H. & DEVARAJ, S.N. 2017. Differential cytotoxic activity of Quercetin on colonic cancer cells depends on ROS generation through COX-2 expression. *Food and Chemical Toxicology*, 106:92-106.

RAMOS, M.A.D.S., DA SILVA, P.B., SPOSITO, L., DE TOLEDO, L.G., BONIFACIO, B.V., RODERO, C.F., DOS SANTOS, K.C., CHORILLI, M. & BAUAB, T.M. 2018. Nanotechnology-based drug delivery systems for control of microbial biofilms: A review. *International Journal of Nanomedicine*, 13:1179-1213.

RAN, C., CHEN, D., XU, M., DU, C., LI, Q. & JIANG, Y. 2016. A study on characteristic of different sample pretreatment methods to evaluate the entrapment efficiency of liposomes. *Journal of Chromatography B*, 1028:56-62.

RAO, N.M. & SANKAR, D.G. 2015. Development and validation of stability-indicating HPLC method for simultaneous determination of lamivudine, tenofovir, and dolutegravir in bulk and their tablet dosage form. *Future Journal of Pharmaceutical Sciences*, 1:73-77.

RAZI, M.A., WAKABAYASHI, R., TAHARA, Y., GOTO, M. & KAMIYA, N. 2018. Genipin-stabilized caseinate-chitosan nanoparticles for enhanced stability and anti-cancer activity of curcumin. *Colloids and Surfaces B: Biointerfaces*, 164:308-315.

REFAHI, S., MINAEI, B., HADDADI, G.H., KHOEI, S., BAKHTIARIAN, A., POURISSA, M. & TAKAVAR, A. 2016. Histopathological evaluation of the effectiveness of glycyrrhizic

acid as a radioprotector against the development of radiation-induced lung fibrosis. *Iran Journal of Radiology*, 13(2):e21012.

RETTIE, A.E. & JONES, J.P. 2005. Clinical and toxicological relevance of CYP2C9: Drug-drug interactions and pharmacogenetics. *Annual Review of Pharmacology and Toxicology*, 45:477-494.

RIEHEMANN, K., SCHNEIDER, S.W., LUGER, T.A., GODIN, B., FERRARI, M. & FUCHS, H. 2009. Nanomedicine-challenge and perspectives. *Angewandte Chemie*, 48(5):872-897.

ROCHE. 2008. Lariam® brand of mefloquine hydrochloride tablets. *The FDA* [Online]. Available from: https://www.accessdata.fda.gov/drugsatfda_docs/label/2008/019591s024s025lbl.pdf [Accessed: 03/08/2019].

RODRIGUEZ-FRAGOSO, L., MARTINEZ-ARISMENDI, J.L., OROZCO-BUSTOS, D., REYES-ESPARZA, J., TORRES, E. & BURCHIEL, W. 2011. Potential risks resulting from fruit/vegetable-drug interactions: Effects on drug metabolising enzymes and drug transporters. *Journal of Food Science*, 76(4):112-124.

ROMITI, N., TONGIANI, R., CERVELLI, F. & CHIELI, E. 1998. Effects of curcumin on p-glycoprotein in primary cultures of rat hepatocytes. *Life Sciences*, 62(25):2349-2358.

ROMPICHARLA, S.V.K., BHATT, H., SHAH, A., KOMANDURI, N., VIJAYASARATHY, D., GHOSH, B. & BISWAS, S. 2017. Formulation optimization, characterisation, and

evaluation of *in vitro* cytotoxic potential of curcumin loaded solid lipid nanoparticles for improved anticancer activity. *Chemistry and Physics of Lipids*, 208:10-18.

SAHU, P.K. 2016. Design, structure activity relationship, cytotoxicity and evaluation of antioxidant activity of curcumin derivatives/analogues. *European Journal of Medicinal Chemistry*, 121:510-516.

SAHU, P.K., SAHU, P.K., SAHU, P.L. & AGARWAL, D.D. 2016. Structure activity relationship, cytotoxicity and evaluation of antioxidant activity of curcumin derivatives. *Bioorganic and Medicinal Chemistry Letters*, 26:1342-1347.

SALEH-E-IN, M.M., SULTANA, N., HOSSAIN, M.N., HASAN, S. & ISLAM, M.R. 2016. Pharmacological effects of the phytochemicals of *Anethum sowa* L. root extracts. *BMC Complementary and Alternative Medicine*, 16(464):1-14.

SALVA, E., TURAN, S.O., EREN, F. & AKBUGA, J. 2015. The enhancement of gene silencing efficiency with chitosan-coated liposome formulations of siRNAs targeting HIF-1α and VEGF. *International Journal of Pharmaceutics*, 478:147-154.

SALVA, E., TURAN, S.O., EREN, F. & AKBUGA, J. 2015. The enhancement of gene silencing efficiency with chitosan-coated liposome formulations of siRNAs targeting HIF-1α and VEGF. *International Journal of Pharmaceutics*, 478:147-154.

SARASWATHI, V.S., SARAVANAN, D. & SANTHAKUMAR, K. 2017. Isolation of quercetin from the methanolic extract of lagerstroemia speciose by HPLC technique, its cytotoxicity against MCF-7 cells and photocatalytic activity. *Journal of Photochemistry and Photobiology, B: Biology*, 171:20-26.

SATOH, T., WATANABE, Y., IKARASHI, N., ITO, K. & SUGIYAMA, K. 2009. Effects of Kampo medicines on p-glycoprotein. *Biological and Pharmaceutical Bulletin*, 32:2018-2021.

SAURAJ, S., KUMAR, U., KUMAR, V., PRIYADARSHI, R., GOPINATH, P. & NEGI, Y.S. 2018. pH-responsive prodrug nanoparticles based on xylan-curcumin conjugate for the efficient delivery of curcumin in cancer therapy. *Carbohydrate Polymers*, 188:252-259.

SAUVAGE, F., FRANZE, S., BRUNEAU, A., ALAMI, M., DENIS, S., NICOLAS, V., LESIEUR, S., LEGRAND, F., BARRATT, G., MESSAOUDI, S. & VERGNAUD-GAUDUCHON, J. 2016. Formulation and *in vitro* efficacy of liposomes containing the Hsp90 inhibitor 6BrCaQ in prostate cancer cells. *International Journal of Pharmaceutics*, 499:101-109.

SCAMBIA, G., RANELLETTI, F.O., PANICI, P.B., DE VINCENZO, R., BONANNO, G., FERRANDINA, G., PIANTELLI, M., BUSSA, S., RUMI, C., CIANFRIGLIA, M. & MANCUSO, S. 1994. Quercetin potentiates the effect of adriamycin in a multidrug-resistant MCF-7 human breast-cancer cell line: P-glycoprotein as a possible target. *Cancer Chemotherapy and Pharmacology*, 34(6):459-464.

SCHUTTE, M.E., ALINK, G.M., FREIDIG, A.P., SPENKELINK, B., VAESSEN, J.C.H., VAN DE SANDT, J.J.M., GROTEN, J.P. & RIETJENS, I.M.C.M. 2008. Quercetin increases the bioavailability of 2-amino-1-methyl-6-phenylimidazo[4,5 b]pyridine (PhIP) in rats. *Food and Chemical Toxicology*, 46:3422-3428.

SERCOMBE, L., VEERATI, T., MOHEIMANI, F., WU, S.Y., SOOD, A.K. & HUA, S. 2015. Advances and challenges of liposome assisted drug delivery. *Frontiers in Pharmacology*, 6:1-13.

SHAPIRO, AB. & LING, V. 1997. Effect of quercetin on Hoechst 33342 transport by purified and reconstituted p-glycoprotein. *Biochemical Pharmacology*, 53(4):587-596.

SHIN, J.H., PARK, S.J., JO, Y.K., KIM, E.S., KANG, H., PARK, J., LEE, E.H. & CHO, D. 2012. Suppression of autophagy exacerbates mefloquine-mediated cell death. *Neuroscience Letters*, 515:162-167.

SHIN, S.C., CHOI, J.S. & LI, X. 2006. Enhanced bioavailability of tamoxifen after oral administration of tamoxifen with quercetin in rats. *International Journal of Pharmaceutics*, 313:144-149.

SHIRASAKA, Y., LI, Y., SHIBUE, Y., KURAOKA, E., SPAHN-LANGGUTH, H., KATO, Y., LANGGUTH, P. & TAMAI, I. 2009. Concentration-dependent effect of naringin on intestinal absorption of β1-adrenoceptor antagonist talinolol mediated by p-glycoprotein and organic anion transporting polypeptide (OATP). *Pharmaceutical Research*, 26(3):560-567.

SHRINGIRISHI, M., MAHOR, A., GUPTA, R., PRAJAPATI, S.K., BANSAL, K. & KESHARWANI, P. 2017. Fabrication and characterisation of nifedipine loaded b-cyclodextrin nanosponges: An *in vitro* and *in vivo* evaluation. *Journal of Drug Delivery Science and Technology*, 41:344-350.

SINGH, A., DUTTA, P.K., KUMAR, H., KUREEL, A.K. & RAI, A.K. 2018. Synthesis of chitin glucan-aldehyde-quercetin conjugate and evaluation of anticancer and antioxidant activities. *Carbohydrate Polymers*, 193:99-107.

SINGH, A., LAVKUSH, A., KUREEL, K., DUTTA, P.K., KUMAR, S. & RAI, A.K. 2018. Curcumin loaded chitin-glucan quercetin conjugate: Synthesis, characterisation, antioxidant, *in vitro* release study, and anticancer activity. *International Journal of Biological Macromolecules*, 110:234-244.

SINGH, R.P., GANGADHARAPPA, H.V. & MRUTHUNJAYA, K. 2017. Phospholipids: Unique carriers for drug delivery systems. *Journal of Drug Delivery Science and Technology*, 39:166-179.

SMEJKALOVA, D., MUTHNY, T., NESPOROVA, K., HERMANNOVA, M., ACHBERGEROVA, E., HUERTA-ANGELES, G., SVOBODA, M., CEPA, M., MACHALOVA, V., LUPTAKOVA, D. & VELEBNY, V. 2017. Hyaluronan polymeric micelles for topical drug delivery. *Carbohydrate Polymers*, 156:86-96.

SOUPPOURIS, A. 2013. Nanosponges could soak up deadly infections like MRSA from your bloodstream. *The Verge* [Online], April 15. Available from: https://www.theverge.com/2013/4/15/4225834/nanosponges-kill-deadly-bacteria-mrsa-clinical-trial [Accessed: 30/07/2019].

SPARREBOOM, A., VAN ASPEREN, J., MAYER, U., SCHINKEL, A.H., SMIT, J.W., MEIJER, D.K.F., BORST, P., NOOIJEN, W.J., BEIJNEN, J.H. & VAN TELLINGEN, O. 1997. Limited oral bioavailability and active epithelial excretion of paclitaxel (taxol) caused

by p-glycoprotein in the intestine. *Proceedings of the Academy of Sciences of the United States of America*, 94(5):2031-2015.

STRAUCH, S., JANTRATID, E., DRESSMAN, J.B., JUNGINGER, H.E., KOPP, S., MIDHA, K.K., SHAH, V.P., STAVCHANSKY, S. & BARENDS, D.M. 2011. Biowaiver monographs for immediate release solid oral dosage forms: Mefloquine hydrochloride. *Journal of Pharmaceutical Sciences*, 100(1):11-21.

SUN, S., GONG, F., LIU, P. & MIAO, Q. 2018. Metformin combined with quercetin synergistically repressed prostate cancer cells via inhibition of VEGF/PI3K/Akt signaling pathway. *Gene*, 664:50-57.

SUN, Y., LI, G., TANG, Z. & WU, B. 2010. Modulation on the p-glycoprotein in the jejunum by combined use of *Glycyrrhiza inflata* and *kansui*. *Acta Pharmeutica Sinica*, 45:510-516.

TAMBE, A., MOKASHI, P. & PANDITA, N. 2019. *Ex-vivo* intestinal absorption study of boswellic acid, cyclodextrin complexes and poloxamer solid dispersions using everted gut sac technique. *Journal of Pharmaceutical and Biomedical Analysis*, 167:66-73.

TARIRAI C., VILJOEN, A.M. & HAMMAN, J.H. 2012. Effects of dietary fruits, vegetables and a herbal tea on the *in vitro* transport of cimetidine: Comparing the Caco-2 cell model with porcine jejunum tissue. *Pharmaceutical Biology*, 50(2):254-263.

TARIRAI, C., VILJOEN, A.M. & HAMMAN, J.H. 2010. Herb-drug pharmacokinetic interaction reviewed. *Expert Opinion on Drug Metabolism and Toxicology*, 6(12):15151538.

TATIRAJU, D.V., BAGADE, V.B., KARAMBELKAR, P.J., JADHAV, V.M. & KADAM, V. 2013. Natural Bioenhancers: An overview. *Journal of Pharmacognosy and Phytochemistry*, 2(3):55-60.

THE CENTERS FOR DISEASE CONTROL AND PREVENTION. 2019. The stages of HIV infection. *AIDSINFO* [Online], June 25. Available from: https://aidsinfo.nih.gov/understanding-hiv-aids/fact-sheets/19/46/the-stages-of-hiv-infection [Accessed: 06/08/2019].

THE JENNER INSTITUTE. 2019. *About malaria* [Online]. Available from: https://www.jenner.ac.uk/about-malaria [Accessed: 06/08/2019].

TIAN, Y., XIA, J., ZHANG, L., ZHANG, J., JIANG, Y., ZHANG, Y., YANG, L., ZHANG, Q. & XIA, L. 2016. Ionic liquid based polymeric liposomes: A stable and biocompatible soft platform for bioelectrochemistry. *Bioelectrochemistry*, 111:41-48.

TOUW, D.J. 1997. Clinical implications of genetic polymorphisms and drug interactions mediated by cytochrome P450 enzymes. *Drug Metabolism and Drug Interactions*, 14:55-82.

TRIPATHY, S. & ROY, S. 2014. A review of age-old antimalarial drug to combat malaria: Efficacy upgradation by nanotechnology-based drug delivery. *Asian Pacific Journal of Tropical Medicine*, 673-679.

UBEAUD, G., HAGENBACH, J., VANDENSCHRIECK, S., JUNG, L. & KOFFEL, J.C. 1999. *In vitro* inhibition of simvastatin metabolism in rat and human liver by naringenin. *Life Sciences*, 65(13):1403-1415.

UMATHE, S.N., DIXIT, P.V., KUMAR, V., BANSOD, K.U. & WANJARI, M.M. 2008. Quercetin pretreatment increases the bioavailability of pioglitazone in rats: Involvement of CYP3A inhibition. *Biochemical Pharmacology*, 75:1670-1676.

UNIVERSITY OF NEBRASKA-LINCOLN. 2015. Research team models new atomic structures of gold nanoparticle. *Phys.org* [Online], April 27. Available from: https://phys.org/news/2015-04-team-atomic-gold-nanoparticle.html [Accessed: 06/08/2019].

VAN HOOGEVEST, P. & WENDEL, A. 2014. The use of natural and synthetic phospholipids as pharmaceutical excipients. *European Journal of Lipid Science and Technology*, 116:1088-1107.

VERSANTVOORT, C.H.M., ROMPELBERG, C.J.M. & SIPS, A.J.A.M. 2000. Methodologies to study human intestinal absorption: A review. *Research for Man and Environment*, RIVM report 630030 001.

VIJAYAKUMAR, T.M., KUMAR, R.M., AGRAWAL, A., DUBEY, G.P. & ILANGO, K. 2015. Comparative inhibitory potential of selected dietary bioactive polyphenols, phytosterols on CYP3A4 and CYP2D6 with fluorometric high-throughput screening. *Journal of Food Science and Technology*, 52(7):4537-4543.

VILACA, R., MENDES, V., MENDES, M.V., CARRETO, L., AMORIM, M.A., DE FREITAS, V., MORADAS-FERREIRA, P., MATEUS, N. & COSTA, V. 2012. Quercetin protects saccharomyces cerevisiae against oxidative stress by inducing trehalose biosynthesis and the cell wall integrity pathway. *PLoS ONE*, 7(9):e45494.

VOLAK, L.P., GHIRMAI, S., CASHMAN, J.R. & COURT, M.H. 2008. Curcuminoids inhibit multiple human cytochromes P450 (CYP), UDP-glucuronosyltransferase (UGT), and sulfotransferase (SULT) enzymes, while piperine is a relatively selective CYP3A4 inhibitor. *Drug Metabolism and Disposition,* 36(8):1594-1605.

WANG, J., MA, C., GUO, C., YUAN, R. & ZHAN, X. 2016. CTG-loaded liposomes as an approach for improving the intestinal absorption of asiaticoside in *Centella* total glucosides. *International Journal of Pharmaceutics*, 509:296-304.

WANG, L., ZHAO, P., FENG, C., WU, Y., DING, Y. & HU, A. 2018. Controlled synthesis of water-dispersible conjugated polymeric nanoparticles for cellular imaging. E*uropean Polymer Journal*, 105:1-6.

WANG, M., ZHAO, T., LIU, Y., WANG, Q., XING, S., LI, L., WANG, L., LIU, L. & GAO, D. 2017. Ursolic acid liposomes with chitosan modification: Promising antitumor drug delivery and efficacy. *Materials Science and Engineering C*, 71:1231-1240.

WANG, Y., CUI, Y., ZHAO, Y., ZHAO, Q., HE, B., ZHANG, Q. & WANG, S. 2018. Effects of surface modification and size on oral drug delivery of mesoporous silica formulation. *Journal of Colloid and Interface Science*, 513:736-747.

WANG, Y.H., CHAO, P.D., HSIU, S.L., WEN, K.C. & HOU, Y.C. 2004. Lethal quercetin-digoxin interaction in pigs. *Life Sciences*, 74:1191-1197.

WORLD HEALTH ORGANISATION. 2005. Proposal to Waive *In vivo* Bioequivalence Requirements for the WHO Model List of Essential Medicines Immediate Release, Solid Oral Dosage Forms. Geneva.

WORLD HEALTH ORGANISATION. 2015. World HIV/AIDS Report 2015. Geneva.

WORLD HEALTH ORGANISATION. 2015. World Malaria Report 2015. Geneva.

XIAO, Y., LIU, Y., YANG, S., ZHANG, B., WANG, T., JIANG, D., ZHANG, J., YUB, D. & ZHANG, N. 2016. Sorafenib and gadolinium co-loaded liposomes for drug delivery and MRI-guided HCC treatment. *Colloids and Surfaces B: Biointerfaces*, 141:83-92.

XING, P., WU, W., DU, P., HAN, F. & CHEN, Y. 2011. Effects of brucine combined with glycyrrhetinic acid or liquiritin on rat hepatic cytochrome P450 activities *in vivo*. *Acta Pharmaceutica Sinica*, 46:573-580.

YANG, R., ZHANG, X., LI, F., DING, L., LI, B., SUN, H. & GAN, Y. 2013. Role of phospholipids and copolymers in enhancing stability and controlling degradation of intravenous lipid emulsions. *Colloids and Surfaces A: Physicochemical and Engineering Aspects*, 436:434-442.

YAO, H., FU, X., XIE, Q., HUANG, B., SUN, Y. & LI, G. 2009. Effect of liquorice decoction on rat intestinal p-glycoprotein. *Journal of Southern Medical University*, 29:1571-1573.

YAO, Y.M., CAO, W., CAO, Y.J., CHENG, N.Z., OU-YANG, D.S., LIU, Z.Q. & ZHOU, H.H. 2007. Effect of sinomenine on human cytochrome P450 activity. *International Journal of Clinical Chemistry*, 379(1-2):113-118.

YOON, H.Y., KWAK, S.S., JANG, M.H., KANG, M.H., SUNG, S.W., KIM, C.H., KIM, S.R., YEOM, D.W., KANG, M.J. & CHOI, Y.W. 2017. Docetaxel-loaded RIPL peptide

(IPLVVPLRRRRRRRRC)-conjugated liposomes: Drug release, cytotoxicity, and antitumor efficacy. *International Journal of Pharmaceutics*, 523:229-237.

YUCEL, C., DEGIM, Z. & YILMAZ, S. 2013. Nanoparticle and liposome formulations of doxycycline: Transport properties through Caco-2 cell line and effects on matrix metalloproteinase secretion. *Biomedicine and Pharmacotherapy*, 67:459-467.

ZENG, Y., GU, B., JI, X., DING, X., SONG, C. & WU, F. 2007. Sinomenine, an antirheumatic alkaloid, ameliorates clinical signs of disease in the Lewis rat model of acute experimental autoimmune encephalomyelitis. *Biological and Pharmaceutical Bulletin*, 30(8):1438-1444.

ZHANG, D., YE, L., CHENG, H., YU, W., YANG, J. & GUO, P. 2008. Cytoprotective effect and its mechanisms of isoliquiritigenin on acetaminophen induced acute injury of hepatocytes. *Chinese Journal of Clinical Pharmacology and Therapeutics*, 13:293-298.

ZHANG, H., GONG, W., WANG, Z., YUAN, S., XIE, X., YANG, Y., YANG, Y., WANG, S., YANG, D., XUAN, Z. & MEI, X. 2014. Preparation, characterisation, and pharmacodynamics of thermosensitive liposomes containing docetaxel. *Journal of Pharmaceutical Sciences*, 103:2177-2183.

ZHANG, H., WONG, C.W., COVILLE, P.F. & WANWIMOLRUK, S. 2000. Effect of the grapefruit flavonoid naringin on pharmacokinetics of quinine in rats. *Drug Metabolism and Drug Interactions*, 17:351-363.

ZHANG, W., TAN, T.M.C. & LIM, L.Y. 2007. Impact of curcumin-Induced changes in p-glycoprotein and CYP3A expression on the pharmacokinetics of peroral celiprolol and midazolam in Rats. *Drug Metabolism and Disposition*, 35(1):110-115.

ZHANG, Y., DONG, K., WANG, F., WANG, H., WANG, J., JIANG, Z. & DIAO, S. 2018. Three dimensional macroporous hydroxyapatite/chitosan foam-supported polymer micelles for enhanced oral delivery of poorly soluble drugs. *Colloids and Surfaces B: Biointerfaces*, 170:497-504.

ZHAO, T., LIU, Y., GAO, Z., GAO, D., LI, N., BIAN, Y., DAI, K. & LIU, Z. 2015. Self-assembly and cytotoxicity study of PEG-modified ursolic acid liposomes. *Materials Science and Engineering C,* 53:196-203.

ZHOU, D. & RAKARIYATHAM, K. 2018. Phospholipids. In: *Reference Module in Food Science*, 1-4.

ZHOU, Y., QUAN, G., WU, Q., ZHANG, X., NIU, B., WU, B., HUANG, Y., PAN, X. & WU, C. 2018. Mesoporous silica nanoparticles for drug and gene delivery. *Acta Pharmaceutica Sinica B*, 8(2):165-177.

ZUO, T., GUAN, Y., CHANG, M., ZHANG, F., LU, S., WEI, T., SHAO, W. & LIN, G. 2016. RGD(Arg-Gly-Asp) internalized docetaxel-loaded pH sensitive liposomes: Preparation, characterisation and antitumor efficacy *in vivo* and *in vitro*. *Colloids and Surfaces B: Biointerfaces*, 147:90-99.